

**POLITECNICO DI TORINO**

**Master's Degree in Aerospace Engineering**



**Master's Degree Thesis**

**Multi-objective optimization of low-thrust  
orbit transfers in LEO using Q-law and  
direct collocation**

**Supervisors**

**Prof. Lorenzo CASALINO**

**Dr. Federica PAGANELLI AZZA**

**Candidate**

**Angelo Luca MORELLO**

**July 2022**



# Ringraziamenti

Un ringraziamento particolare va all'azienda AIKO, per avermi permesso di studiare a fondo e di mettermi alla prova nell'argomento che più mi ha appassionato durante questo lungo percorso di studi fornendomi tutti gli strumenti necessari per farlo, per avermi fatto sentire come uno di loro dal primo giorno in cui ho iniziato a lavorare su questa tesi, e per essere sempre stati disponibili quando ho avuto bisogno di consigli.

Ringrazio di cuore Federica, per avermi seguito ed aiutato personalmente dall'inizio alla fine di questa ultima tappa del percorso, condividendo delusioni, vittorie, ma soprattutto tante idee e confronti che mi hanno portato ad una importante crescita sia personale che culturale. E grazie al mio amico Christian, per avermi fatto conoscere quasi per caso, tra una partita di calcetto e una birra, questa interessante opportunità.

Un sentito ringraziamento va al Professore Casalino, per la disponibilità dimostrata e per i preziosissimi consigli che hanno creato spiragli anche in quei momenti in cui non sembrava esserci una via d'uscita.

Infine ai miei genitori, a cui dedico questo traguardo. La testardaggine che scorre nel mio sangue "per colpa" vostra è stata l'arma che più mi è stata utile in tutti in questi anni di studio. Questo giorno, questo ultimo lavoro, questo percorso, senza quello che per me rappresentate non sarebbe andato così. I sacrifici che, facendo finta di niente, avete continuamente fatto in questi anni solo perchè avete sempre creduto ciecamente in me, mi hanno trasmesso dei valori forti quanto veri che porterò per sempre con me e che cercherò di trasmettere a mia volta. Siete le fondamenta di tutto quello che ho costruito, le colonne portanti che più di tutti hanno subito il peso dei miei sfoghi, dei miei bronci, ma soprattutto dei miei infiniti silenzi. Sono grato di tutte le esperienze vissute in questi ultimi anni, ma oggi se ne va anche un peso: spero tanto che vedendomi sorridere così ne sia valsa la pena averlo sopportato insieme a me.

# Summary

The increased fuel efficiency makes electric propulsion systems particularly suitable when large  $\Delta V$  increments are required, such as during orbital transfers around a central body. On the other hand, low thrust systems operate for a significant amount of mission time, producing long thrusting arcs that have to be designed through appropriate continuous optimization techniques. The corresponding optimal control problem is indeed strongly nonlinear and it is much harder to solve than conventional high-thrust trajectory optimization.

In this work, a flexible approach for the optimization of low thrust trajectories is presented. The orbit transfer problem is addressed, introducing a two-stage technique to produce continuous spacecraft trajectories that satisfy initial and terminal conditions defined along two different orbits while minimizing the fuel consumption and/or time of flight (TOF). The devised method takes into account the impact of external perturbations in order to generate a reliable solution. The multi-objective formulation of the optimization problem offers a practical way to trade off fuel consumption and time of flight, providing an adaptable framework able to deal with several use-cases.

The proposed optimization strategy relies on a method that combines Lyapunov control guidance algorithms with direct collocation approaches, offering lower computational demands with respect to existing techniques. A peculiar feature of this work is the single-phase formulation of the optimal control problem that requires no prior information about the solution structure. The Q-law results, already close to the global optima, are then used to warm up the optimization routine, that employs direct collocation techniques to transcribe the optimal control problem (OCP) into a nonlinear programming problem (NLP). The transcription process is particularly effective when paired with the Q-law output because of the direct collocation capability of exploiting the entire initial guess, relying on the computed path and controls to produce optimal trajectories while satisfying desired endpoint constraints. The resulting NLP is easily solved with a general-purpose solver such as IPOPT or SNOPT.



# Table of Contents

<b>List of Tables</b>	VII
<b>List of Figures</b>	IX
<b>Acronyms</b>	XII
<b>1 Introduction</b>	1
1.1 Problem definition . . . . .	1
1.2 State of the art . . . . .	3
1.3 Objectives of the thesis . . . . .	5
1.4 Main contributions . . . . .	10
1.5 Structure of the thesis . . . . .	11
<b>2 System dynamics model</b>	12
2.1 Orbital mechanics . . . . .	12
2.1.1 Energy and relation to the geometry of an orbit . . . . .	14
2.2 Coordinate systems . . . . .	18
2.2.1 Earth-centered inertial system . . . . .	18
2.2.2 RTN frame . . . . .	19
2.2.3 Classical orbital elements . . . . .	20
2.2.4 Modified Equinoctial Elements . . . . .	24
2.3 Perturbations . . . . .	24
2.3.1 Gauss's Variational Equations . . . . .	26
2.3.2 Propulsion . . . . .	27
2.3.3 Asphericity of the Earth . . . . .	28
2.4 Eclipses . . . . .	34
2.5 Spacecraft model . . . . .	37
<b>3 Q-law</b>	38
3.1 Control Lyapunov Functions and Q-law . . . . .	38
3.1.1 Minimum time solution . . . . .	42

3.1.2	Optimal fuel solution . . . . .	44
3.1.3	Asphericity of the Earth . . . . .	45
3.2	Example results . . . . .	46
3.2.1	Minimum time . . . . .	47
3.2.2	Optimal fuel . . . . .	49
3.3	Q-law vs optimal thrust angles maneuvers . . . . .	54
3.4	Q-law weights analysis . . . . .	58
3.5	Eclipses . . . . .	60
3.5.1	Mesh refinement . . . . .	66
<b>4</b>	<b>Direct optimization</b> . . . . .	<b>70</b>
4.1	Optimal trajectory design problem . . . . .	70
4.2	NLP . . . . .	71
4.3	Direct transcription and collocation . . . . .	72
4.3.1	Local discretization methods . . . . .	74
4.4	<i>PSOPT</i> setup . . . . .	76
4.4.1	Problem formulation . . . . .	76
4.5	Example results . . . . .	78
4.5.1	Minimum time . . . . .	78
4.5.2	Optimal fuel . . . . .	81
<b>5</b>	<b>Simulation results</b> . . . . .	<b>85</b>
5.1	Minimum time . . . . .	85
5.1.1	Orbit change . . . . .	86
5.1.2	Disposal . . . . .	90
5.2	Optimal fuel . . . . .	95
5.2.1	Orbit change . . . . .	95
5.2.2	Disposal . . . . .	99
5.3	GMAT validation . . . . .	104
5.3.1	Orbit change . . . . .	104
5.3.2	Disposal . . . . .	106
<b>6</b>	<b>Conclusions</b> . . . . .	<b>109</b>
6.1	Future work . . . . .	110
	<b>Bibliography</b> . . . . .	<b>111</b>

# List of Tables

1.1	Direct and indirect optimization methods: pros and cons . . . . .	6
1.2	Objective mission of the thesis . . . . .	9
2.1	Simulation parameters and initial orbital elements for propagation .	31
2.2	Spacecraft parameters . . . . .	37
2.3	Model parameters . . . . .	37
3.1	Q-law transfer parameters for example scenario . . . . .	46
3.2	Examples of time of flight and fuel mass consumption resulting as a function of $\eta_{a_{cut}}$ and $\eta_{a_{cut}}$ . . . . .	51
3.3	Optimal thrust angles for the maximum instantaneous change of each orbital element . . . . .	55
3.4	Estimates of velocity increment required to obtain a change in each orbital element . . . . .	56
3.5	Q-law vs benchmark: comparison of procedure results, target errors and computational time . . . . .	58
3.6	Weights analysis results . . . . .	59
3.7	Parameters for eclipses example transfer . . . . .	62
3.8	Eclipses impact on time of flight and fuel consumption . . . . .	62
3.9	Mesh refinement impact on Q-law algorithm performance . . . . .	69
4.1	Transfer for solver example results . . . . .	78
4.2	Algorithm options for solver minimum time example results . . . . .	79
4.3	Comparison between Q-law and <i>PSOPT</i> results . . . . .	79
4.4	Optimization parameters for optimal fuel trade-off . . . . .	82
4.5	Solutions for optimal fuel problem . . . . .	82
4.6	Comparison between solutions for optimal fuel problem . . . . .	84
5.1	Q-law parameters for initial guess generation . . . . .	85
5.2	Minimum time orbit change: initial and final state variables . . . . .	86
5.3	Minimum time orbit change: results . . . . .	86
5.4	5 years propagation: initial and final state variables . . . . .	90

5.5	Minimum time disposal: initial and final state variables . . . . .	91
5.6	Minimum time disposal: results . . . . .	91
5.7	Optimal fuel orbit change: initial and final state variables . . . . .	95
5.8	Optimal fuel orbit change: results . . . . .	99
5.9	Optimal fuel disposal: initial and final state variables . . . . .	100
5.10	Optimal fuel disposal: results . . . . .	100

# List of Figures

1.1	Sun-synchronous orbits position relatively to the Sun . . . . .	7
1.2	Relation between altitude and inclination for a SSO . . . . .	8
2.1	Two-body problem . . . . .	13
2.2	$m$ moving from point 1 to point 2 under the gravitational force of $M$	14
2.3	Conic sections . . . . .	16
2.4	Geometrical properties of conic sections . . . . .	17
2.5	ECI frame . . . . .	18
2.6	RTN frame . . . . .	19
2.7	Thrusting angles . . . . .	20
2.8	Classical orbital elements . . . . .	21
2.9	Correlation between classical orbital elements, ECI and RTN frames	23
2.10	Orbital perturbations at low altitudes [4] . . . . .	25
2.11	Orbital elements evolution: GMAT propagation vs $J_2$ secular effect propagation . . . . .	32
2.12	Ideal vs $J_2$ perturbed scenario. 400 km altitude increase transfer with fixed eccentricity . . . . .	33
2.13	Eclipse model . . . . .	35
2.14	Eclipse logistic function . . . . .	36
3.1	Influence of $k$ parameter on penalty function $P$ , with $r_p^{min} = 6578$ km	40
3.2	Orbital elements and mass evolution for Q-law minimum time solution	48
3.3	Orbit visualization for Q-law minimum time solution . . . . .	48
3.4	Thrust directions for Q-law minimum time solution . . . . .	49
3.5	Time of flight and fuel mass consumption as a function of $\eta_{a_{cut}}$ and $\eta_{r_{cut}}$ . . . . .	50
3.6	Zoom on results as a function of cutoff for low $\eta_{a_{cut}}$ and $\eta_{r_{cut}}$ values	51
3.7	Orbital elements and mass evolution for Q-law optimal fuel solution with $\eta_{a_{cut}} = 0.6$ . . . . .	52
3.8	Thrust magnitude and directions for Q-law optimal fuel solution with $\eta_{a_{cut}} = 0.6$ . . . . .	53

3.9	Orbit visualization for Q-law optimal fuel solution with $\eta_{a_{cut}} = 0.6$	53
3.10	Details of inclination evolution due to cutoff effects with $\eta_{a_{cut}} = 0.6$	54
3.11	Comparison between Q-law and benchmark results in orbital elements evolution	57
3.12	Weights analysis results - Time of flight result for each Q-law weights combination in the three analysis	60
3.13	Orbital elements evolution for the transfer summarized in Table 3.7	63
3.14	Thrust direction for the transfer summarized in Table 3.7	64
3.15	Orbital trajectory for the transfer summarized in Table 3.7 with eclipses	65
3.16	Orbital trajectory for for the transfer summarized in Table 3.7 without eclipses	65
3.17	Orbital trajectory for the example transfer with mesh refinement	67
3.18	Thrust and eclipse function profiles without mesh refinement	68
3.19	Thrust and eclipse function profiles with mesh refinement	68
4.1	State variables evolution: minimum time optimization vs minimum time Q-law	80
4.2	Thrust directions: minimum time optimization vs minimum time Q-law	81
4.3	Optimal fuel solutions and initial guesses	83
5.1	Minimum time orbit change: state variables	88
5.2	Minimum time orbit change: thrust directions	89
5.3	Minimum time disposal: state variables	93
5.4	Minimum time disposal: thrust directions	94
5.5	Optimal fuel orbit change: state variables	97
5.6	Optimal fuel orbit change: thrust throttle and directions	99
5.7	Optimal fuel disposal: state variables	102
5.8	Optimal fuel disposal: thrust throttle and directions	103
5.9	Orbit change: GMAT validation on orbital elements evolution	106
5.10	Disposal: GMAT validation on orbital elements evolution	108



# Acronyms

**AOP**

Argument of periapsis

**CLF**

Control Lyapunov function

**COE**

Classical orbital element

**ECI**

Earth-centered inertial

**GEO**

Geostationary Earth orbit

**GMAT**

General Mission Analysis Tool

**GTO**

Geostationary transfer orbit

**GVE**

Gauss variational equations

**IADC**

Inter-Agency Space Debris Coordination Committee

**LEO**

Low-Earth orbit

**MEE**

Modified equinoctial elements

**NLP**

Nonlinear programming

**OCP**

Optimal control problem

**RAAN**

Right ascension of the ascending node

**RTN**

Radial - Tangential - Normal reference frame

**SEP**

Solar electric propulsion

**SRP**

Solar radiation pressure

**SSO**

Sun-synchronous orbit

**TOF**

Time of flight

# Chapter 1

## Introduction

### 1.1 Problem definition

Electric propulsion is gaining popularity for both planetary and interplanetary space missions, offering appealing efficiency for a wide variety of applications. Even though these systems provide a lower thrust magnitude, their specific impulse improvement of approximately one order of magnitude compared to chemical propulsion allows a greater total change in velocity ( $\Delta V$ ) with smaller propellant mass, making these systems suitable for many missions, such as many-revolution transfers in Earth orbits when changes in one or more orbital elements are desired, exploiting solar radiation as an external power source through photovoltaic panels.

Based on their low-thrust characteristics, solar electric propulsion (SEP) systems are the object of many research for their potential use on small satellites and Cubesats, whose use has constantly grown in recent years. This particular term refers to a miniaturised satellite made up of cube units with 10 cm sides, such that  $1 \text{ U} = (10 \times 10 \times 10) \text{ cm}^3$  with mass of no more than 2 kg [1]. Cubesats were initially developed by universities to facilitate access to space for educational purposes, targeting students. After some years, they have gained popularity and they are now widely used and studied in countless companies worldwide, thanks to low cost of developing, building and launching associated to them. In addition, the opportunity of having these satellites work together in constellations along with the continuous technological improvements of miniaturised components, lead to numerous advantages in performances related to Earth observation and telecommunications, such as coverage and revisit rate, often at lower cost compared to regular satellites. However, the small size causes drawbacks too, such as limits on data downlink capability or picture resolution. For now, only a limited amount of Cubesats have been equipped with a propulsion system, most of which were chemical cold gas solution. Meanwhile, the research and the technological development of

miniaturized electric propulsion systems is improving, leading to in-orbit validation for some of these systems such as Hall effect thrusters [2]. The possibility for Cubesats to have on-board propulsion paves the way to new opportunities, allowing orbital correction maneuvers that are extremely useful to improve performances or to enable new missions, that can be, taking as example an Earth observation mission:

- Orbit raising to augment coverage
- Orbit lowering to improve picture resolution
- Inclination corrections
- Station keeping to counteract perturbations and augment satellite lifespan

Another important operation that electric propulsion allows is the end-of-life disposal, in order to propel the satellite back into the atmosphere at the end of the mission, essential to mitigate the space debris issue especially when LEO (Low-Earth Orbit) Cubesats constellations are considered. Indeed, in case of collision not only the satellite and the mission are lost, but the entire orbit becomes unusable for a long time. It is therefore essential to include this maneuver when designing a mission, mainly because the number of active satellites is set to increase significantly in the future, providing improved services but at the same time complicating the challenge of space debris removal.

Finally, propulsion on Cubesats also allows to plan a more flexible launch strategy, using rideshare launches to a parking orbit followed by maneuvers in order to reach the operational orbit. It is demonstrated that this strategy leads to a reduction of the total cost of the mission [3].

However, the use of low-thrust electric propulsion is associated with a higher need of electric power, typically generated by deployable solar arrays, and a longer time of flight due to small values of acceleration compared to chemical propulsion systems, which work through impulsive high-thrust maneuvers. Moreover, the system operates for a significant amount of mission time, leading to long continuous thrusting arcs. Therefore, one of the main challenges is to accurately design these arcs, since the thrust magnitude and its direction have to be defined for each instant. These elements can be determined, given a desired transfer from a specified initial state, through an optimization of the orbital trajectory that consists in the determination of a control law that either maximizes or minimizes a defined performance index, returning a time history of the thrust magnitude and direction vector.

The optimization of mission design gets more difficult considering LEO Cubesats constellations. Because of its low distance from Earth's surface that advantages operations related to global monitoring, telecommunications and astronomical

observations, and because of the lower cost for a low-altitude launch compared to any other space mission, most of the existing satellites orbits in this region [4]. However, LEO is also the most dynamical perturbed environment for Earth satellites, so the presence of perturbations must be taken into account in order to obtain significant solutions but, at the same time, it further complicates the mission design optimization.

## 1.2 State of the art

The three most important categories of low-thrust trajectory optimization methods are indirect methods, direct methods and dynamic programming approach. In the following section a brief overview about these methods, based on [5], is presented.

An indirect method discretizes the system in its dualized form: the states and costates are both solved. These approaches rely on the calculus of variations, and the necessary conditions of optimality require the solution of a multi-point boundary value problem (MPBVP) that results from applying the Pontryagin minimum principle (PMP) [6]. Even if these types of methods are really accurate, there are a lot of difficulties in the implementation, such as that analytical forms of the optimal control necessary conditions must be expressed, including the costate differential equations, the Hamiltonian, the optimality condition, and transversality conditions. Numerically speaking, this also makes the problem size large due to discretization of the costates. Furthermore, the mission analyst must guess certain aspects of the optimal control solution, such as the portion of the time domain containing constrained or unconstrained control arcs, when using a gradient-based methods, and since these approaches also require initial guesses for the costates, the domain of convergence may be very small and highly sensitive to the initial costates.

In a direct method instead, the system is discretized in its original form without the need to express the optimal control necessary conditions and costate equations. The state and control variables are discretized, and the optimal control problem is converted into a nonlinear programming (NLP) problem [7], where the objective function is directly optimized. The transcription process requires the discretization of the control variables in a time-grid. The goal of a NLP problem is to determine a vector of unknown decision variables that comply with a set of non-linear constraints, including equality and inequality restrictions. These methods are easier to implement than indirect methods and generally robust, having a larger domain of convergence. Moreover they can easily accomodate path constraints, maintaining a reduced problem size. On the other hand, they are less accurate than indirect methods and computationally sensitive and expensive.

The last optimization method is the Dynamic Programming Approach, either

based on the Bellman's principle of optimality [8] for discrete-time systems, or based on the Hamilton-Jacobi-Bellman theorem [9] for continuous-time systems. The whole state space is searched, so the optimal solution is also the global optimum. On the other hand, dimensionality is the main drawback of these methods: memory expense and computational time grow quickly with the number of state variables and thus these methods become impractical for high-dimensional state space.

Historically, low-thrust many-revolution problems have been solved with indirect and direct optimal control methods. These typically involve one of the following techniques to impose the dynamical equations in the solution:

- Single shooting: The trajectory is integrated using time-marching methods [10] from the initial time  $t_0$  upon reaching the final time  $t_f$ . Initial states are unknowns to be determined, and boundary constraints are imposed at the end of the integration.
- Multiple shooting: The time interval  $[t_0, t_f]$  is broken up into subintervals, and the trajectory is integrated over each subinterval. Initial states of subintervals are unknowns to be determined, and continuity conditions have to be imposed at the interface of each subinterval.
- Collocation: The states are discretized over a predefined time-grid, such that they are known only at discrete points. The equations that describe the system are transformed into discrete defect constraints, which relate the values at the beginning to the values at the end of each subinterval. Collocation methods can be divided in local and global, depending on the rule to approximate differential equations between adjacent subintervals.

These approaches are used to convert the optimal control problem to the problem of determining a vector of decision variables. Methods for solving NLP problems, resulting from direct approaches, and MPBVP, resulting from indirect approaches, are iterative methods that use a different set of rules for evolving, and they can be classified as follows:

- Gradient-based: An initial guess is made of the unknown decision vector  $\mathbf{z}$ . At each  $k^{th}$  iteration, a search direction  $\mathbf{p}_k$  and a step length  $\alpha_k$  are defined. The former provides a direction in  $\mathbb{R}^{n_z}$  along which to change the current value  $\mathbf{z}_k$ , while the latter provides the magnitude of the change, such that the update has the form  $\mathbf{z}_{k+1} = \mathbf{z}_k + \alpha_k \mathbf{p}_k$ . The procedure continues until optimality conditions are reached.
- Heuristic: The search is performed in a stochastic manner with no need of gradient information. The most known examples of these methods are evolutionary algorithm and heuristics based on Lyapunov control.

- Hybrid: This approach is based on combining a set of rules that exploits gradient information and a set of rules based on heuristic searches to iteratively operate over a candidate solution. Gradient information is used to drive the constraints to zero, while heuristic methods are applied to explore wide design domains.

It is interesting to also introduce direct methods that approximate the control law by predefined guidance schemes. These methods have been developed in order to rapidly generate sub-optimal trajectories. A class of these utilizes closed form feedback control laws derived from Lyapunov functions. One of the most known method is the Proximity Quotient guidance law (Q-law), presented by Petropoulos [11]. This concept relies on the calculation of a proximity quotient  $Q$ , that is an assessment of the proximity of the osculating orbit to the target orbit. The algorithm is a closed loop Lyapunov-based control method that determines the instantaneously optimal thrust direction to reduce  $Q$  at each point along the trajectory towards the target orbit. The advantage of this law lies in the speed of computation, which can be orders of magnitude greater than that for direct and indirect optimization methods, while the disadvantage is that the solutions are non-optimal, even though Genetic Algorithms can be exploited to optimize Q-law free parameters, as seen in Chapter 2.

### 1.3 Objectives of the thesis

The possibility to maneuver satellites paves the way to the opportunity of exploiting orbit changes such that mission requirements, in terms of orbital parameters as altitude and eccentricity, can be satisfied also starting the mission from a different orbit than the operational one, rather than starting and remaining on the same orbit throughout the mission. As a matter of fact, most of Cubesats and small satellites exploits rideshares of larger satellites for a parking orbit injection, using launch broking company such as ISIS or Spaceflight Industries [3]. These companies generally offer launches opportunity between 450 km and 650 km of altitude on Sun-Synchronous Orbits, with the majority of these being around 550 km SSO, associated with an orbital inclination of  $97.5977^\circ$ . From the parking orbit, propulsion allows to maneuver the satellite in order to improve selected performances, as discussed in section 1.1. In this particular case, the mission will start from the parking orbit described above and the operations will be:

- Orbit raising in order to improve revisit rate and augment satellite coverage
- Inclination correction maneuver in order to reach a SSO
- Disposal maneuver, reaching a perigee of 400 km and an apogee of 800 km

	<b>Direct methods</b>	<b>Indirect methods</b>
<b>Pros</b>	Easier to initialize, thanks to a larger domain of convergence and a physically intuitive optimization variable	Offer theoretical insight into mathematical and physical problem characteristics
	Robust, larger domain of convergence, at least a sub-optimal solution is reached	
	Can easily accommodate complex control, state or path constraints, with no need to know a priori the sequence of constrained and free arcs	Greater accuracy than direct methods when convergence is met
	Reduced problem size	
<b>Cons</b>	Strongly dependent on the initial guess, may not converge often to the global optimal	Explicit derivations of the costate and control equations required, not flexible
		Small domain of convergence, accurate initial guess of the costates required to converge
	Often require much computational effort	Not intuitive, costates do not have physical interpretations
		More difficult to reformulate in case new states, constraints or dynamics are given
		Not suitable to solve highly constrained optimization problems

**Table 1.1:** Direct and indirect optimization methods: pros and cons

Sun-Synchronous Orbits are nearly polar orbits, i.e. with inclination around  $90^\circ$ , that have the particular characteristic to have a  $360^\circ$  nodal precession (presented when perturbations are deeply discussed in section 2.3.3) in one year, so it always maintains the same position relatively to the Sun, as seen in Fig. 1.1, where a SSO is compared to an unperturbed orbit to better grasp the difference in the relative position of the orbits with respect to the Sun.

This characteristic is given by the  $J_2$  perturbation effect, that causes the arise of a shift in the value of the right ascension of the ascending node (RAAN, also

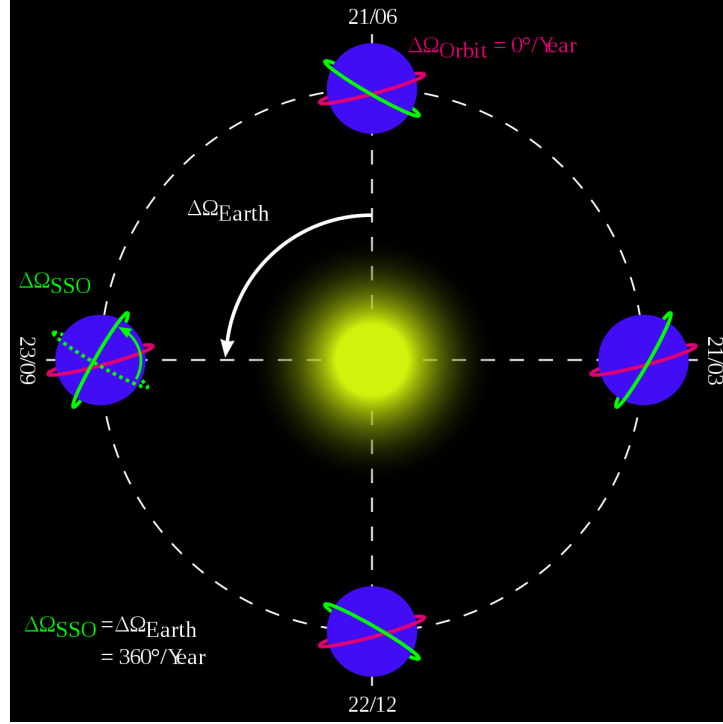


**Figure 1.1:** Sun-synchronous orbits position relatively to the Sun

known as  $\Omega$ ), such that:

$$\Delta RAAN \left[ \frac{\text{rad}}{\text{s}} \right] = -3\pi J_2 \left( \frac{R_E}{p} \right)^2 \frac{\cos i}{\tau} \quad (1.1)$$

where  $J_2$  is the coefficient for the zonal harmonic term related to Earth oblateness,  $R_E$  is Earth radius,  $p$  is the orbit semilatus rectum,  $i$  is the orbital inclination and  $\tau$  is the orbital period. For quasi-circular orbits, i.e. the majority of LEO orbits,  $p \approx a$  where  $a$  is the semi-major axis of the orbit. These elements will be further discussed in Chapter 2, but considering that:

$$\Delta RAAN_{SSO} = \frac{2\pi}{1 \text{ sidereal year}} = 1.9909869 \cdot 10^{-7} \frac{\text{rad}}{\text{s}} \quad (1.2)$$

they are now introduced just to highlight the fact that for a SSO there is a direct relationship between orbit altitude, expressed by means of the semi-major axis, and orbital inclination. This relation is derived equaling Eq. 1.1 and Eq. 1.2:

$$i \text{ [rad]} = \arccos \left[ - \left( \frac{a \text{ [km]}}{12350.23 \text{ km}} \right)^{\frac{7}{2}} \right] \quad (1.3)$$

and it is shown in Fig. 1.2. If this relation is respected, the orbit results to be a Sun-Synchronous orbits.

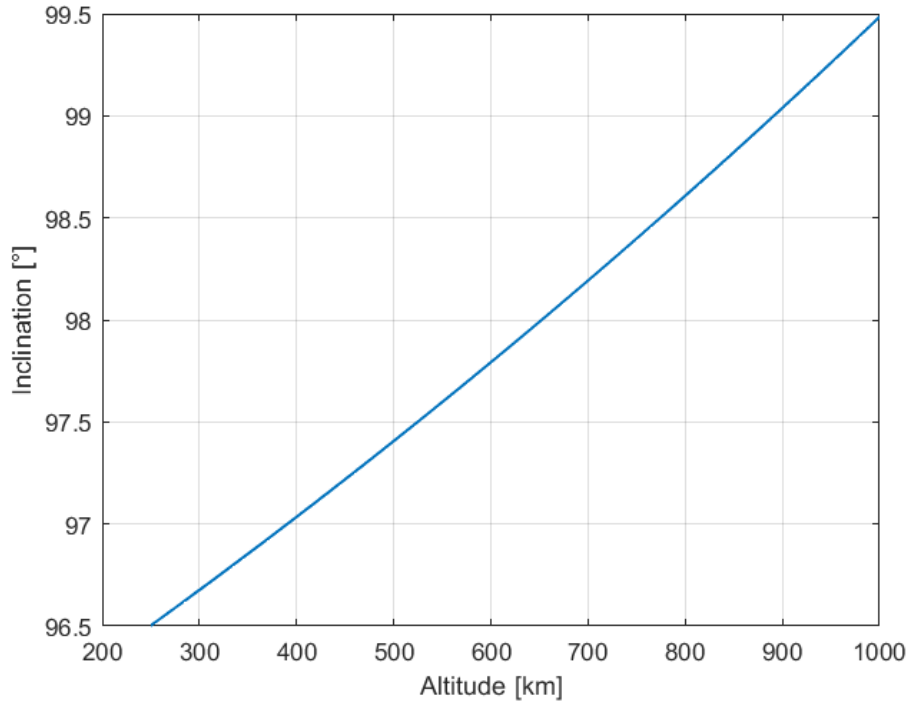


**Figure 1.2:** Relation between altitude and inclination for a SSO

The advantage of orbiting in a SSO is given by the main characteristic of always maintaining the same position with respect to the Sun. Based on the orbit RAAN value that determines the orbit position relatively to the Sun, different properties can be achieved: a mission can be designed in a way that, for example, the satellite never passes during its lifetime through eclipse arcs, crucial issue for solar electric propulsion since the propulsion system, when not illuminated by solar light, cannot generate thrust. This issue is further discussed in section 2.4. Another example of use-case scenario is a mission whose goal is to have a spacecraft that always orbits following the terminator line, i.e. the moving line that divides a planetary body's surface in sunlight side and dark side. This is done knowing that the terminator line, as well as a SSO, rotates of  $360^\circ$  around the Sun in 1 sidereal year.

This SSO introduction is important especially to calculate the orbital inclination correction that represents the second desired operation for the objective mission. However it is essential to note that the first two maneuvers will be conducted in a combined way, since, as it is successively proven in section 3.3, combined maneuvers always cost less than the respective separate maneuvers. From Eq. 1.3,

the inclination of a 800 km SSO is  $98.6081^\circ$ .

The last maneuver is conducted as an end-of-life disposal after 5 years of in-orbit operations, in order to comply with IADC regulations and recommendations on space debris mitigation [12] that give a 25-years limit for the presence of a deactivated space system in LEO region. It is demonstrated in [3] that, after carrying out this maneuver, the satellite will de-orbit in a bit more than 13 years. To reach this target orbit a combined change of altitude and eccentricity has to be planned.

These operations are summed up in Table 1.2. Classical orbital elements, described in section 2.2.3, are used to define the initial and the target orbit of the transfers. Values of not targeted orbital elements are considered arbitrary for simplicity and because they have not a significant impact on the transfer, so their initial values are conventionally set to zero. Initial values of orbital elements for the second transfer are derived and discussed in Chapter 5.

Orbital element	Orbit change		Disposal		Unit
	Initial value	Target value	Initial value	Target value	
$a$	6928	7178	7178	6978	km
$e$	0.01	0.01	0.01	0.02866151	-
$i$	97.5977	98.6081	98.6081	Free	$^\circ$
$\Omega$	0	Free	12.5416	Free	$^\circ$
$\omega$	0	Free	23.1151	Free	$^\circ$
$\theta$	0	Free	0	Free	$^\circ$

**Table 1.2:** Objective mission of the thesis

The goal is to have an optimal transfer between these orbits, either in terms of time or cost. Therefore, the objective of this thesis is to investigate on the most suitable optimization methods for orbital transfers design.

After comparing the advantages and disadvantages of direct and indirect approaches, briefly summed up in Table 1.1, it has been decided to focus the attention on direct optimization methods. Moreover, the introduced Q-law is thoroughly analyzed in this work too: it is surely worth to explore how much the advantage of having a quicker solution is balanced to the disadvantage of having a sub-optimal trajectory, observing the difference compared to a direct-optimized trajectory.

Finally, after analyzing these different types of orbital trajectory generation, the objective is trying to understand if any benefits may derive from a two-phase hybrid optimization in which the sub-optimal method and the direct optimization method are combined. In this case, the sub-optimal method is represented by the Q-law algorithm, deeply presented and discussed in Chapter 3, while the

direct optimization is implemented using PSOPT, an open source optimal control solver based on direct collocation methods, presented in Chapter 4. This hybrid optimization is conducted by using, either for minimum time solution or for optimal fuel solution, the sub-optimal trajectory generated by the Q-law algorithm as an initial guess input in the solver, that will optimize the already close to optimal solution, minimizing a certain performance index that varies with respect to the objective of the problem: if a minimum time problem is defined, the total time of flight will represent the performance index, whereas an optimal fuel problem is considered, the final mass value, with negative sign, will be the performance index.

Analyzing the objective scenario, the goal is to examine the performances together with the ease of use of these different guidance laws approaches, with the possibility of achieving significant optimal results for minimum time solutions while obtaining, for optimal fuel solutions, an appropriate trade-off between total time of flight and fuel consumption.

## 1.4 Main contributions

The main contributions of this thesis are:

- A deep analysis of a Lyapunov control-based guidance for LEO transfers, with the possibility of integrating a mechanism for fuel optimal solution. The results are then compared with state-of-the-art optimal maneuvers results.
- An examination of the most suitable ways to integrate the main LEO perturbation, that is the  $J_2$  zonal harmonic effect, in the Q-law algorithm and in the direct optimization process, after a GMAT validation of the assumed perturbation model.
- The integration of eclipse constraints in the Q-law procedure, after the derivation of a logistic eclipse model.
- An analysis of the effectiveness of direct collocation optimization methods for low-thrust trajectory problems, reaching a trade-off for optimal fuel transfers and comparing the optimized results with the ones obtainable through a faster strategy such as the Q-law.
- An investigation on the benefits deriving from combining a sub-optimal rapidly generated trajectory, through the Q-law, with a direct collocation optimization for low-thrust trajectory problems.
- A validation of the controls given in output by the Q-law algorithm through GMAT.

## 1.5 Structure of the thesis

This discussion is presented as follows:

- **Chapter 1:** An introduction to the problem is presented, together with an overview on state-of-the-art of electric propulsion systems. The available approaches to deal with the design of their trajectories are discussed and the objective of the thesis is then defined.
- **Chapter 2:** The orbital transfer problem is introduced, with a discussion on orbital perturbations, and the main modelling choices are described.
- **Chapter 3:** The Q-law mechanisms are deeply studied for both minimum time and optimal fuel scenario, together with example results and analysis in order to illustrate the benefits of the chosen Lyapunov control guidance. Then, an overview on eclipses integration and effects on this method is presented.
- **Chapter 4:** The adopted direct optimization technique is addressed, focusing on the optimizer setup and presenting some results in order to prove the effectiveness of the proposed optimization method.
- **Chapter 5:** The objective scenario of this thesis is deeply analyzed. Minimum-time and fuel optimal results for the objective scenario are shown and compared, demonstrating the suitability of a hybrid approach to address the low thrust trajectory design problem.
- **Chapter 6:** Conclusions and a discussion on future work are presented.

## Chapter 2

# System dynamics model

The following chapter will focus on the presentation of the fundamentals of orbital mechanics, essential to better understand the contents of this thesis. The employed spatial model will be presented and discussed, with the explanation of used reference frames and equations of motions. After that, the considered perturbations will be introduced and the spacecraft model will be defined.

For an even deeper understanding and for further details on orbital mechanics not reported in this discussion, precise and in-depth explanations can be found in [13], from which most of the following summarizing sections are excerpted.

### 2.1 Orbital mechanics

The basis of orbital mechanics is described by Kepler's laws of planetary motion described below:

- **First Law** The orbit of each planet is an ellipse, with the Sun at a focus.
- **Second Law** The line joining the planet to the Sun sweeps out equal areas in equal times.
- **Third Law** The square of the period of a planet is proportional to the cube of its mean distance to the Sun.

Together with these, to better comprehend the influences between masses in orbital motion, it is essential to keep in mind Newton's law of universal gravitation:

$$\vec{F}_g = -G \frac{Mm}{r^2} \frac{\vec{r}}{r} \quad (2.1)$$

where  $M$  and  $m$  are two masses,  $\vec{F}_g$  is the force on mass  $m$ , and  $\vec{r}$  is the vector from  $M$  to  $m$ , that can be written in cartesian coordinates as  $[x, y, z]^T$  based on

the origin of the defined reference system.  $G$  represents the universal gravitational constant and it is equal to  $6.67 \cdot 10^{-11} \text{ Nm}^2/\text{kg}^2$ .

The most basic spacecraft trajectory occurs in the two-body problem, following the assumption of bodies deemed as points with constant mass. Furthermore, only the gravitational force between bodies is considered for now in this presentation.

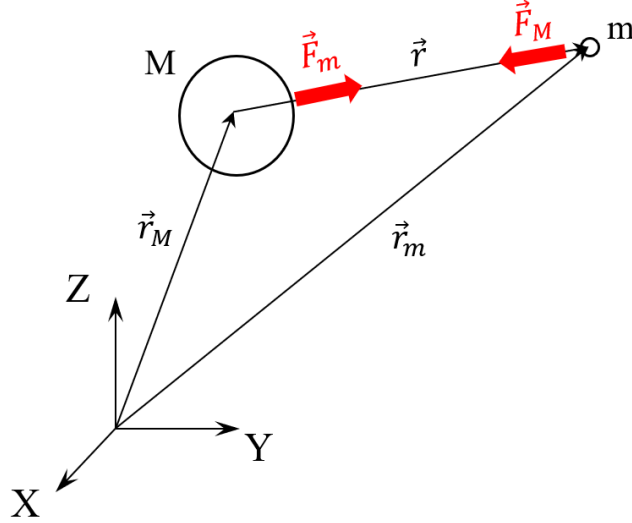


**Figure 2.1:** Two-body problem

The two-body problem is derived from the N-body problem, when one body has negligible mass and the other is a point mass central body, and it describes the motion of a body relative to another one. As demonstrated in [13], the equation of motion in the two-body problem is expressed as:

$$\ddot{\vec{r}} = -G \frac{M + m}{r^3} \vec{r} \quad (2.2)$$

where  $\ddot{\vec{r}}$  is the acceleration of  $m$  relative to  $M$ . To take the studied case as an example, the mass  $m$  could be a spacecraft orbiting around Earth, that represents the mass  $M$ . In this equation, the gravitational forces acting between the two masses and all of the other bodies (i.e. Sun, Moon, other planets) are neglected, since the force between the spacecraft and Earth is much bigger than others.

When  $M \gg m$ , as in the defined example, a simplifying assumption can be made by totally neglecting  $m$  such that:

$$G(M + m) \approx GM = \mu \quad (2.3)$$

where  $\mu$  is called gravitational parameter, and it depends on the mass of the considered central body. The Earth gravitational parameter is  $\mu_{Earth} =$

398600.4419 km<sup>3</sup>/s<sup>2</sup>.

Following this assumption, the equation of motion (Eq. 2.2) for the two-body problem can now be rewritten as:

$$\ddot{\vec{r}} + \frac{\mu}{r^3}\vec{r} = 0 \quad (2.4)$$

### 2.1.1 Energy and relation to the geometry of an orbit

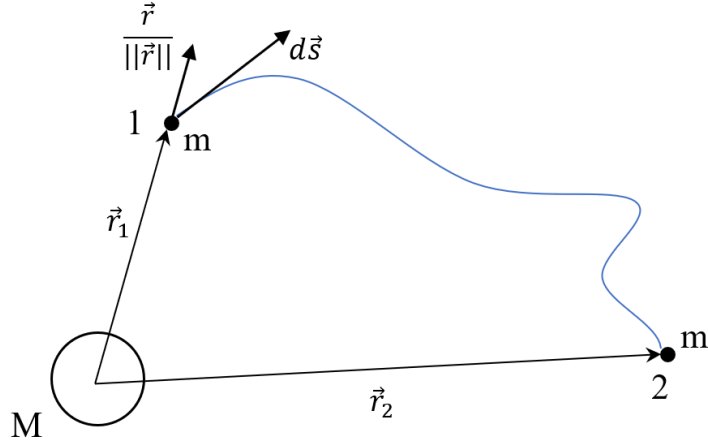


**Figure 2.2:**  $m$  moving from point 1 to point 2 under the gravitational force of  $M$

The mechanical work per unit mass done by the gravitational force of the primary mass  $M$  to achieve a change of position from point 1 to point 2 of the secondary body  $m$  is expressed as:

$$\mathcal{L}_{12} = \int_1^2 \frac{\vec{F}_g}{m} \cdot d\vec{s} = \int_1^2 \ddot{\vec{r}} \cdot d\vec{s} = \int_1^2 -\frac{\mu}{r^2} \frac{\vec{r}}{r} \cdot d\vec{s} = \int_1^2 -\frac{\mu}{r^2} dr = \frac{\mu}{r_2} - \frac{\mu}{r_1} \quad (2.5)$$

It can be seen from this result that the mechanical work does not depend on the trajectory. Therefore the gravitational field is conservative, as the mechanical work is zero if a closed path in which initial and final point coincide is taken into consideration. A body moving in this field does not increase or reduce its mechanical energy, but only transfers it from potential to kinetic energy and vice versa. Moreover, in a conservative field the mechanical work can be expressed as the variation of potential energy from the initial point to the final point:

$$\mathcal{L}_{12} = -\Delta\varepsilon_g = \varepsilon_{g1} - \varepsilon_{g2} \quad (2.6)$$

Comparing Eq. 2.5 and Eq. 2.6, a new definition of the potential energy per unit mass (also called specific potential energy) can be obtained:

$$\varepsilon_g = -\frac{\mu}{r} + c \quad (2.7)$$

where  $c$  is an arbitrary constant representing the potential energy of a reference point. Knowing that this choice is arbitrary,  $c$  is conventionally set to zero, as the reference point is considered at  $r \rightarrow \infty$  from the primary body, so the equation becomes:

$$\varepsilon_g = -\frac{\mu}{r} \quad (2.8)$$

After that, the energy constant of motion can be derived as seen in [13]. Firstly, Eq. 2.4 is scalar multiplied by  $\dot{\vec{r}}$ , leading to:

$$\dot{\vec{r}} \cdot \ddot{\vec{r}} + \dot{\vec{r}} \cdot \frac{\mu}{r^3} \vec{r} = 0 \quad (2.9)$$

Knowing that for scalar product  $\vec{a} \cdot \dot{\vec{a}} = a\dot{a}$ ,  $\vec{v} = \dot{\vec{r}}$  and  $\dot{\vec{v}} = \ddot{\vec{r}}$ :

$$v\dot{v} + \frac{\mu}{r^3} r\dot{r} = 0 \quad (2.10)$$

and noticing that:

$$\frac{d}{dt} \left( \frac{v^2}{2} \right) = v\dot{v} \quad (2.11)$$

$$\frac{d}{dt} \left( -\frac{\mu}{r} \right) = \frac{\mu}{r^2} \dot{r} \quad (2.12)$$

it can be written that:

$$\frac{d}{dt} \left( \frac{v^2}{2} - \frac{\mu}{r} \right) = 0 \quad (2.13)$$

When the time rate of change of an expression is zero, the expression must be constant. In this case the constant is called specific mechanical energy (or mechanical energy per unit mass), and it is expressed as:

$$\varepsilon = \frac{v^2}{2} - \frac{\mu}{r} = \text{const.} \quad (2.14)$$

The first term is the specific kinetic energy of the body, while the second is the specific potential energy as seen in Eq. 2.8. This energy remains constant along the orbit, the energy exchange takes place only between potential and kinetic energy.

This formulation is very important since the mechanical energy can be related to the geometry of the orbit. As a matter of fact, every orbit is a conic section, i.e. a curve obtained from the intersection of a plane and a right circular cone, as seen in Fig. 2.3.

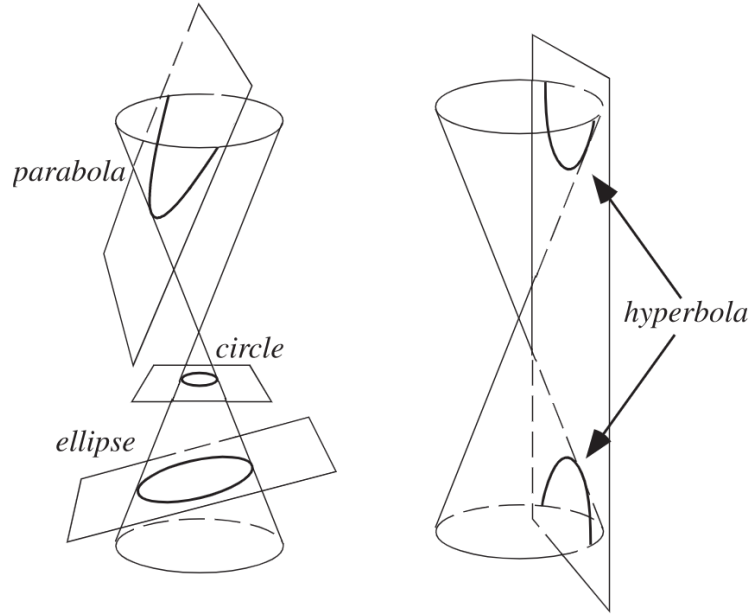


**Figure 2.3:** Conic sections

As thoroughly demonstrated in [13], a relation between the mechanical energy and orbit geometry can be found, and it is expressed through the following:

$$\varepsilon = -\frac{\mu}{2a} \quad (2.15)$$

where  $a$  is called semi-major axis of the orbit, and its value depends on the type and on the size of the orbit. The different values of  $a$  associated to the respective type of conic sections are presented in Fig. 2.4, together with the other geometrical properties:  $p$  is a geometrical constant of the conic section known as semilatus rectum;  $2c$  is the distance between the two foci ( $F$  and  $F'$ ) of the conic section;  $b$  is the semi-minor axis, defined for elliptical orbits.

This equation is valid for all conic orbits and tells that the semi-major axis of an orbit depends only on the specific mechanical energy of the body, which in turn depends on  $\vec{r}$  and  $\vec{v}$  at any point on the orbit. Studying the Eq. 2.15 together with Fig. 2.4, it can be seen that for closed orbits (ellipse and circle)  $a$  is positive and so  $\varepsilon$  is negative; for a parabolic orbit  $a$  is infinite, and so  $\varepsilon$  is zero; for a hyperbolic orbit  $a$  is negative, and so  $\varepsilon$  is positive. Therefore, the specific mechanical energy of the body alone defines the geometry of the orbit in which the body is moving.

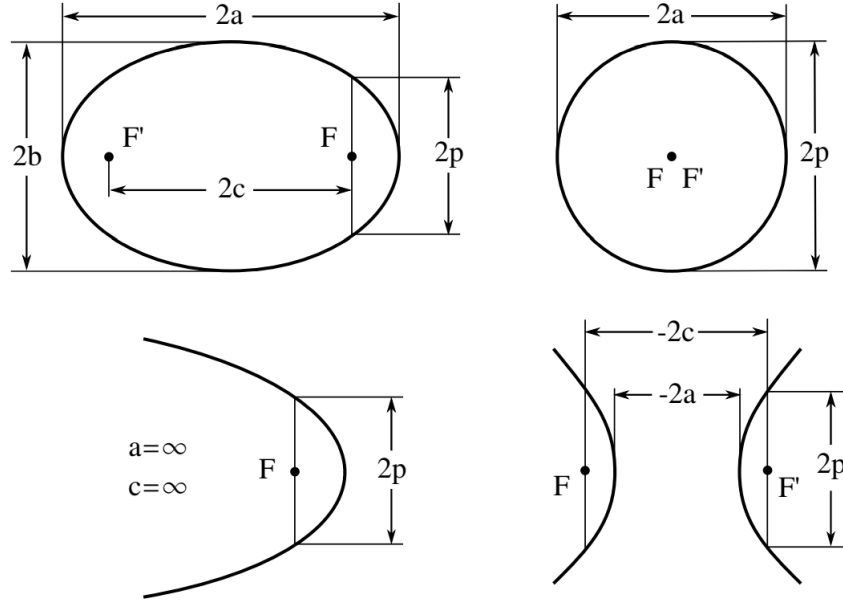


**Figure 2.4:** Geometrical properties of conic sections

Another important geometric relation is defined as follows:

$$e = \sqrt{1 + \frac{2\varepsilon h^2}{\mu^2}} \quad (2.16)$$

where  $e$  is called eccentricity of the conic section, and  $h$  is the magnitude of  $\vec{h} = \vec{r} \times \vec{v}$ , which is the specific angular momentum that, as demonstrated in [13], remains constant along the orbit for any type of conic section and it is equal to:

$$h = \sqrt{\mu p} \quad (2.17)$$

The eccentricity is a non-negative geometrical property that characterizes every conic section, and it can be interpreted as a measure of how far a conic section is from being a circle: for a circle  $e = 0$ , for an ellipse  $0 < e < 1$ , for a parabola  $e = 1$  and for a hyperbola  $e > 1$ . As a matter of fact, these values are consistent with the mechanical energy values seen above: if  $\varepsilon$  is negative, either  $e$  is positive and less than 1 (ellipse), or  $\varepsilon = -\mu^2/2h^2$  and  $e = 0$  (circle); if  $\varepsilon$  is zero,  $e$  is 1 (parabola); if  $\varepsilon$  is positive,  $e$  is greater than 1 (hyperbola). It is important to note that, if  $h = 0$  the eccentricity will be  $e = 1$  yet the orbit will not be a parabola, but it will be a degenerate conic, such as a point or a straight line. As a matter of fact, all parabolas are characterized by  $e = 1$ , but an orbit with  $e = 1$  is not necessarily a parabola, as it could be a degenerate conic.

Every orbit studied in this work will be elliptical orbits.

## 2.2 Coordinate systems

The first requirement to describe an orbit in a three dimensional space is a suitable inertial reference frame, that's a coordinate system whose axes point in a fixed direction with respect to the fixed stars. This choice strongly depends on the mission type. In the case of planets, asteroids and deep space probes orbiting around the Sun, the heliocentric-ecliptic coordinate system is the most suitable. However, orbits around the Sun are not the object of this work so the mentioned coordinate system will not be presented here. For spacecrafts orbiting around Earth instead, the Earth-centered inertial (ECI) system is convenient. The elements that fulfill the description of a coordinate system are the position of the origin, the orientation of the fundamental plane (X-Y plane), the principal direction (the direction of X-axis) and the positive direction of the Z-axis, perpendicular to the fundamental plane. Following the right hand rule, the Y-axis is automatically defined after these elements.

### 2.2.1 Earth-centered inertial system

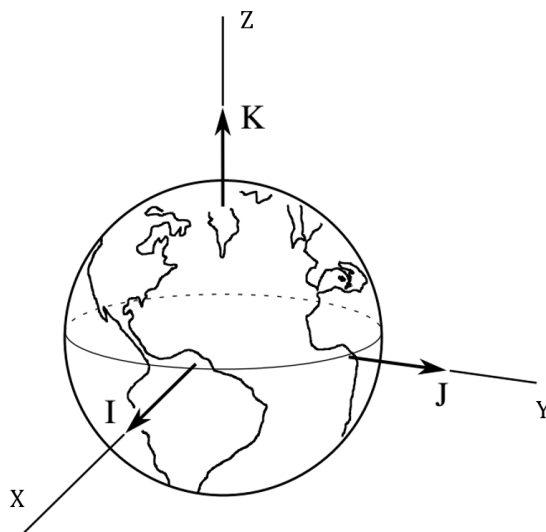


Figure 2.5: ECI frame

The Earth-centered inertial coordinate system, also known as Geocentric-Equatorial coordinate system, has its origin at the Earth's center of mass. This coordinate frame is inertial with respect to the fixed stars, neglecting the precession of the equinoxes, so it does not rotate with Earth's surface. Its fundamental plane is the equatorial plane and the positive X-axis is permanently fixed pointing in the direction of vernal equinox. The Z-axis is perpendicular to the fundamental plane

and points in the direction of the north pole. The Y-axis is defined by completing a right handed set. This reference system is described, as seen in Fig. 2.5, by the unit vectors  $\hat{I}$ ,  $\hat{J}$  and  $\hat{K}$  that respectively lie along the X,Y, and Z axes, and it is useful to describe the body motion relatively to the Earth.

### 2.2.2 RTN frame

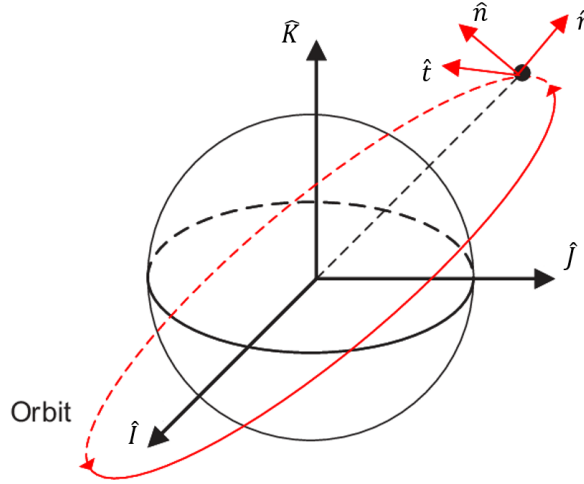


Figure 2.6: RTN frame

Another set of coordinates that is extremely useful to describe the orbital motion of a satellite is its local frame. As a matter of fact, the equations of motion that will be presented and discussed in the following section and that will be used to model the system dynamics are described by variational equations defined in this local frame. This coordinate system has its origin at the spacecraft's center of mass, and it is formed by the unit vectors  $\hat{r}$ ,  $\hat{t}$  and  $\hat{n}$ , defined as:

$$\hat{r} = \frac{\vec{r}}{\|\vec{r}\|}, \quad \hat{n} = \frac{\vec{r} \times \vec{v}}{\|\vec{r} \times \vec{v}\|}, \quad \hat{t} = \hat{n} \times \hat{r} \quad (2.18)$$

The set of unit vectors gives the name to this reference frame, that is called Radial-Tangential-Normal (RTN) frame, also known as Local-Vertical-Local-Horizontal (LVLH) frame.

The principal direction is given by the unit vector  $\hat{r}$ , that goes along the instantaneous radius vector  $\vec{r}$ , from Earth to the spacecraft. The fundamental plane is the instantaneous orbital plane, such that the unit vector  $\hat{t}$  is rotated  $90^\circ$  in the orbital plane with respect to  $\hat{r}$  in the instantaneous direction of motion. The unit vector  $\hat{n}$  is perpendicular to the fundamental plane, and its direction is defined

by completing a right handed set. It is important to note that this reference frame is not influenced by the spacecraft attitude and rotation, since it is defined from the spacecraft's center of mass. It is the reference frame that will be used throughout this entire work to describe the spacecraft's center of mass motion relatively to the instantaneous orbit, as it also allows to define a pair of thrusting angles through which the thrusting spatial components will be derived. As seen in Fig. 2.7, the thrust angles are defined as  $\alpha$  and  $\beta$ . The first is measured in the orbit plane off of the tangential direction  $\hat{t}$ , positive away from the gravitational centre and it is defined in the interval  $[-\pi, \pi]$ ; the latter is measured off of the orbital plane and perpendicular to it, positive in the direction of the angular momentum and defined in the interval  $[-\pi/2, \pi/2]$ .

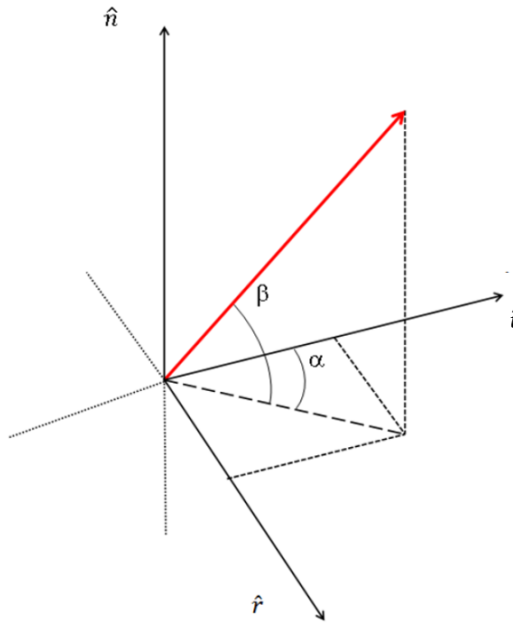
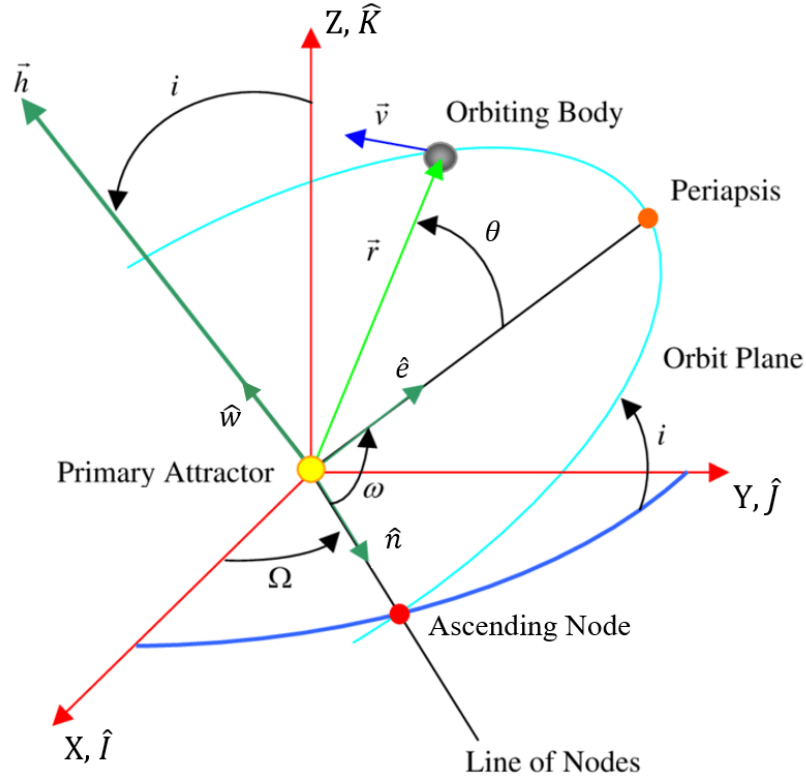


Figure 2.7: Thrusting angles

### 2.2.3 Classical orbital elements

The classical orbital elements (COE), also known as Keplerian orbital elements, are very useful to describe the fundamental properties of the orbit and represent the most used method for description and visualization of orbits around celestial bodies. This set is composed by six parameters, among which five are independent quantities sufficient to completely describe the size, shape and orientation of an orbit. The sixth element is essential to identify the spacecraft position on the orbit at a certain time. These parameters are dependent on  $\vec{r}$  and  $\vec{v}$  and can be



**Figure 2.8:** Classical orbital elements

determined directly from them. This set of orbital elements is presented in Fig. 2.8, and they are defined as:

- $a$ , semi-major axis. It defines the size of the orbit, and it is calculated as the sum of periapsis and apoapsis distance divided by two, or as:

$$a = \frac{p}{1 - e^2} \quad (2.19)$$

knowing that

$$p = \frac{h^2}{\mu} \quad (2.20)$$

$$h = \|\vec{h}\| = \|\vec{r} \times \vec{v}\| \quad (2.21)$$

- $e$ , eccentricity. It defines the shape of the orbit, defining the conic sections geometrical property already discussed in section 2.1. It can be calculated as:

$$e = \|\vec{e}\| = \left\| \frac{\vec{v} \times \vec{h}}{\mu} - \frac{\vec{r}}{\|\vec{r}\|} \right\| \quad (2.22)$$

- $i$ , inclination. It is the angle between the orbital plane and the fundamental plane of the coordinate system, i.e. the equatorial plane in this case, in the intersection identified by the ascending node. Its value can vary between 0 and  $\pi$ , and can be calculated as:

$$i = \arccos(\hat{K} \cdot \hat{w}) \quad (2.23)$$

where:

$$\hat{w} = \frac{\vec{h}}{\|\vec{h}\|} \quad (2.24)$$

Orbits are categorized as direct when  $i < \pi/2$  and retrograde when  $\pi/2 < i < \pi$

- $\Omega$ , also known as RAAN, right ascension of the ascending node. It is defined as the angle in the fundamental plane between the X-axis of the coordinate system, in this case  $\hat{I}$  that points to the vernal equinox, and the line of nodes, that is the line of intersection between the orbital plane and the fundamental plane that points towards the ascending node. This angle is measured eastward from X-axis, it varies between 0 and  $2\pi$ , and it is defined as:

$$\Omega = \begin{cases} \arccos(\hat{I} \cdot \hat{n}) & \text{if } \hat{J} \cdot \hat{n} \geq 0 \\ 2\pi - \arccos(\hat{I} \cdot \hat{n}) & \text{if } \hat{J} \cdot \hat{n} < 0 \end{cases} \quad (2.25)$$

where

$$\hat{n} = \frac{(\hat{K} \times \vec{h})}{\|\hat{K} \times \vec{h}\|} \quad (2.26)$$

- $\omega$ , argument of periapsis. It is the angle between the ascending node and the periapsis of the orbit, so it defines the orientation of the conic section in the orbital plane. It is measured from the line of nodes in the direction of motion, it varies from 0 to  $2\pi$ , and it is defined as:

$$\omega = \begin{cases} \arccos(\hat{n} \cdot \hat{e}) & \text{if } \hat{e} \cdot \hat{K} \geq 0 \\ 2\pi - \arccos(\hat{n} \cdot \hat{e}) & \text{if } \hat{e} \cdot \hat{K} < 0 \end{cases} \quad (2.27)$$

- $\theta$ , true anomaly. It is the angle between periapsis and the current position of the spacecraft. It is measured from the periapsis in the direction of motion, it varies from 0 to  $2\pi$  and it is defined as:

$$\theta = \begin{cases} \arccos\left(\frac{\vec{r}}{\|\vec{r}\|} \cdot \hat{e}\right) & \text{if } \vec{r} \cdot \vec{v} \geq 0 \\ 2\pi - \arccos\left(\frac{\vec{r}}{\|\vec{r}\|} \cdot \hat{e}\right) & \text{if } \vec{r} \cdot \vec{v} < 0 \end{cases} \quad (2.28)$$

In some particular cases this set of orbital elements is undefinable [13]: when  $i = 0^\circ$  (equatorial orbit) the line of nodes is not defined and consequently  $\Omega$  and  $\omega$  are undefined too; when  $e = 0$  (circular orbit) periapsis cannot be defined, and consequently  $\omega$  and  $\theta$  are also undefined. However, the scenarios studied in this work do not include any of these identified cases, so the classical orbital elements are chosen as a suitable representation for the adopted model.

Finally, in Fig. 2.9 a comparison between the two discussed frames, together with the classical orbital elements, is presented to better grasp the correlation between these reference system.

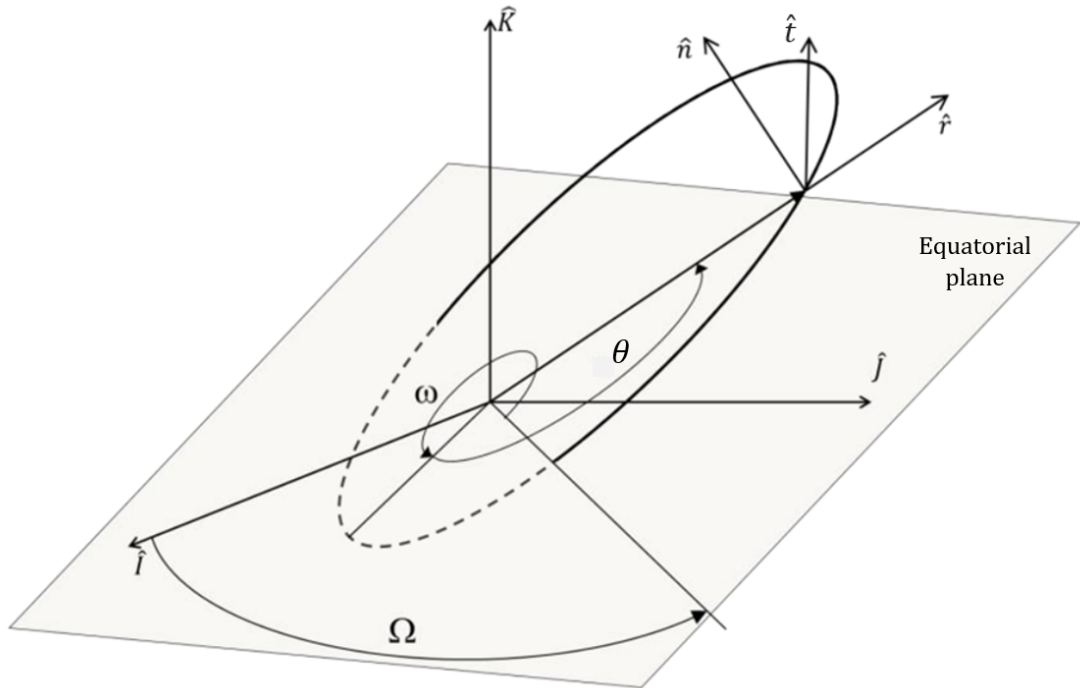


**Figure 2.9:** Correlation between classical orbital elements, ECI and RTN frames

### 2.2.4 Modified Equinoctial Elements

The modified equinoctial elements (MEE) [14][15][16] are another set of orbital elements that can be useful for trajectory analysis and optimization, as reported in the following section. They are suitable for circular, elliptic and hyperbolic orbits. Plus, singularities discussed for classical orbital elements when  $i = 0^\circ$  or  $e = 0$  do not arise in this set. However, two of the components are singular (infinite) for  $i = 180^\circ$ . In this work they will be useful for the determination of the eclipses model.

These elements are defined as a function of classical orbital elements, and they are given by:

$$\begin{aligned}
 p &= a(1 - e^2) \\
 f &= e \cos(\omega + \Omega) \\
 g &= e \sin(\omega + \Omega) \\
 h &= \tan\left(\frac{i}{2}\right) \cos \Omega \\
 k &= \tan\left(\frac{i}{2}\right) \sin \Omega \\
 L &= \Omega + \omega + \theta
 \end{aligned} \tag{2.29}$$

The inverse equations that give the values of classical orbital elements as a function of modified equinoctial elements can be found in [16].

## 2.3 Perturbations

The previous dissertation about the two-body problem has been based on some assumptions presented at the beginning of the section, such as the one that stated that only gravitational forces between the two masses are considered to describe their relative motion. So, no form of perturbations has been taken into account until now. While under the action of gravity alone the only orbital element that varies is true anomaly, a real spacecraft orbiting around Earth is subjected to perturbations that lead to variations in all of the six orbital elements throughout its trajectory, changing the trajectory predicted by the two-body problem. Because of perturbations that are always present, the orbital elements slightly change at any instant, therefore the spacecraft continuously goes from one Keplerian orbit to another. To indicate an orbit, its geometrical properties or its orbital elements that, given a certain time, refer to a real trajectory in which all the perturbations are included, the term "osculating" is used [13].

The restricted two-body equation of motion (Eq. 2.4) can be rewritten as:

$$\ddot{\vec{r}} = \frac{\mu}{r^3}\vec{r} + \vec{\delta}_P \quad (2.30)$$

where  $\vec{\delta}_P$  is the perturbing acceleration vector in the considered coordinate system, in this case ECI frame.

Generally, the perturbations acting on orbiting bodies are due to thrust from spacecraft's propulsion system, gravitational attraction by third bodies, atmospheric drag and lift, asphericity of the attracting body, solar radiation pressure and magnetic effects. These perturbations are usually associated with three categories of effects:

- **Short-period variations:** oscillating perturbations with a period similar or less than the orbital period
- **Long-period variations:** oscillating perturbations with a period greater than the orbital period
- **Secular variations:** aperiodic variations that vary as a function of the osculating orbital elements and that are associated with long-term effects on the orbit

Depending on the mission, some perturbations becomes more relevant than others, as seen in Fig. 2.10.

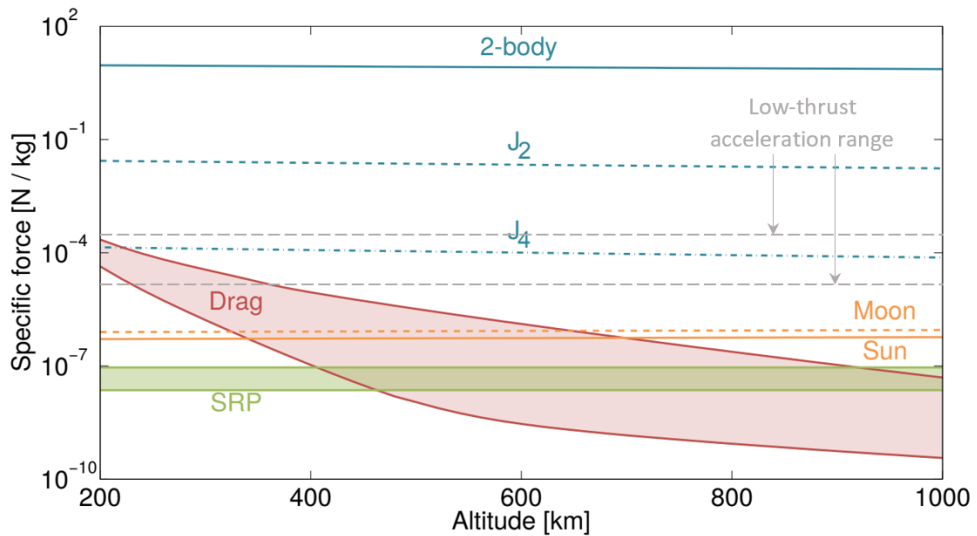


Figure 2.10: Orbital perturbations at low altitudes [4]

Considering that the work in this thesis is focused only on LEO-LEO transfers (altitude below 2000 km) the included orbital perturbations will concern the

Earth's oblateness, associated with the  $J_2$  zonal harmonic, and of course the thrust acceleration given by the propulsion system and Earth's gravitational attraction. Furthermore, considered altitudes are not low enough to make drag a relevant perturbation, so it is neglected. All the other perturbations are considered negligible too.

### 2.3.1 Gauss's Variational Equations

Perturbations can be applied to the classical orbital elements through a set of variational equations, defined in the spacecraft's local frame presented in section 2.2.2, that describes how orbital elements vary with time through an analytical definition of the rate of change of elements due to perturbations. The equations used throughout this work is the Gauss's Variational Equations, also known as Gauss's Planetary Equations. Their derivation is accurately presented in [17]. These equations provide the instantaneous rates of change of the orbital elements for an assigned acceleration vector in the RTN frame, as a function of the osculating orbital elements. The rates of change are expressed as [18]:

$$\begin{aligned}
 \frac{da}{dt} &= \frac{2a^2}{h} \left( e \sin \theta f_r + \frac{p}{r} f_t \right) \\
 \frac{de}{dt} &= \frac{1}{h} \{ p \sin \theta f_r + [(p+r) \cos \theta + re] f_t \} \\
 \frac{di}{dt} &= \frac{r \cos(\theta + \omega)}{h} f_n \\
 \frac{d\Omega}{dt} &= \frac{r \sin(\theta + \omega)}{h \sin i} f_n \\
 \frac{d\omega}{dt} &= \frac{1}{eh} [-p \cos \theta f_r + (p+r) \sin \theta f_t] - \frac{r \sin(\theta + \omega) \cos i}{h \sin i} f_n \\
 \frac{d\theta}{dt} &= \frac{h}{r^2} + \frac{1}{eh} [p \cos \theta f_r - (p+r) \sin \theta f_t]
 \end{aligned} \tag{2.31}$$

where  $t$  is the time,  $p$  is the osculating semilatus rectum,  $h = \sqrt{\mu p}$  is the magnitude of the specific orbital angular momentum,  $\mu$  is the gravitational parameter of Earth.  $r$  is the radius from Earth and it is defined using the general equation of any conic section in polar coordinates [13]:

$$r = \frac{p}{1 + e \cos \theta} \tag{2.32}$$

$f_r$ ,  $f_t$ , and  $f_n$  are the three spatial components of the perturbations acceleration expressed in the RTN frame, respectively in the radial, tangential (circumferential) and normal (out of plane) directions.

The discussed equations exhibit singularities for equatorial orbit ( $i = 0^\circ$ ) and for circular orbit ( $e = 0$ ). To avoid these singularities, a set of variational equations as a function of osculating modified equinoctial elements can be used. This set is introduced in [14][15], and can be reformulated using matrix notation as seen in [19]. However, since the cases that cause singularities are not cases of interest in this work as already discussed in section 2.2.3, the equations expressed through classical orbital elements (Eq. 2.31) will be used.

### 2.3.2 Propulsion

The spacecraft's propulsion system is able to generate thrust, that can be used as an active control to achieve the desired rates of change of orbital elements. As stated in section 1.1, a low-thrust electric propulsion system is used throughout this thesis.

Following the thrust angles discussion in section 2.2.2, the thrust acceleration components can be expressed as:

$$\begin{bmatrix} f_r \\ f_t \\ f_n \end{bmatrix}_{thrust} = \begin{bmatrix} f \cos \beta \sin \alpha \\ f \cos \beta \cos \alpha \\ f \sin \beta \end{bmatrix} \quad (2.33)$$

where:

$$f = \frac{T}{m} \quad (2.34)$$

is the thrust acceleration magnitude, being  $T$  the thrust value equal, and  $m$  the total mass of the body subjected to the acceleration.

The thrust value  $T$  can be modulated and it mostly depends on the mission objective: in general, when a minimum time optimization is desired, the thrust value is always set to  $T = T_{max}$ , whereas for optimal fuel optimization the thrust value is  $0 \leq T \leq T_{max}$ . The thrust can be then formulated as:

$$T = T_{max}\eta \quad (2.35)$$

where  $0 \leq \eta \leq 1$  is the thrust throttle and its value depends on the optimization problem.

The fuel mass flow rate due to thrust is also dependent on the on the throttle. Based on the model presented in [20] and assuming no mass leakage, it is modeled as:

$$\dot{m} = -\frac{T}{g_0 I_{sp}} = -\frac{T_{max}\eta}{g_0 I_{sp}} \quad (2.36)$$

where  $g_0 = 9.80665 \text{ m/s}^2$  is the standard Earth gravitational acceleration, and  $I_{sp}$  is the specific impulse of the propulsion system. Consequently, it can be seen that the value of  $\dot{m}$  only depends on the optimization problem by means of the throttle  $\eta$ , and:

$$0 \leq \dot{m} \leq \dot{m}_{max} \quad (2.37)$$

where  $\dot{m}_{max}$  is the fuel mass flow rate associated to  $\eta = 1$  and  $T_{max}$ .

### 2.3.3 Asphericity of the Earth

Generally it is assumed that Earth is a perfect sphere, however it is well known that this is an approximation. The assumption of geometrical and mass symmetry of Earth cannot stand when real perturbed trajectories are considered in the problem. As a matter of fact, Earth is an oblate body called "Geoid", flattened at the poles and bulged at the equator, and it is characterized by asymmetrical density variations. The excess of mass at the equator produces a slight torque on the satellite, which is exposed to effects not included in the expression for the gravitational potential of the Earth seen in Eq. 2.8. Thus, the latter has to be reformulated introducing new terms that represent this perturbation. Several gravitational models of increasing fidelity have been employed in the past to describe the gravitational field of the Earth (WGS-84, JGM-2, EGM-2008 are some examples [21][22]). All of them are based upon using the expression of the gravitational potential written in terms of harmonics, associated with Legendre polynomials.

The gravitational potential of the Earth using the WGS-84 model can be expressed as [23][24]:

$$\begin{aligned} \varepsilon_g = & \frac{\mu}{r} - \frac{\mu}{r} \sum_{n=2}^{\infty} J_n \left( \frac{R_E}{r} \right)^n \mathcal{P}_n \sin \phi \\ & - \frac{\mu}{r} \sum_{n=2}^{\infty} \sum_{m=1}^n J_{n,m} \left( \frac{R_E}{r} \right)^n \mathcal{P}_n^m \sin \phi \cos [m(\lambda_g - \lambda_{n,m})] \quad (2.38) \end{aligned}$$

where  $\phi$  is the latitude,  $\lambda_g$  is the geographical longitude of the point at which the potential is evaluated.  $J_n$  is the coefficient associated with harmonics  $n$ , called zonal harmonics, and are associated with the North-South deviation;  $J_{n,m}$  and  $\lambda_{n,m}$  are coefficients associated with harmonics of degree  $n$  and order  $m$ , which are called tesseral harmonics if  $n \neq m$  and sectorial harmonics if  $n = m$ , and they are associated with the deviation in the East-West direction.

The function  $\mathcal{P}_n$  is the Legendre's polynomial of degree  $n$  and order 0, defined by:

$$\mathcal{P}_n(x) = \frac{1}{n!2^n} \frac{d^n}{dx^n} [(x^2 - 1)] \quad (2.39)$$

while the function  $\mathcal{P}_n^m$  is the associated Legendre's polynomial of degree  $n$  and order  $m$ , expressed as:

$$\mathcal{P}_n^m(x) = (-1)^m (1 - x^2)^{\frac{m}{2}} \frac{d^m}{dx^m} [\mathcal{P}_n(x)] \quad (2.40)$$

where  $x = \sin \phi$ .

Accuracy of the Earth gravitational model depends on the accuracy of the coefficients  $J_n$  and  $J_{n,m}$ . With EGM-2020 set to be a new release, the latest introduced gravitational model is EGM-2008 [25].

As seen in [23], the term related to Earth's oblateness, that is  $J_2 = 1.082639 \cdot 10^{-3}$ , dominates among all harmonics being at least three orders of magnitude greater than the other harmonics. Furthermore, the effect of tesseral and sectorial harmonics is not important in LEO, since their effect is compensated by the relative rotation of the Earth with respect to the spacecraft frame (the relevance of this effect is proportional to the spacecraft altitude). These elements therefore explain the choice of including Earth asphericity in the considerations, throughout the entire work, by integrating the effect of  $J_2$  zonal harmonic only.

As studied in [26], the acceleration acting on the spacecraft due to the considered zonal harmonic can be defined in the RTN frame as:

$$\vec{a}_{J_2} = \frac{3\mu J_2 R_E^2}{2r^4} \begin{bmatrix} 3 \sin^2 i \sin^2 (\omega + \theta) - 1 \\ - \sin^2 i \sin 2(\omega + \theta) \\ - \sin 2i \sin \omega + \theta \end{bmatrix} \quad (2.41)$$

As already presented above in this section, the change in orbital elements due to  $J_2$  effect through this acceleration can be divided into three categories: short period, long period and secular variation. In literature, the first two are often neglected since they are cyclical, meaning that the orbital element return to its original value after a certain period of oscillation. The secular variation instead is not negligible, since it produces long-term effects on the orbit's RAAN and argument of periapsis.

In the first attempt,  $J_2$  effect has been implemented adding the three acceleration components to Eq. 2.33, so the total acceleration acting on the spacecraft through Eq. 2.31 becomes:

$$\vec{f} = \begin{bmatrix} \vec{f}_r \\ \vec{f}_t \\ \vec{f}_n \end{bmatrix}_{thrust} + \vec{a}_{J_2} \quad (2.42)$$

However, as also seen in [27], it has been found out that this formulation is not appropriate for the optimization problem, since the algorithm that generates the

orbital trajectory might spend propellant and time to fight the periodic terms of the perturbation, instead of taking advantages of the secular variations.

So the following step has been to try to make the algorithm work by including only the secular variations due to  $J_2$  perturbation, which are expressed as [28]:

$$\left(\frac{d\Omega}{dt}\right)_{J_2} = -3\pi J_2 \left(\frac{R_E}{p}\right)^2 \frac{1}{\tau} \cos i \quad (2.43)$$

$$\left(\frac{d\omega}{dt}\right)_{J_2} = \frac{3}{2}\pi J_2 \left(\frac{R_E}{p}\right)^2 \frac{1}{\tau} (5 \cos^2 i - 1) \quad (2.44)$$

where:

$$\tau = 2\pi \sqrt{\frac{a^3}{\mu}} \quad (2.45)$$

represents the orbital period of the osculating orbit.

The first variation causes the nodal precession (or regression), the most relevant perturbation effect for LEO. For direct orbits ( $i < 90^\circ$ ) the line of the nodes regresses ( $\Delta\Omega/\Delta t < 0$ ), while for retrograde orbits ( $i > 90^\circ$ ) it precesses ( $\Delta\Omega/\Delta t > 0$ ). This effect is enhanced as inclination approaches  $0^\circ$  or  $180^\circ$ , and/or as altitude decrease.

The second variation causes the apsidal precession (or regression), not as relevant as nodal precession since studied LEO orbits are in most cases circular or near circular. In this case the line of apsides regresses ( $\Delta\omega/\Delta t < 0$ ) for  $63.4^\circ < i < 116.6^\circ$  and it precesses ( $\Delta\omega/\Delta t > 0$ ) for  $i < 63.4^\circ$  and  $i > 116.6^\circ$ . For  $i = 63.4^\circ$  and  $i = 116.6^\circ$  there is no effect on the line of apsides: in fact these two values are exploited for the particular Molniya orbits [29].

Thus, the model that includes secular variations due to  $J_2$  can be described rewriting the Eq. 2.31 with the integration of the secular variations expressed in Eq. 2.43 and Eq. 2.44:

$$\begin{aligned}
 \frac{da}{dt} &= \frac{2a^2}{h} \left( e \sin \theta f_r + \frac{p}{r} f_t \right) \\
 \frac{de}{dt} &= \frac{1}{h} \{ p \sin \theta f_r + [(p+r) \cos \theta + re] f_t \} \\
 \frac{di}{dt} &= \frac{r \cos(\theta + \omega)}{h} f_n \\
 \frac{d\Omega}{dt} &= \frac{r \sin(\theta + \omega)}{h \sin i} f_n + \left( \frac{d\Omega}{dt} \right)_{J_2} \\
 \frac{d\omega}{dt} &= \frac{1}{eh} [-p \cos \theta f_r + (p+r) \sin \theta f_t] - \frac{r \sin(\theta + \omega) \cos i}{h \sin i} f_n + \left( \frac{d\omega}{dt} \right)_{J_2} \\
 \frac{d\theta}{dt} &= \frac{h}{r^2} + \frac{1}{eh} [p \cos \theta f_r - (p+r) \sin \theta f_t]
 \end{aligned} \tag{2.46}$$

To justify this assumption and to demonstrate its validity, a GMAT orbit propagation has been carried out, considering the JGM-2 gravitational model already integrated in the software, and not including any other perturbations (such as thrust, drag and SRP) to focus the attention on the  $J_2$  effect throughout the propagation. Then, the GMAT propagation results and the results of a propagation carried out using the GVEs secular model described in Eq. 2.46 are plotted together in Fig. 2.11, using the parameters listed in Table 2.1.

Parameter	Value	Unit
$a_{initial}$	6928	km
$e_{initial}$	0.01	-
$i_{initial}$	97.5977	°
$\Omega_{initial}$	0	°
$\omega_{initial}$	0	°
$\theta_{initial}$	0	°
Propagation time	25	days
Gravitational harmonics model	JGM-2	-
Gravitational harmonics max degree	2	-
Gravitational harmonics max order	0	-

**Table 2.1:** Simulation parameters and initial orbital elements for propagation

It is interesting to highlight the fact that, as seen in Fig. 2.11, the cyclical behavior does not imply that the orbital element value of the model is the mean value of the oscillation. In fact the semi-major axis corresponds to the superior limit of the oscillation, while the inclination is the inferior limit of the oscillation.

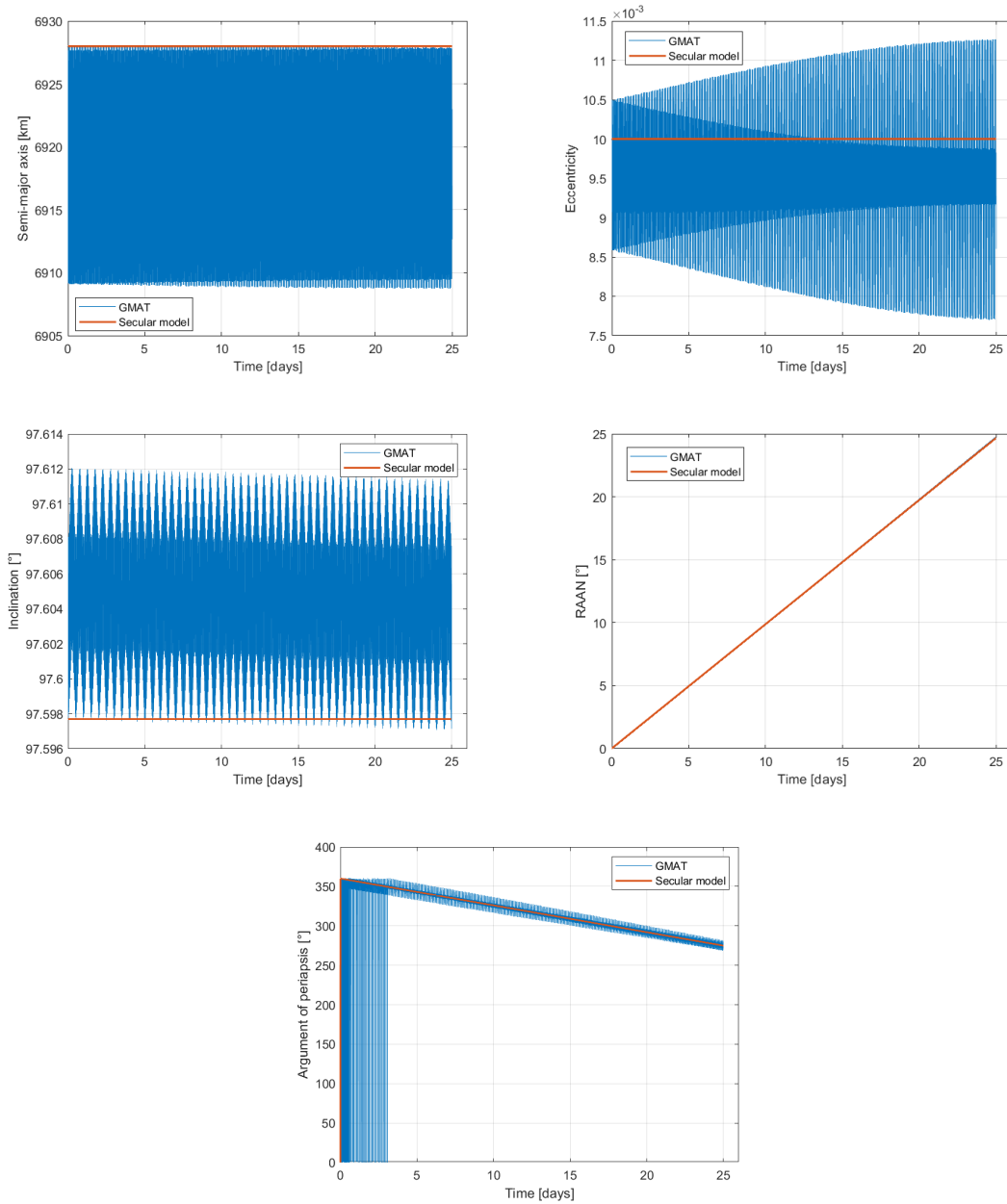
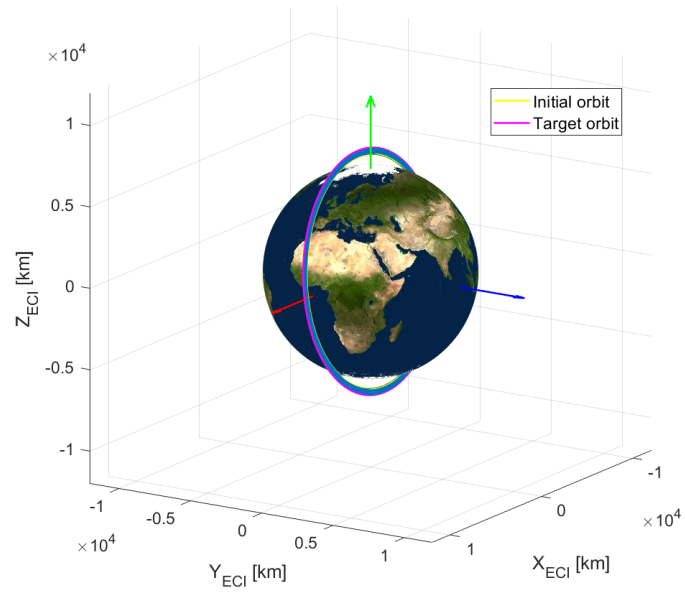
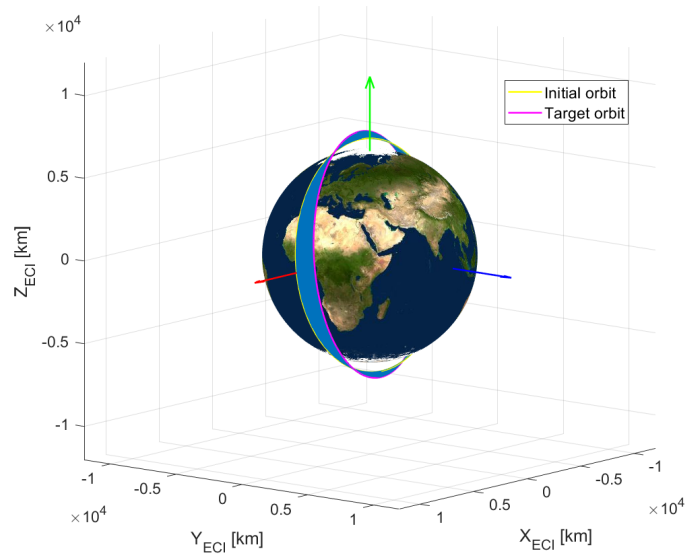


**Figure 2.11:** Orbital elements evolution: GMAT propagation vs  $J_2$  secular effect propagation

The propagation results however confirm that it is reasonable to consider only the secular variation when considering  $J_2$  perturbation, since this leads to a model that is faithful to reality.



(a) Ideal transfer



(b)  $J_2$  perturbed transfer

**Figure 2.12:** Ideal vs  $J_2$  perturbed scenario. 400 km altitude increase transfer with fixed eccentricity

## 2.4 Eclipses

To accurately model the solar electric propulsion system it is necessary to take into account trajectory arcs in which the spacecraft passes through the shadow of the Earth, where there is no available solar energy, considering the worst case in which batteries are not planned for the mission. Therefore, when the vehicle is in eclipses the propulsion is unavailable and thrust is zero. This phenomenon is not included among perturbations, since it does not cause any variation in orbital elements.

An accurate dissertation is presented in [30] and [31] where, with the assumption of spherical shapes of the Sun and the occulting body, in this case Earth, a standard definition for the shadow is proposed as:

$$\Psi = \begin{cases} 0 & \text{if } aD \leq aBR + aSR \\ 1 & \text{if } aD > aBR + aSR \end{cases} \quad (2.47)$$

where  $\Psi = 0$  means that the spacecraft is shadowed,  $\Psi = 1$  means that it is in solar light.  $aD$ ,  $aBR$  and  $aSR$  are angles defined as:

$$\begin{aligned} aSR &= \arcsin\left(\frac{R_{\odot}}{\|\vec{r}_{\odot/sc}\|}\right) \\ aBR &= \arcsin\left(\frac{R_B}{\|\vec{r}_{B/sc}\|}\right) \\ aD &= \arccos\left(\frac{\vec{r}_{B/sc} \cdot \vec{r}_{\odot/sc}}{\|\vec{r}_{B/sc}\| \|\vec{r}_{\odot/sc}\|}\right) \end{aligned} \quad (2.48)$$

with  $R_B$  and  $R_{\odot}$  that are respectively the radius of Earth and the radius of Sun;  $\vec{r}_{B/sc}$  and  $\vec{r}_{\odot/sc}$  are respectively the Earth and Sun position vectors relative to the spacecraft, as seen in Fig. 2.13, such that:

$$\vec{r}_{\odot/sc} = \vec{r}_s(t) + \vec{r}_{B/sc} \quad (2.49)$$

where  $\vec{r}_s(t)$  is the instantaneous ECI position vector of the Sun, available from ephemeris data, and  $\vec{r}_{B/sc}$  is analytically available knowing orbital elements, and further discussed in [31].

Another eclipse model is derived in [32], and it relies on the calculus of the instantaneous position of the spacecraft relative to Earth and Sun using the modified equinoctial elements described in section 2.2.4 and the current date expressed as Julian Date relative to J2000 [33]. The function  $l$  is defined as:

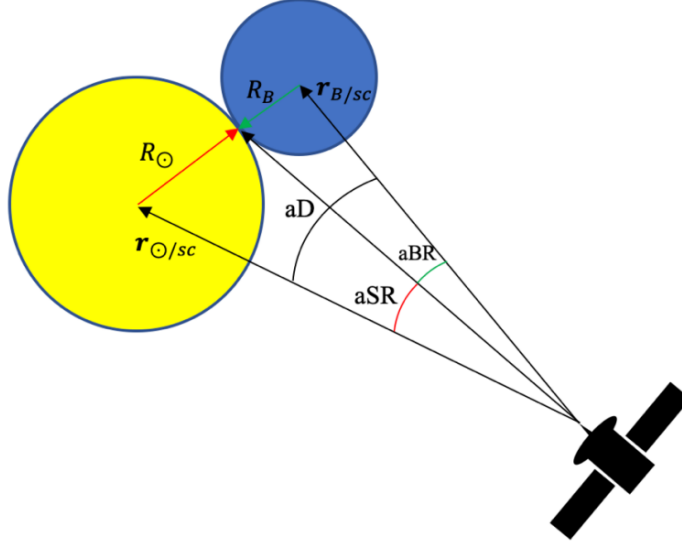


Figure 2.13: Eclipse model

$$\begin{aligned}
 l = & -p\{[(h^2 - k^2 + 1) \cos L + 2hk \sin L] \cos \theta_S + \\
 & + [(k^2 - h^2 + 1) \sin L + 2hk \cos L] \sin \theta_S \cos \varepsilon_S + \\
 & + 2(h \sin L - k \cos L) \sin \theta_S \sin \varepsilon_S\} + \\
 & - (h^2 + k^2 + 1) \sqrt{p^2 - R_E^2 (1 + f \cos L + g \sin L)^2}
 \end{aligned} \tag{2.50}$$

such as when  $l \leq 0$  the spacecraft is in eclipses.  $R_E$  is Earth radius and it is equal to 6378 km;  $\varepsilon_S$  is the ecliptic obliquity and it is equal to 23.4°;  $\theta_S$  is the instantaneous angular position of the Sun with respect to the Earth, and it is defined as:

$$\theta_S = \theta_{S0} + \omega_S t \tag{2.51}$$

where  $\omega_S$  is the constant angular rate of the Sun in its apparent motion relative to Earth, that is:

$$\omega_S = \frac{2\pi}{1 \text{ sidereal year}} = \frac{2\pi}{365.2563 \text{ days}} = 1.9909869 \cdot 10^{-7} \frac{\text{rad}}{\text{s}} \tag{2.52}$$

$t$  is the time in seconds from the reference time  $t_0$ , and  $\theta_{S0}$  denotes the value of  $\theta_S$  at the reference time. In this case J2000 has been taken as reference time, so:

$$t [\text{days}] = JD_{\text{current}} - J2000 = JD_{\text{current}} - 2451545.0 \tag{2.53}$$

$$\theta_{S0} = \theta_S(J2000) = 280.460^\circ \quad (2.54)$$

Combining this formulation with the one presented in Eq. 2.47, a new shadow function can be modeled as:

$$\Psi = \begin{cases} 0 & \text{if } l \geq 0 \\ 1 & \text{if } l < 0 \end{cases} \quad (2.55)$$

For the purpose of numerical optimization, Eq. 2.55 has been smoothed by using the following logistic function [30][31]:

$$\psi_l = \frac{1}{1 + e^{cl}} \quad (2.56)$$

where  $c$  is an arbitrary assignable gain greater than zero and  $l$  is defined in Eq. 2.50. The transformation from step function to logistic function does not involve a decrease of modeling accuracy, since eclipse transitions are truly smooth physical events. In Fig. 2.14 the gain influence on the eclipse transition can be examined. Throughout this work  $c = 298.78$  has been defined, in accordance with [30] and [31] which refer to it as a realistic value for Earth orbital transfers.

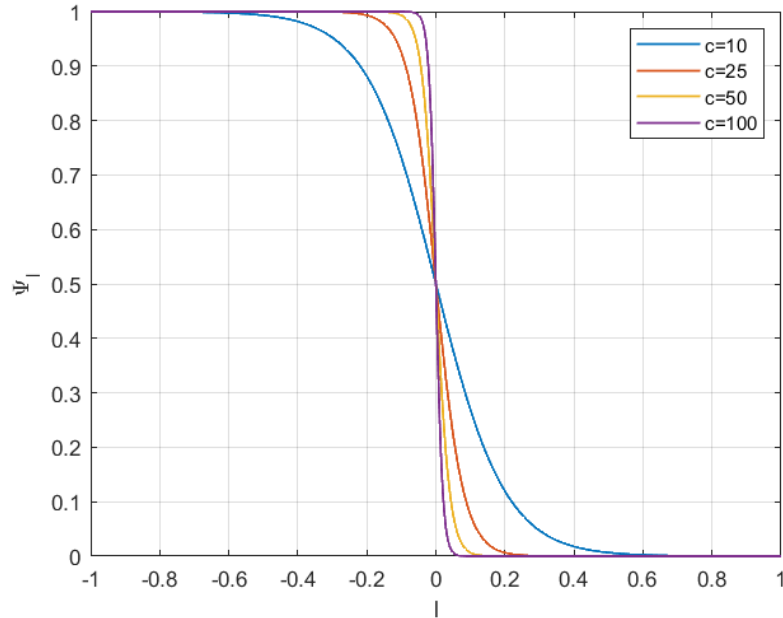


**Figure 2.14:** Eclipse logistic function

As introduced, when the spacecraft is in eclipses arcs thrusting is not available. Therefore when this phenomenon is included in the problem, it influences the thrust value such that Eq. 2.35 can be rewritten as:

$$T = T_{max}\eta\Psi_l \quad (2.57)$$

Using this formulation, thrust value is zero in eclipses arcs ( $\Psi_l = 0$ ) and it depends only on the throttle when the spacecraft is illuminated ( $\Psi_l = 1$ ). The same measure is taken for the fuel mass flow rate expression (Eq. 2.36).

## 2.5 Spacecraft model

Throughout this thesis, following the assumptions made in this chapter, the spacecraft will be modeled as a point mass, coincident with its center of mass.

The values of mass,  $T_{max}$  and  $I_{sp}$  have been defined in accordance with state of the art cubesats and small satellites' electric propulsion systems [34][35][36][37][38]. These values are reported in Table 2.2.

Parameter	Value	Unit
$m_{dry}$	12	kg
$m_{fuel}$	3	kg
Total mass $m$	15	kg
Max thrust $T_{max}$	2.5	mN
Specific impulse $I_{sp}$	1200	s

**Table 2.2:** Spacecraft parameters

$m_{dry}$  is the structural mass, and it is constant, while  $m_{fuel}$  decreases throughout the transfer. Their sum represents the spacecraft's total mass  $m$ .  $I_{sp}$  remains constant throughout the transfer.

The other parameters that represent the assumed dynamical model and that are used throughout this work, are summed up in Table 2.3.

Parameter	Value	Unit
Gravitational parameter $\mu$	398600.4419	km <sup>3</sup> /s <sup>2</sup>
Gravitational acceleration $g_0$	9.80665	m/s <sup>2</sup>
$J_2$ coefficient	$1.082639 \cdot 10^{-3}$	-
Earth radius $R_E$	6378	km

**Table 2.3:** Model parameters

# Chapter 3

## Q-law

In this chapter the proposed approach for the generation of a feasible orbital trajectory given a desired mission will be introduced. It consists of a closed-loop guidance algorithm, that is the Q-Law procedure. This approach can be modeled to achieve minimal time solutions, optimal fuel solutions or an hybrid between these two. Some example results will be shown and analyzed, and analysis will be carried out to explore the influence of Q-law parameters on the results.

### 3.1 Control Lyapunov Functions and Q-law

In control theory, Control Lyapunov Function (CLF) is a concept that associate the idea of Lyapunov functions to the non-linear system synthesis. While the ordinary Lyapunov function is used to test whether a dynamical system is stable, or asymptotically stable, the CLF is used to test whether a system is asymptotically stabilizable, that is whether for any state  $\mathbf{x}$  there is a set of controls  $\mathbf{u}(\mathbf{x}, t)$  such that the non-linear system can be brought to the zero state asymptotically applying controls  $\mathbf{u}$ .

For example, let's assume a dynamical system expressed as:

$$\dot{\mathbf{x}} = f(\mathbf{x}, \mathbf{u}) \quad (3.1)$$

where  $\mathbf{x} \in \mathbb{R}^n$  is the state vector that identify the current system state through  $n$  variables,  $\mathbf{u} \in \mathbb{R}^m$  is the control vector of  $m$  control variables, and the objective is to drive the states to an equilibrium, that in the studied case may be represented by the target orbit defined by the associated orbital elements  $\mathbf{x} = \mathbf{x}_{target}$ , from every initial state in a domain  $\mathbb{D} \subset \mathbb{R}^n$ . A CLF is a function  $V : \mathbb{D} \subset \mathbb{R}$  that is continuously differentiable, positively definite (so always positive except for the equilibrium state where it is zero), such that:

$$\forall \mathbf{x} \neq \mathbf{x}_{target}, \exists \mathbf{u} : \dot{V}(\mathbf{x}, \mathbf{u}) = \nabla V(\mathbf{x}) \cdot f(\mathbf{x}, \mathbf{u}) < 0 \quad (3.2)$$

So in other words, a CLF of a non-linear system is a positively definite function of states such that there always are, for each state  $\mathbf{x}$ , some control inputs which make its derivative, function of states and controls, negative. This means that, if a suitable CLF for the non-linear problem can be found, it is mathematically possible to reach a reduction of  $V$  in each state, meaning that the state is asymptotically brought to the equilibrium where  $V(\mathbf{x}) = 0$  [39].

The proximity quotient concept [18] relies on the calculation of a proximity quotient  $Q$ , that is an assessment of the proximity of the osculating orbit to the target orbit, and it represents the candidate CLF chosen for this work. It is essentially a systematic encapsulation of the principles of the time-to-go concept, explained in Petropoulos' studies [11], and it captures the complexity of a wide variety of orbit transfers, including those involving multiple coast arcs, with few input parameters. In this work the proximity quotient is expressed as:

$$Q = (1 + W_P P) \sum_{oe} W_{oe} S_{oe} \left[ \frac{d(oe, oe_T)}{\dot{oe}_{xx}} \right]^2 \quad \text{for } oe = a, e, i, \omega, \Omega \quad (3.3)$$

We note that the true anomaly  $\theta$  is not considered in the orbital elements, because a variation of it would just require a coasting phase without any kind of thrusting action, unlike the other elements. Furthermore, it is not in this work's interest to consider scenarios with a target on argument of periapsis, so for simplicity only four parameters will be considered from now on as targets, i.e.  $[a, e, i, \Omega]$ .

$W_P$  and  $W_{oe}$  are scalar weights greater than or equal to zero, typically unitary if there is no interest in weights optimization; the subscript  $T$  denotes the target orbit element value, and the osculating value is indicated without any subscript;  $\dot{oe}_{xx}$  indicates the maximum rate of change of the orbital element  $oe$  due to thrust, over thrust direction and over true anomaly on the osculating orbit, and its value will be discussed hereafter for every orbital parameter considered;  $P$  is a penalty function and it is used to impose a minimum-periapsis radius constraint, taking the form:

$$P = \exp \left[ k \left( 1 - \frac{r_p}{r_p^{min}} \right) \right] \quad (3.4)$$

where  $k$  is a scalar, usually set in concert with the value of  $r_p$ , that is the osculating periapsis radius.  $r_p^{min}$  indicates the lowest permissible value of  $r_p$ , chosen by the mission designer. This is very important to take into consideration when a mission includes low semi-major axis and/or high eccentricity values, since the risk of impact with Earth's surface may arise with these conditions. The size of  $k$

determines how steeply the exponential barrier rises at  $r_p = r_p^{min}$ : typical values for it are  $10^2 \div 10^3$ .

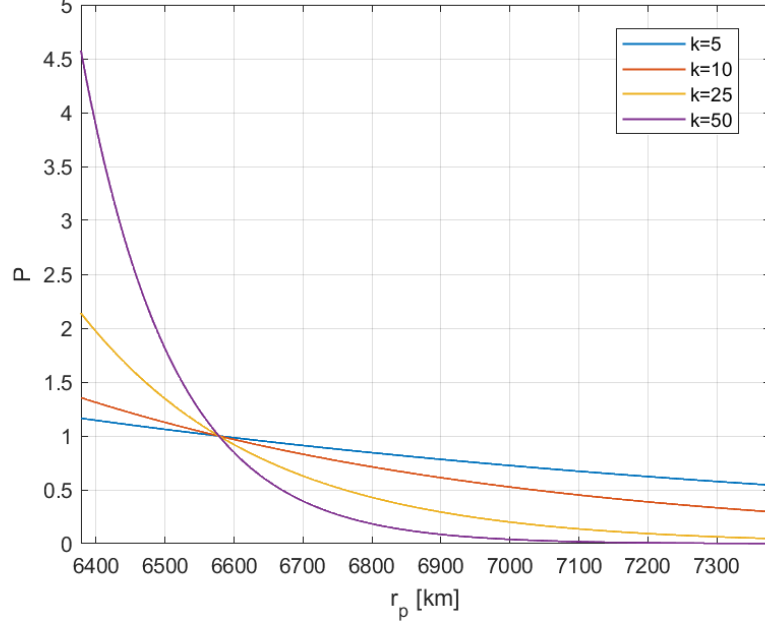


**Figure 3.1:** Influence of  $k$  parameter on penalty function  $P$ , with  $r_p^{min} = 6578$  km

As it can be seen in Fig. 3.1, the penalty function is positive, causing a potential increase of  $Q$ , when  $r_p$  goes below the minimum value: since Q-law procedure, following the definition of CLF seen in Eq. 3.2, aims to always find an action that reduces of  $Q$ , the actions that would cause the periapsis to go below its minimum value, and so to increase  $Q$ , are automatically avoided. Moreover, the further the periapsis is from its minimum value, the less the penalty function influences the value of  $Q$  and the whole procedure. A very high value of  $k$  indicates that only in the nearest proximity of the minimum periapsis value the procedure would start to be influenced by the penalty function.

$S_{oe}$  is a scaling function used principally to prevent non-convergence to the target orbit and in this work it is expressed as:

$$S_{oe} = \begin{cases} \left[1 + \left(\frac{a-a_T}{ma_T}\right)^n\right]^{\frac{1}{r}} & \text{for } oe = a \\ 1 & \text{for } oe = e, i, \Omega \end{cases} \quad (3.5)$$

where  $m, n$  and  $r$  are scalars, whose typical values are 3, 4 and 2 respectively.

$d(oe, oe_T)$  is a distance function that intuitively indicates the distance from the osculating orbital parameter to the target orbital parameter, and it is defined as:

$$d(oe, oe_T) = \begin{cases} oe - oe_T & \text{for } oe = a, e, i \\ \cos^{-1} [\cos(oe - oe_T)] & \text{for } oe = \Omega \end{cases} \quad (3.6)$$

where the distance function for  $\Omega$  is defined in a more particular form: being a difference between two angles, this function is needed to provide the shortest angular measure of the distance between these two positions on a circle. To make it clearer, if  $\Omega_T = 1^\circ$  and  $\Omega = 359^\circ$ , the distance must be the shortest, that is  $2^\circ$ , and using the distance function written in Eq. 3.6 it is possible to always have the short way round the circle, having a distance that varies in the interval  $[0, \pi]$ , in the quickest and simplest way possible. Apart from this, the function thus expressed is differentiable with respect to  $oe$  (except when it is equal to  $\pi$ ) and the sign of the derivative indicates whether  $oe$  leads or lags  $oe_T$ , and so the sign of the variation needed, based on the shortest angular distance.

Regarding  $\dot{oe}_{xx}$  values, analytical expressions are available. They identify the maximum variation achievable for each orbital parameter over thrust direction and over true anomaly of the osculating orbit. Every orbital parameter's rate of change depends indeed on the true anomaly  $\theta$  and on the thrust direction, by means of thrust acceleration components expressed through thrust angles. This can also be seen in Eq. 2.46, used to model orbital elements' changes throughout this procedure.

In this work, the following expression is used for  $\dot{oe}_{xx}$ :

$$\dot{oe}_{xx} = \max_{\alpha, \beta, \theta}(\dot{oe}) \quad \text{for } oe = a, e, i, \Omega \quad (3.7)$$

that is, for each orbital parameter:

$$\begin{aligned} \dot{a}_{xx} &= 2f \sqrt{\frac{a^3(1+e)}{\mu(1-e)}} \\ \dot{e}_{xx} &= \frac{2pf}{h} \\ \dot{i}_{xx} &= \frac{pf}{h(\sqrt{1-e^2 \sin^2 \omega} - e|\cos \omega|)} \\ \dot{\Omega}_{xx} &= \frac{pf}{h \sin i (\sqrt{1-e^2 \cos^2 \omega} - e|\sin \omega|)} \end{aligned} \quad (3.8)$$

It is interesting to note that  $Q$  captures the best possible rate of change for each of the osculating orbital elements through the ratio  $[d(oe, oe_T) / \dot{oe}_{xx}]$  that is, for each orbital element, a ratio between the distance from the target at that moment and the maximum rate of change achievable for that element in that

precise osculating orbit: in other words, it indicates the time it would take that orbital element to reach the target value if the maximum possible variation could be achieved at the considered point of the transfer. So, to make it more general, the value of  $Q$  may be considered as an approximation of the square of the time it would take to reach the target orbit from the osculating orbit if the maximum rate of change for every orbital element could be achieved. Actually such change is not concretely possible considering that elements' variations depend on thrust angles, so a pair of thrust angles that implies the maximum rate of change for one orbital element is most likely not the same pair that implies maximum variation for another element.

### 3.1.1 Minimum time solution

The proximity quotient  $Q$  is zero when the osculating orbit equals the target orbit, in accordance to the Control Lyapunov Functions definition. So, the goal of this approach is to drive  $Q$  to zero. Doing this, for the minimum time solution the goal is to do it, and so to reach the target orbit, in the quickest way. Knowing that the time variation of the proximity quotient is:

$$\dot{Q} = \sum_{oe} \frac{\partial Q}{\partial oe} \dot{oe} \quad (3.9)$$

where the expressions for  $\dot{oe}$  are available from the Gauss's variational equations, while the term  $\partial Q/\partial oe$  has to be calculated analytically for every orbital element. It is important to note that this term has to be calculated for each of the five orbital elements, even for the ones which are unconstrained i.e. do not have a target value to reach, because the term  $\dot{oe}_{xx}$  may be dependent on unconstrained elements too, causing  $Q$  to vary as a function of them.

We can also note that  $Q$  is a function of the five orbital elements and the thrust acceleration; unlike it, its derivative  $\dot{Q}$  is also a function of the thrust angles and the true anomaly, since both of these terms appear in the Gauss's variational equations. Knowing this, the minimum time solution can be reached by finding, at each instant, the thrust angles  $\alpha_n$  and  $\beta_n$  that identifies the Lyapunov-optimal thrust components, minimising the variation  $\dot{Q}$  (i.e. maximize its magnitude, since the searched value is negative):

$$\dot{Q}_n = \min_{\alpha, \beta} \dot{Q} \quad (3.10)$$

Rewriting the  $\dot{Q}$  equation as seen in [27]:

$$\dot{Q} = D_1 \cos \beta \cos \alpha + D_2 \cos \beta \sin \alpha + D_3 \sin \beta \quad (3.11)$$

where:

$$\begin{aligned}
 D_1 &= \sum_{oe} \frac{\partial Q}{\partial oe} \frac{\partial \dot{oe}}{\partial f_t} \\
 D_2 &= \sum_{oe} \frac{\partial Q}{\partial oe} \frac{\partial \dot{oe}}{\partial f_r} \\
 D_3 &= \sum_{oe} \frac{\partial Q}{\partial oe} \frac{\partial \dot{oe}}{\partial f_n}
 \end{aligned} \tag{3.12}$$

and differentiating  $\dot{Q}$  with respect to  $\alpha$  and  $\beta$ :

$$\begin{aligned}
 \frac{\partial \dot{Q}}{\partial \alpha} &= -D_1 \cos \beta \sin \alpha + D_2 \cos \beta \cos \alpha \\
 \frac{\partial \dot{Q}}{\partial \beta} &= -D_1 \sin \beta \cos \alpha - D_2 \sin \beta \sin \alpha + D_3 \cos \beta
 \end{aligned} \tag{3.13}$$

the thrust angles that make the derivative most negative can be obtained equaling the system of the two equations to zero:

$$\begin{aligned}
 \alpha^* &= \arctan_2(-D_2, -D_1) \\
 \beta^* &= \arctan \left( \frac{-D_3}{\sqrt{D_1^2 + D_2^2}} \right)
 \end{aligned} \tag{3.14}$$

Thrust components resulting from this pair of angles make sure that  $Q$  is being driven to zero as quickly as possible at any point of the transfer. This does not mean that every orbital element will be sent to its corresponding target value uniformly during the transfer: in fact, one of the strengths of this approach is that it understands when an "overshooting" is beneficial for the transfer, i.e. an osculating orbital element value that moves away from the target value instead of moving towards it. This happens because reducing  $Q$  does not only involve the reduction of the distance function, but also the increase of  $\dot{oe}_{xx}$  values. So, far-from-target changes in one orbit element may be automatically made (increasing the distance function for  $oe_1$ ) if this leads to a greater benefit for another element (increase of  $\dot{oe}_{2xx}$ ) and so a larger reduction of  $Q$ .

The procedure is stopped when  $Q$  goes below a defined tolerance value, which must be defined in accordance with the integration step as it strongly depends on it: the greater is the integration step, the greater must be the tolerance on  $Q$  to satisfy the stopping criterion, and so the less is the accuracy that can be reached on targets.

### 3.1.2 Optimal fuel solution

The Q-law approach also has an optional mechanism for coasting through an effectivity cutoff. In fact, the thrust angles  $\alpha_n$  and  $\beta_n$  described before are chosen to make the reduction of  $Q$  the quickest possible at the current true anomaly, without taking into consideration how effective the action is compared to the same action in other locations of the osculating orbit. So, two thrust effectivities at the current true anomaly are defined as:

$$\eta_a = \frac{\dot{Q}_n}{\dot{Q}_{nn}} \quad (3.15)$$

$$\eta_r = \frac{\dot{Q}_n - \dot{Q}_{nx}}{\dot{Q}_{nn} - \dot{Q}_{nx}} \quad (3.16)$$

where:

$$\dot{Q}_{nn} = \min_{\theta} \dot{Q}_n \quad (3.17)$$

$$\dot{Q}_{nx} = \max_{\theta} \dot{Q}_n \quad (3.18)$$

This concept relies on the choice of these values, in order to completely turn off thrusting actions at the points where the effectivity would be below these chosen values. The mission designer is free to choose whether to use the relative effectivity  $\eta_r$  or the absolute effectivity  $\eta_a$ , even with possibility of having a variable cut-off value depending on the proximity to the target orbit. As explained in [18], the relative approach is most suited to planar transfers involving circular orbits, since the absolute effectivity will be close to unity around the whole orbit. In general, consistently with the definition of effectivity, the greater these cutoff value, the less the fuel mass consumed during the transfer: thrust takes place only when its effectivity is above a certain value, causing a reduced waste of fuel but also a longer time of flight, since this process will lead to multiple coasting arcs.

The values of  $\dot{Q}_{nn}$  and  $\dot{Q}_{nx}$  are not analytically available. The minimum value of  $\dot{Q}$  over  $\alpha$  and  $\beta$  with a fixed true anomaly is determined as:

$$\dot{Q}_n = \dot{Q}(\alpha^*, \beta^*) = -\sqrt{D_1^2 + D_2^2 + D_3^2} \quad (3.19)$$

but  $D_1, D_2$  and  $D_3$  are also a function of true anomaly, making the minimum and maximum values of  $\dot{Q}_n$  over true anomaly not as simple to find, so a numerical approach must be employed. In this work, following the example of [20], this is done calculating for each integration step (and respective osculating orbital elements)  $\dot{Q}_n$  values over a grid of 90 equally spaced true anomaly points, along the

interval  $[0, 2\pi]$ . Then, the minimum and the maximum among these 90 values of  $\dot{Q}_n$  respectively identify  $\dot{Q}_{nn}$  and  $\dot{Q}_{nx}$  of the osculating orbit. This number of true anomaly points has been defined as a compromise between computational time and precision of the results for these two values: a more refined grid would lead to an unnecessary addition of computational expense, since the improvement of results becomes negligible. In order to avoid useless time waste and computational expense, this whole procedure is set to take place only when a non-zero cut-off value is specified.

### 3.1.3 Asphericity of the Earth

As introduced in section 2.3.3 and in [27], the implementation of  $J_2$  perturbation effects through RTN acceleration components (Eq. 2.41) causes oscillatory behaviours on orbital elements evolution that are not suitable for the Q-law procedure, that still leads to a solution, yet too affected by the periodic terms and quite far from optimal. That is the reason why the model with only secular variations on RAAN and argument of periapsis has been adopted for the implementation in the Q-law approach, through the equations Eq. 2.46.

It is important to draw attention to a strong limit that arises when this perturbation is included in the optimization problem. Considering the formulation of the Q-law approach, the only way to obtain changes in RAAN, different from the variation due to  $J_2$  perturbation, is by having an out-of-plane thrust component as provided by Eq. 2.46. However, considering the available state-of-the-art Cubesat and small satellites thrust acceleration values, it is not possible to exploit Q-law to develop an orbital transfer optimization in which a target on RAAN is imposed, as it can be done for  $a$ ,  $e$  and  $i$ . As a matter of fact, the  $J_2$  acceleration ( $\sim 10^{-5}$  km/s<sup>2</sup>) is much higher than the achievable out-of-plane thrust acceleration component  $f_n$  ( $\sim 10^{-7}$  km/s<sup>2</sup>), so actions provided by the Q-law algorithm are not able to counteract the perturbation effect.

Following other procedures it is however possible to adjust the RAAN [40][41][3], that is imposing a certain  $\Delta\Omega$  between the spacecraft orbit and the orbit that would result from a propagation without thrust. The latter would present  $\Omega = \Omega_0 + \Delta\Omega$  after a certain period of propagation time, due to  $J_2$  effect only, while the former presents  $\Omega' = \Omega_0 + \Delta\Omega'$ . However, changing  $\Omega$  at a rate different from the natural drift rate using out-of-plane thrusting arcs is very costly in terms of propellant. That is why the preferred method for adjusting  $\Omega$  takes advantage of the natural rate of nodal regression and its dependence on altitude and inclination. The procedure is carried out by maneuvering from the initial target orbit to a coasting orbit, with a different semi-major axis and/or a different inclination, where the regression rate changes relatively to the initial orbit. After an optimal coasting duration a maneuver can be performed again to bring the spacecraft from the

coasting orbit to the final orbit, that may also be characterized by the same  $a$ ,  $e$  and  $i$  as the ones of the initial orbit. A shift in  $\Omega$  will build up with time during these three phases following Eq. 2.43, making the RAAN of the spacecraft's orbit slowly drift with respect to the RAAN of the initial orbit.

The discussion and the optimization of this maneuver is not an object of this thesis' work, however it still was worth studying and introducing this method to integrate the phasing maneuver in possible future works, since it can be significant for SSO problems.

## 3.2 Example results

In order to show Q-law results in terms of orbital elements trends and orbit visualization, the transfer presented in Table 3.1 has been analyzed:

	Parameter	Value	Unit
<b>Initial orbit</b>	$a$	6928	km
	$e$	0.01	-
	$i$	97.5977	°
	$\Omega$	0	°
	$\omega$	0	°
	$\theta$	0	°
<b>Target orbit</b>	$a_T$	7078	km
	$e_T$	0.04	-
	$i_T$	98	°
	$\Omega_T$	Free	-
	$\omega_T$	Free	-
	$\theta_T$	Free	-
<b>Simulation parameters</b>	Integration time step $dt$	120	s
	Integration method	RK45	-
	Q-law tolerance	$10^4$	$s^2$
	$W_a$	1	-
	$W_e$	1	-
	$W_i$	1	-
	$r_p^{min}$	6578	km
	k	1000	-

**Table 3.1:** Q-law transfer parameters for example scenario

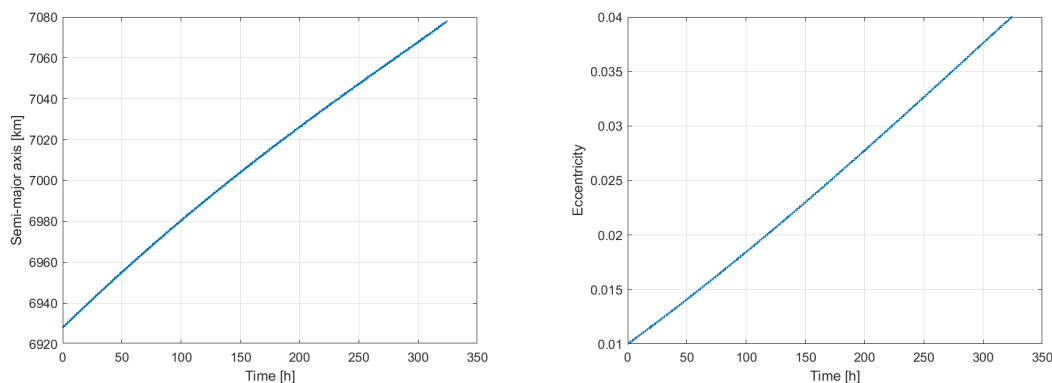
The spacecraft model and the relative parameters are presented and discussed in section 2.5, while simulation parameters has been discussed when Q-law has

been introduced in section 3.1.

The initial and target orbital elements have been chosen in accordance with the objective scenario, presented in section 1.3. As a matter of fact, the initial orbit is the same, but it has been decided to test here a transfer that, differently from the objective scenario in which the eccentricity is fixed, includes changes in semi-major axis, eccentricity and inclination in order to capture as much information as possible and at the same time to not differ so much from the objective scenario. It is important to carry out a simulation that allows to obtain as much information as possible on the results of this approach, especially because it then becomes more relevant to conduct more in-depth investigations about the changes in results as a function of certain parameters or about the comparison with other type of maneuvers, as it can be seen in the following sections. For example, using a scenario that includes a fixed eccentricity for the Q-law weights analysis would lead to an incomplete examination, as the weight associated to eccentricity  $W_E$  would not influence the procedure at all.

### 3.2.1 Minimum time

The first results are studied for the minimum time problem, for which the thrust is active in every point of the transfer ( $\eta_{cut} = 0$ ) and is equal to  $T_{max}$ .



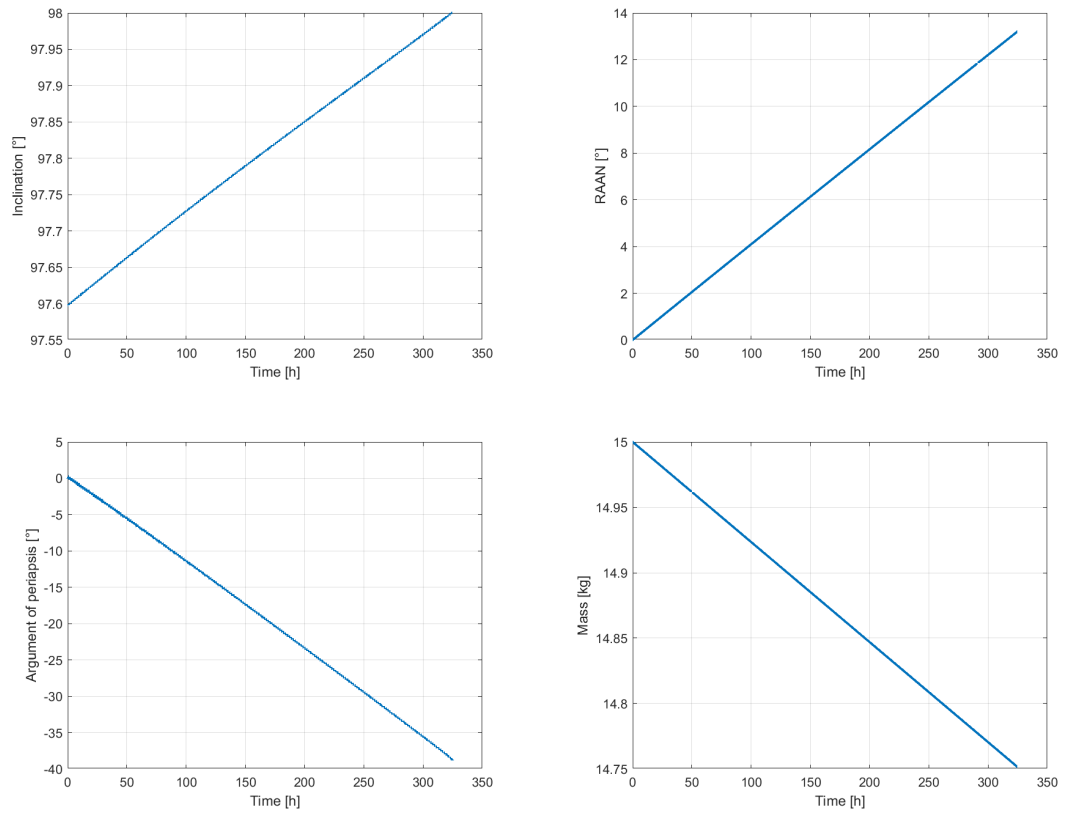


Figure 3.2: Orbital elements and mass evolution for Q-law minimum time solution

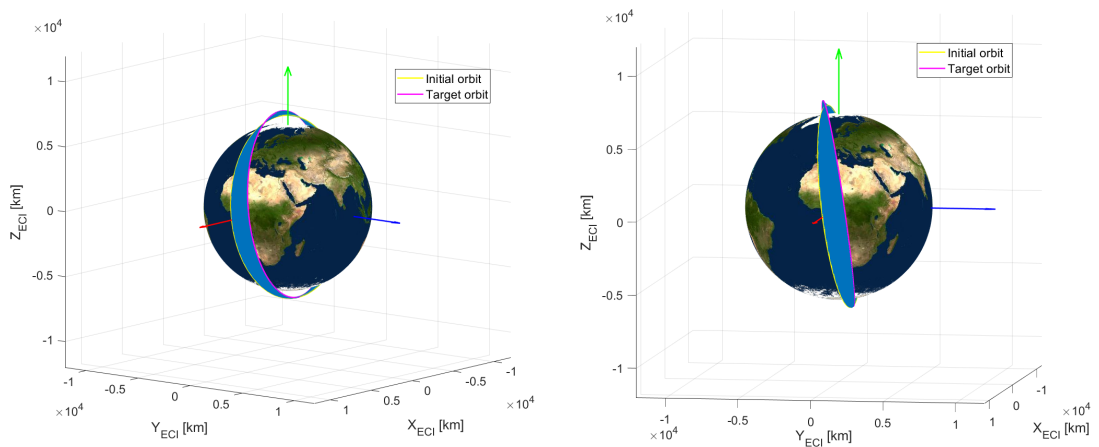
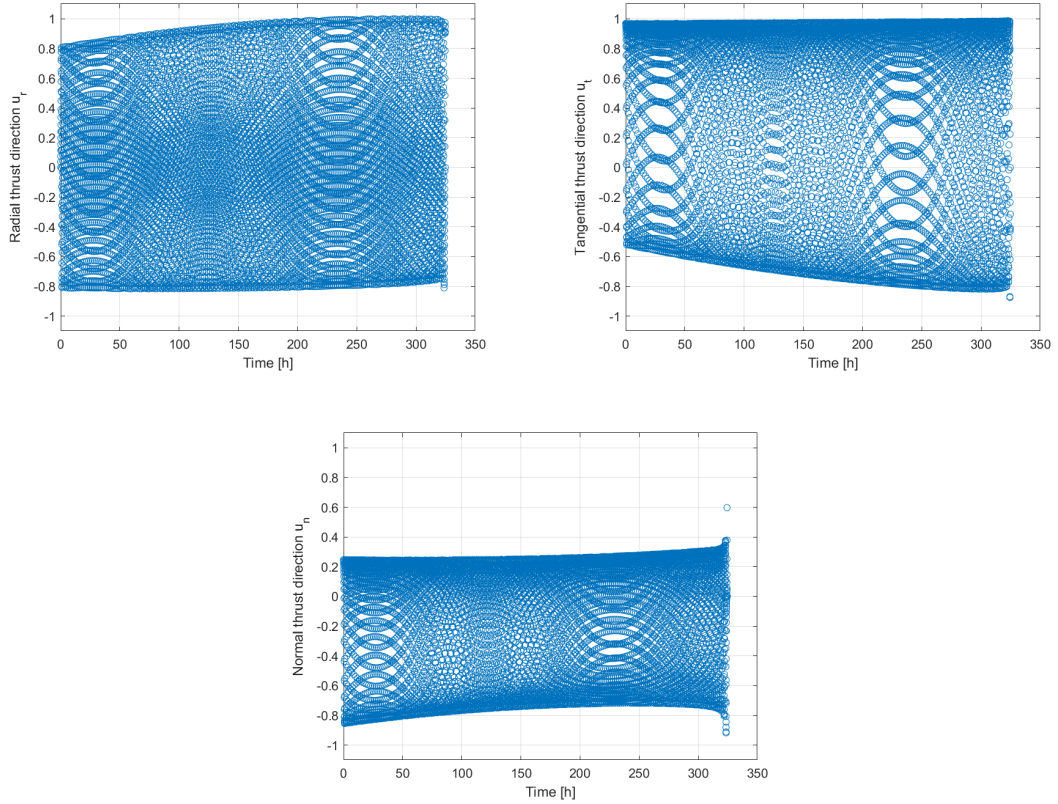


Figure 3.3: Orbit visualization for Q-law minimum time solution



**Figure 3.4:** Thrust directions for Q-law minimum time solution

The results show that the mission is completed with a total time of flight of 324.73 hours, consuming a total fuel mass of 0.2483518837 kg. With the defined stopping tolerance ( $Q = 10^4 \text{ s}^2$ ), the target orbit is reached with  $a_{error} = 0.00249 \text{ km}$ ,  $e_{error} = 3.25 \cdot 10^{-6}$ , and  $i_{error} = 4 \cdot 10^{-13} \text{ }^\circ$ .

### 3.2.2 Optimal fuel

When considering an optimal fuel optimization problem, there is not a unique absolute solution to it. As a matter of fact, using the described effectivity cutoff approach, it is possible to generate different results in terms of time and fuel consumption that do not vary linearly. Analyzing these results, a trade-off between fuel consumption and time of flight is critical. Since there is not an absolute best solution to this problem, the mission designer has to essentially choose which of the proposed solution is the best-fit for the specific interests. That is the reason why it is interesting to propose here an analysis of Q-law results as a function of the effectivity cutoff value, for both relative and absolute approaches. Other examples

of this analysis can be found in [18].

The analyzed transfer is the same as the one analyzed for the minimum time. The first analysis has been carried out following the relative cutoff approach, the second one has been done following the absolute cutoff approach. In both cases, a grid of equally spaced values of  $\eta_{cutoff}$  has been generated, with  $[0, 0.999]$  as grid extremes (included) and step size equal to 0.001. The analysis is essentially the transfer simulation repeated with every cutoff value in the grid, and leads to the results showed in Fig. 3.5 and in Table 3.2.

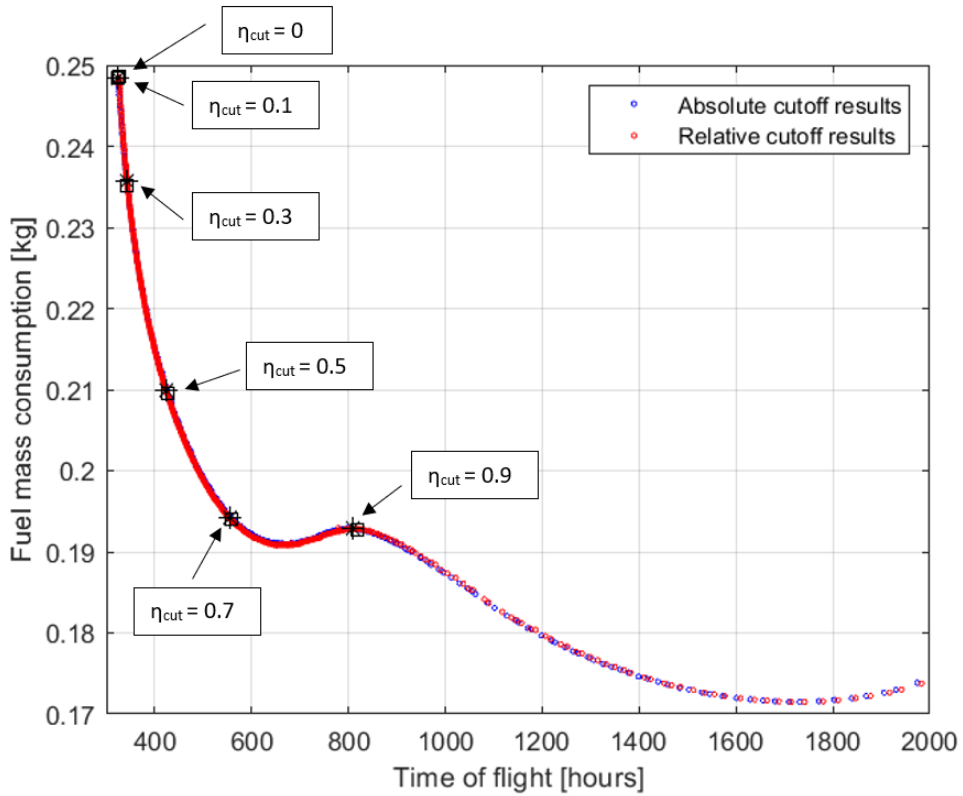


**Figure 3.5:** Time of flight and fuel mass consumption as a function of  $\eta_{acut}$  and  $\eta_{rcut}$

The maximum displayed time of flight has been set to be 2000 hours, enough to have significant results and to not make the plot illegible, especially for the plot area relative to short time of flight. The largest cutoff values that produce results within this time of flight are  $\eta_{rcut} = 0.975$  that generates a solution with a total time of flight of 1973.97 hours, and  $\eta_{acut} = 0.975$  that leads to a solution with a total time of flight of 1982.83 hours. As expected, the case with  $\eta_{rcut} = \eta_{acut} = 0$  yields the same results seen in the minimum time solution, and it is the one that

$\eta_{a\text{cut}}$	ToF [h]	$m_{\text{fuel}}$ [kg]	$\eta_{r\text{cut}}$	ToF [h]	$m_{\text{fuel}}$ [kg]
0	324.733	0.2483518837	0	324.733	0.2483518837
0.1	324.733	0.2483518837	0.1	325.267	0.2485048411
0.3	342.733	0.2357328955	0.3	343.7	0.2351720516
0.5	424.7	0.2098321037	0.5	425.6	0.209500696
0.7	555.133	0.1942049528	0.7	557.2	0.1939755166
0.9	809.9	0.1928538288	0.9	818.867	0.192802843

**Table 3.2:** Examples of time of flight and fuel mass consumption resulting as a function of  $\eta_{a\text{cut}}$  and  $\eta_{r\text{cut}}$

generates the shortest time of flight as thrust is applied continuously, however not the one associated with the absolute maximum fuel consumption, as seen for instance in the case with  $\eta_{r\text{cut}} = 0.1$  (Fig. 3.6) that leads to an increase in both time of flight and fuel consumption. This highlights the fact that a higher value of  $\eta_{\text{cutoff}}$  does not always imply a saving of fuel, despite the increase in time of flight.

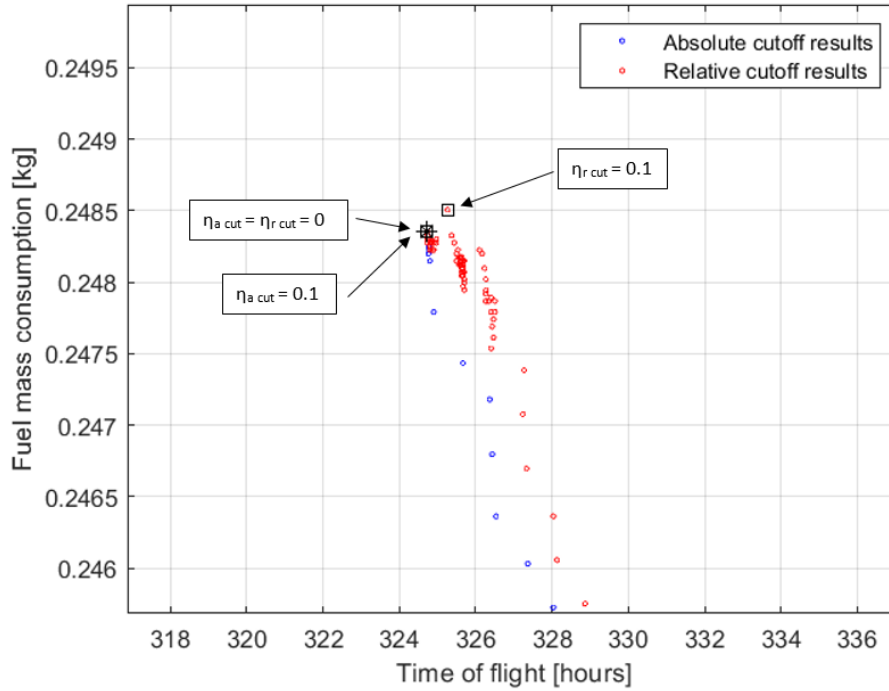


**Figure 3.6:** Zoom on results as a function of cutoff for low  $\eta_{a\text{cut}}$  and  $\eta_{r\text{cut}}$  values

Hereafter, an example of how the effectivity cutoff acts throughout the transfer can be seen, either in the orbit visualization (Fig. 3.9) or in the orbital elements

plots (Fig. 3.7 and Fig. 3.10) as well as in the thrust magnitude and directions (Fig. 3.8). For this specific case and to have enough enhanced cutoff effects,  $\eta_{a\text{cut}} = 0.6$  has been defined.

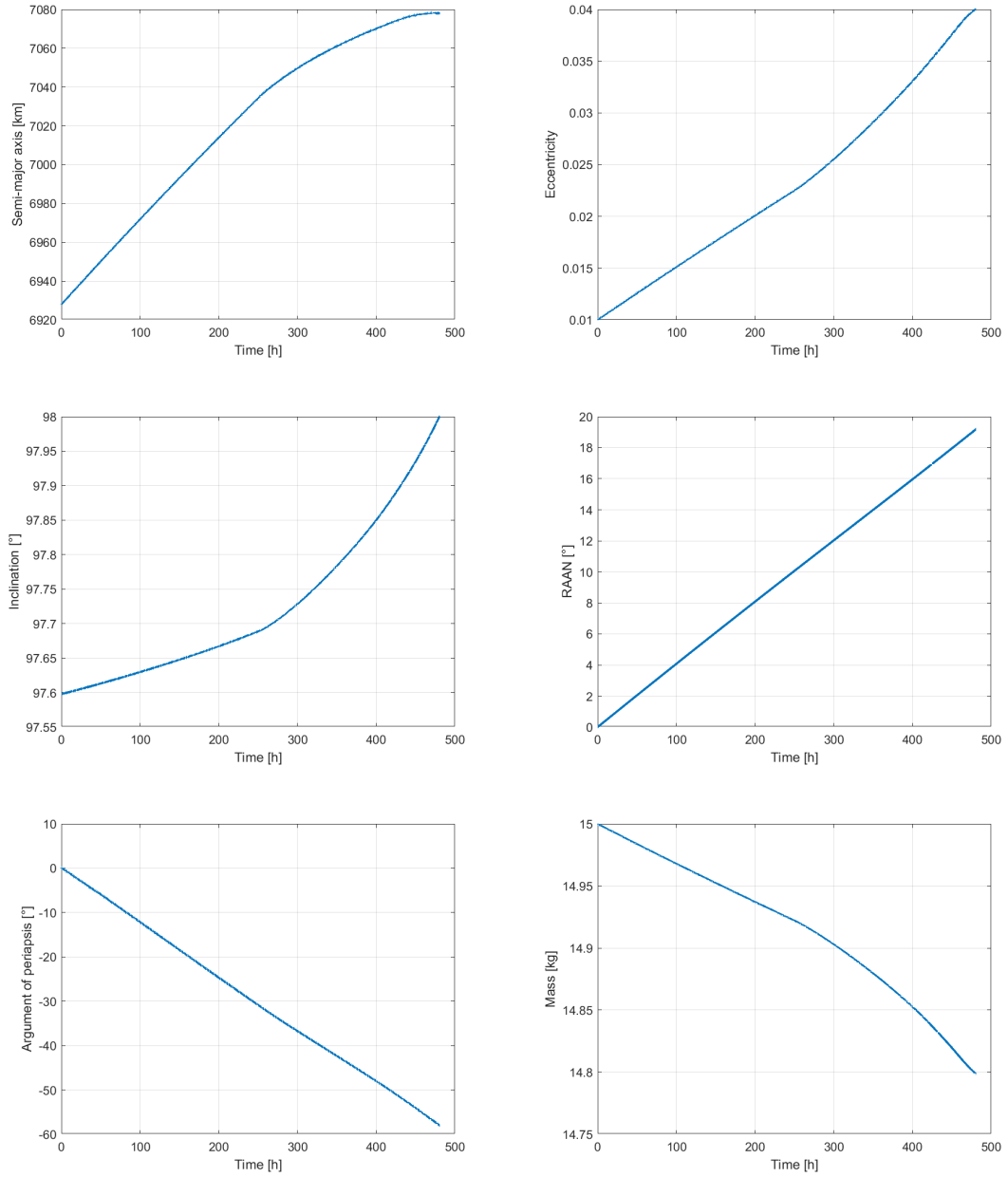


**Figure 3.7:** Orbital elements and mass evolution for Q-law optimal fuel solution with  $\eta_{a\text{cut}} = 0.6$

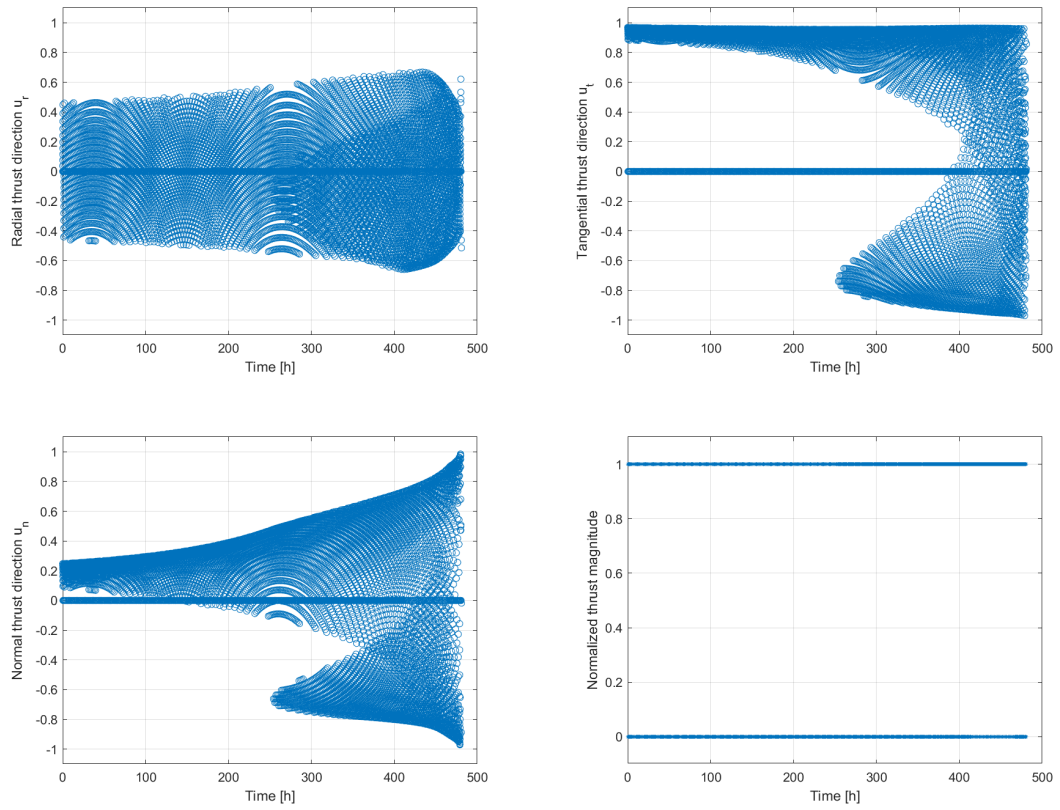


**Figure 3.8:** Thrust magnitude and directions for Q-law optimal fuel solution with  $\eta_{a_{cut}} = 0.6$

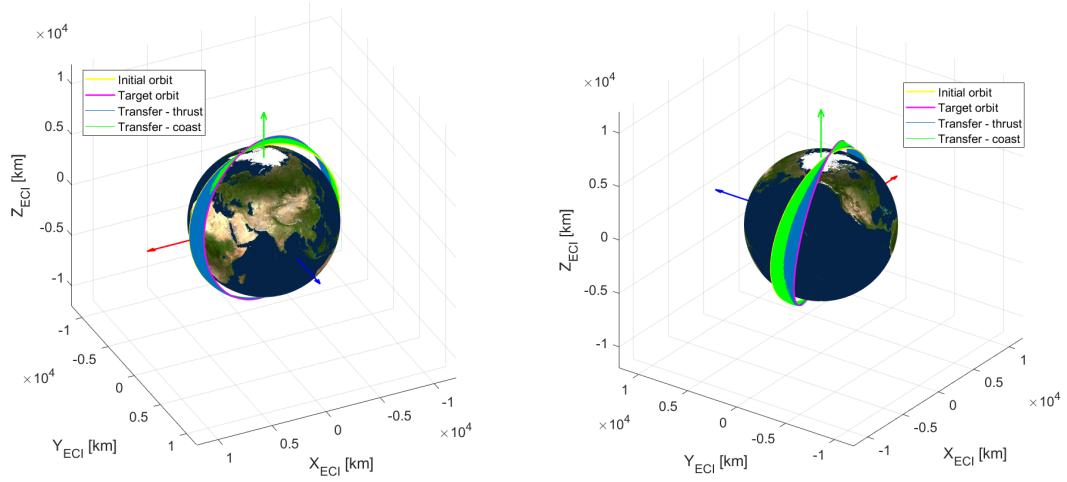


**Figure 3.9:** Orbit visualization for Q-law optimal fuel solution with  $\eta_{a_{cut}} = 0.6$

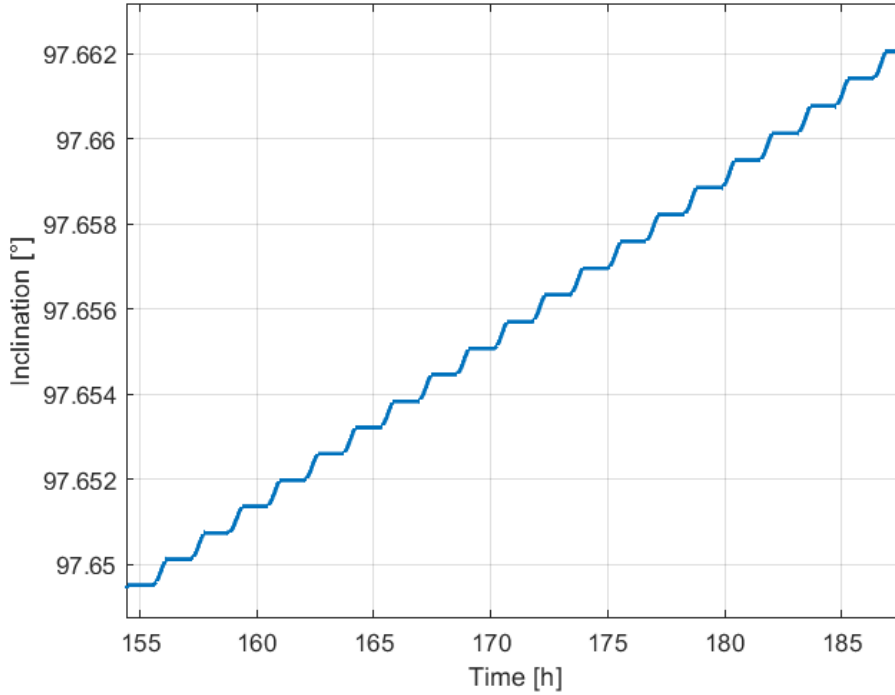


**Figure 3.10:** Details of inclination evolution due to cutoff effects with  $\eta_{a_{cut}} = 0.6$

### 3.3 Q-law vs optimal thrust angles maneuvers

The following section provides a benchmark of the implemented Q-law approach with a well-known approach that derives the instantaneous optimal optimal thrust angles  $\alpha$  and  $\beta$  to obtain a certain change in the orbital elements. Also, the advantages of the chosen CLF are discussed and presented.

The Table 3.3 shows, for each orbital element, the thrust angles providing the highest instantaneous rate of change [42]. Furthermore, the thrust angles cause a change only for the respective orbital element, while the others remain constant or are subjected to negligible changes. It is worth mentioning the definition of  $E$ , that is the osculating eccentric anomaly and it is expressed as:

$$E = \arccos\left(\frac{e + \cos\theta}{1 + e \cos\theta}\right) \quad (3.20)$$

In a more general case, more than one orbital element differ from the initial to the final orbit, so a combined change of all orbital elements involved has to take place, since it is well known that combined changes lead to a save of time and fuel

	Thrusting angles	
$\mathbf{a}$	$\alpha = \arctan\left(\frac{e \sin \theta}{1+e \cos \theta}\right)$	$\beta = 0$
$\mathbf{e}$	$\alpha = \arctan\left(\frac{\sin \theta}{\cos \theta + \cos E}\right)$	$\beta = 0$
$\mathbf{i}$	$\alpha = 0$	$\beta = \operatorname{sgn}(\cos(\omega + \theta)) \cdot \frac{\pi}{2}$
$\mathbf{\Omega}$	$\alpha = 0$	$\beta = \operatorname{sgn}(\sin(\omega + \theta)) \cdot \frac{\pi}{2}$
$\mathbf{\omega}$	$\alpha = \arctan\left(\frac{1+e \cos \theta}{2+e \cos \theta \cot \theta}\right)$	$\beta = \arctan\left(\frac{e \cot i \sin(\omega + \theta)}{\sin(\alpha - \theta)(1+e \cos \theta) - \cos \alpha \sin \theta}\right)$

**Table 3.3:** Optimal thrust angles for the maximum instantaneous change of each orbital element

consumption with respect to separate changes of the same quantity. This combined change has been implemented as seen in [42], where the thrust direction vector is expressed as:

$$\mathbf{u} = \sum_{COE} (1 - \delta_{COE, COE_1}) \frac{COE_1 - COE}{COE_1 - COE_0} \mathbf{u}_{COE} \quad (3.21)$$

where  $COE$ ,  $COE_1$  and  $COE_0$  are respectively the instantaneous osculating, the target and the initial value of the specific orbital element;  $\mathbf{u}_{COE}$  is the instantaneous thrust directions vector of the optimal thrusting for the modification of the specific orbital element;  $\delta_{COE, COE_1}$  is the Kronecker delta. The fraction works as a self-adaptive weight for each orbital element assuring the completion of all maneuvers at the same time. The procedure stops when the tolerance, defined by the mission analyst, is satisfied for each of the target orbital elements. Moreover, it is important to note that the resulting thrust directions vector is not normalized, so it has to be divided by its own norm if a vector with unit magnitude is desired.

Along with this, a script that estimates  $\Delta V$  for any transfer has been implemented based on formulation studied in [42][43] and defined in the Table 3.4, where the marked-above variables ( $\bar{a}$ ,  $\bar{e}$ ,  $\bar{i}$ ) represent the mean value of the specific orbital element.

It is essential to highlight the fact that, for combined maneuvers, the total  $\Delta V$  is  $\Delta V_{total,comb} = \sqrt{\sum_{oe} (\Delta V_{oe})^2}$  and it is always less than the total  $\Delta V$  of the corresponding separate maneuver, which is  $\Delta V_{total,sep} = \sum_{oe} \Delta V_{oe}$ . That is the reason why combined maneuvers are always more convenient than separate maneuvers. However, the goal here is to demonstrate that Q-law controls lead to results not so

	$\Delta V$
$\mathbf{a}$	$ \sqrt{\frac{\mu}{a}} - \sqrt{\frac{\mu}{a_T}} $
$\mathbf{e}$	$\frac{2}{3}\sqrt{\frac{\mu}{a}} \arcsin e - \arcsin e_T $
$\mathbf{i}$	$\frac{\pi}{2}\sqrt{\frac{\mu}{a}} i - i_T $
$\mathbf{\Omega}$	$\frac{\pi}{2}\sqrt{\frac{\mu}{a}} \Omega - \Omega_T  \sin \bar{i}$
$\mathbf{\omega}$	$\frac{2}{3}\sqrt{\frac{\mu}{a}}\frac{\bar{e}}{\sqrt{1-\bar{e}^2}} \omega - \omega_T $

**Table 3.4:** Estimates of velocity increment required to obtain a change in each orbital element

different from this quicker and simpler estimate. Better results are not expected in all cases, since this method may underestimate the necessary  $\Delta V$ .

As said before, it has been decided to implement this comparison testing the same scenario proposed in the example results above with the same parameters, integration method and integration time step. The chosen stopping tolerances are defined in accordance with the integration time step, and they are the following:

$$\begin{aligned}
 a_{tol} &= 30 \text{ m} \\
 e_{tol} &= 10^{-4} \\
 i_{tol} &= (2 \cdot 10^{-4})^\circ
 \end{aligned}
 \tag{3.22}$$

The results of the benchmark maneuver procedure are then showed in Fig. 3.11 and in Table 3.5.

It is immediate to say that Q-law performance leads to better results in terms of time of flight, and consequently fuel consumption since thrust is always active and equal to  $T_{max}$  in minimum time problems. These results are achieved with a very slight increase in computational expense in terms of CPU time, and with way better reached tolerances (in the form of target errors) by the Q-law procedure. Moreover, the combined maneuver method described in Eq. 3.21 is not suitable when an orbital element is fixed to its initial value: when a certain orbital element has coincident target and initial value, if the osculating element changes due to thrust actions that are specific to other orbital elements, the numerator ( $COE_1 - COE$ ) assumes a non-zero value but at the same time the denominator ( $COE_1 - COE_0$ ) is zero, so the division is not possible and the procedure stops. However, as

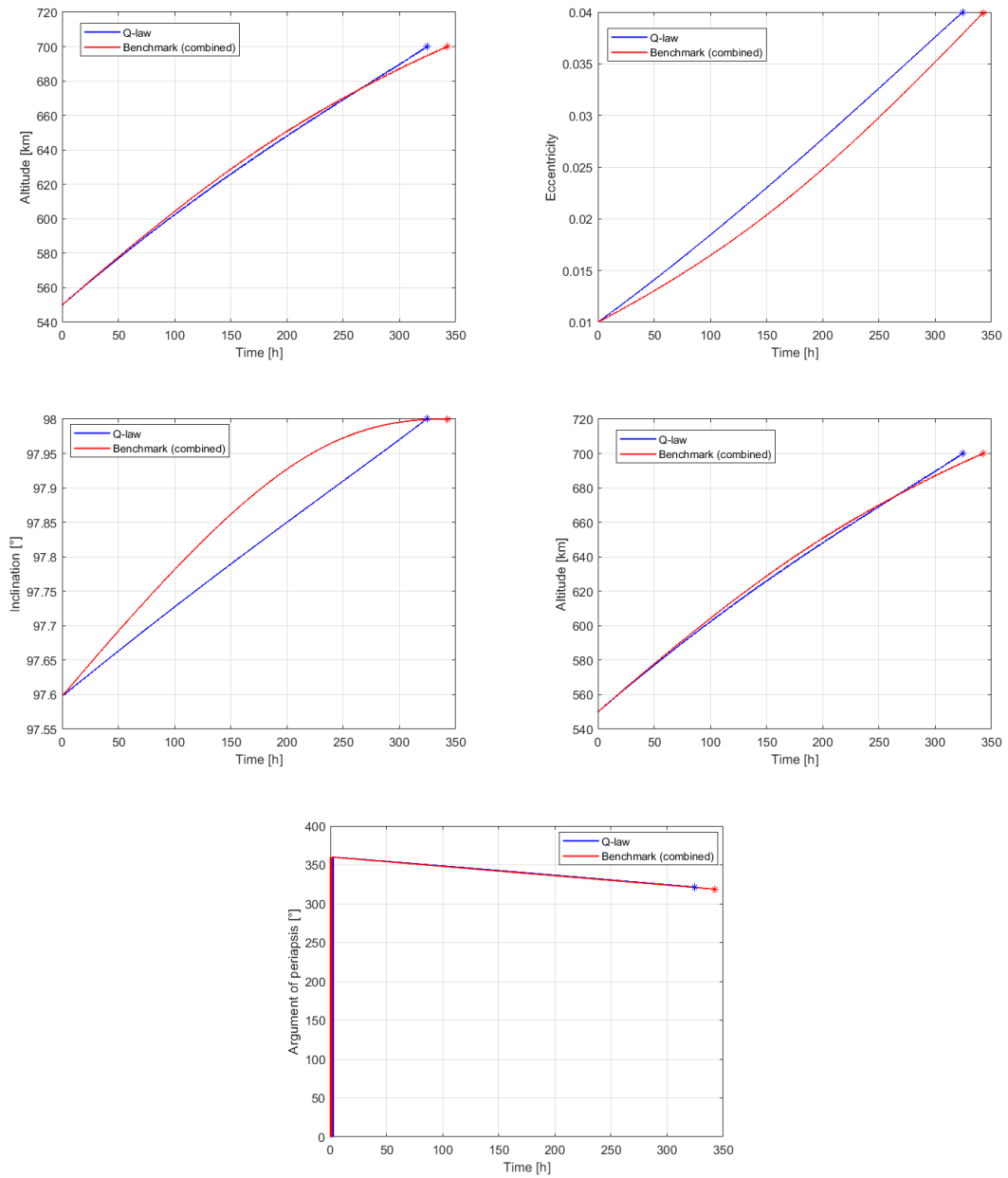


**Figure 3.11:** Comparison between Q-law and benchmark results in orbital elements evolution

highlighted before, these maneuvers make sure that changes only happen for the specific orbital element, with zero or just slight changes on other orbital elements. This means that the problem described can be settled by not defining a target value

	Benchmark estimate	Q-law
ToF [h]	342.5	324.73
$m_{fuel}$ [kg]	0.2619396022	0.2483518837
$\Delta V$ [km/s]	0.190359068	0.196470990
$a_{err}$ [m]	24.208	2.490
$e_{err}$	$7 \cdot 10^{-5}$	$3.25 \cdot 10^{-6}$
$i_{err}$ [°]	$2 \cdot 10^{-4}$	$4 \cdot 10^{-13}$
CPU time [s]	17.1175785	18.8279157

**Table 3.5:** Q-law vs benchmark: comparison of procedure results, target errors and computational time

on orbital elements for which the target value coincides with the initial value. By means of this procedure, the achieved results are still acceptable with reasonable tolerances. Other reasons why the choice of using Q-law has been made for this work are the possibility to include path constraints, such as the minimum periapsis constraint, the possibility to have an effective way to implement an optimal fuel problem through the cutoff mechanism as seen in the previous section, and the possibility to conduct an optimization on orbital elements weights ( $W_{oe}$ ), that may lead to results improvement, as briefly showed in the next section.

### 3.4 Q-law weights analysis

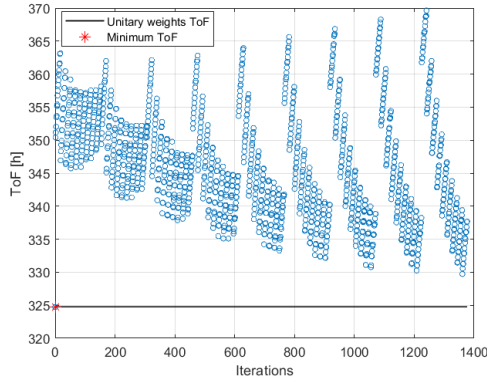
One of the advantage of exploiting Q-law is the possibility to optimize weights. An example of this work can be found in Shannon’s studies [20], where the optimization of Q-law weights causes a significant improvement in total time of flight. In fact, simulating the same transfer with an integration step of 5 minutes, first with unitary weights and then with optimized weights, respectively leads to 135.38 days and 118.56 days of time of flight, so almost a 12.5% improvement. Therefore it seemed interesting to perform a preliminary analysis of Q-law results as a function of weights also for LEO transfers, that represent the object of this work. However it is important to preface that the analysis described below is quite far from an actual optimization. As a matter of fact, the goal of this section is just to demonstrate how Q-law weights tuning affects the results both improving or worsening them. The tested transfer is the one already chosen and discussed in the example results section. The analysis has been carried out generating a grid of equally spaced values for  $W_a$ ,  $W_e$  and  $W_i$ , that are the weights related to the orbital elements that are associated with a target value. Then, after the extremes and the step associated with each grid is defined, the analysis starts and it is essentially the transfer simulation repeated for every possible combination of  $(W_a, W_e, W_i)$ .

	Unitary weights	I	II	III
$W_a$	1	[1:3]	[1:3]	[1:3]
$W_e$	1	[1:3]	[1:3]	[1:3]
$W_i$	1	[6:10]	[1:3]	[1:3]
Grid step	-	0.25	0.25	0.2
N° of iterations	-	1378	729	1331
CPU time [h]	-	6.99	3.877	6.836
N° of better comb.	-	0	20	42
Best ( $W_a, W_e, W_i$ )	-	[1,1,1]	[2.25, 2.75, 2.5]	[1.8, 2.2, 2]
Best ToF [h]	324.733	324.733	324.300	324.300

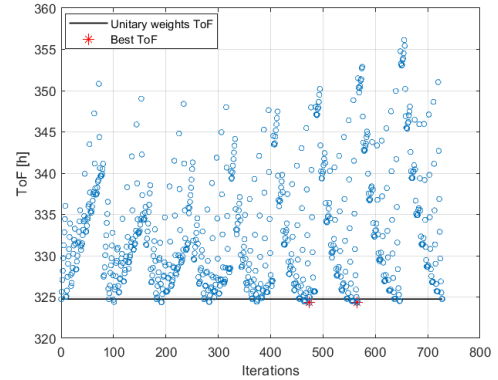
Table 3.6: Weights analysis results

Firstly, the analysis has been carried out setting the three grids extremes suggested in [20] and a grid step size equal to 0.25. No combination of weights has produced better results than the unitary weights simulation results. This, together with the very good results achieved instead in Shannon's work, suggests that the choice of grid extremes, which delimit the optimal weights research area, strongly depends on the transfer type and/or the total time of flight, so it is not possible to define standard extremes values that enclose for sure optimal weights values. In a second attempt, the analysis has been conducted with different extremes for  $W_I$  and the same step size. In this case, some combinations produce better results compared to the results given by unitary weights, yet the best result leads to a save in the total time of flight of just 0.433 hours, that equals an improvement of 0.133%. To see if better results are achieved, a third attempt has been done slightly refining the three grids, through a reduction in step size. The number of combinations that produce better results than the unitary weights increase proportionally with the number of iterations, no results were found to be better than the one already found in the second attempt, in spite of the increase in number of iterations and computational time.

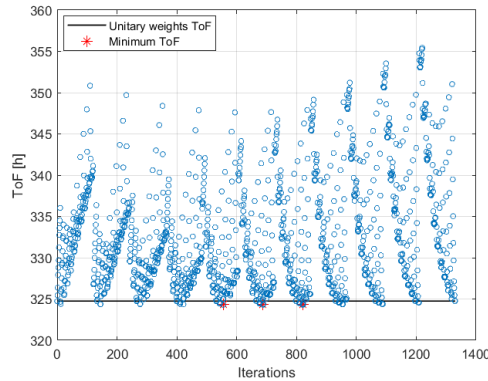
As stated before, these analysis have been disclosed just to demonstrate that weights tuning leads to different results on the same transfer with equal integration step. Obviously the analysis results would be more significant and different from each other with a reduced integration step, staying in the scope of preliminary analysis such as the one conducted, at the cost of an increase in the already huge amount of computational time. Genetic Algorithms optimizations seem the most suitable for this problem, as suggested in [20][27]. However this is a work that is not in the interest of this thesis, and considering that the results obtained with this preliminary analysis show that, in this type of transfers, unitary weights produce a



(a) First analysis, 1378 weights combinations



(b) Second analysis, 729 weights combinations



(c) Third analysis, 1331 weights combinations

**Figure 3.12:** Weights analysis results - Time of flight result for each Q-law weights combination in the three analysis

solution that does not significantly differ from the optimal one, it is reasonable to continue with the unitary weights approach throughout this entire work. In the case of longer transfers, the research of optimal weights becomes crucial to achieve an efficient problem optimization, since, based on this preliminary analysis together with Shannon's results analyzed before, the total time of flight improvement due to optimized weights is likely proportional to the total time of flight of the transfer.

### 3.5 Eclipses

As presented in section 2.4, the integration of eclipses constraints is important in the analysis of low-thrust orbital transfers due to the solar radiation power source.

In the same section, a model to implement these constraints has been proposed.

In this section a transfer will be examined to analyze the impact of the eclipses constraints on the mission. Given an initial date, fundamental to identify the correct relative position of the Sun with respect to Earth, a Q-law minimum time trajectory will be generated and eclipses effects will be discussed. Successively a mesh refinement procedure, important especially when the trajectory is used as an initial guess for optimization processes, will be proposed.

It is important, however, to note that eclipses constraints will be analyzed only for Q-law transfers in this work. The integration of this constraint in the optimization process described in Chapter 4 has led to non-convergence in each of the studied cases, using every possible optimization methods. This issue likely derives from the fact that the optimization problem is set up to be a single-phase problem in this work. As a matter of fact, when events that cause changes in the dynamics of the problem are included, such as the forced coasting arcs when the spacecraft is in eclipses, a multi-phase problem, where only non-eclipsed arcs are optimized, is suggested. Another feasible way to meet the constraints without adding significant computational time is suggested in [20], and it is the use of a gain-tuned Q-law as a means to identify eclipses while quickly producing an initial solution close to the optimal, successively performing an optimization of the Q-law trajectory just after the last eclipse to increase the solution optimality. However, this is not suitable for LEO transfers, since the orbital period is very short: the trajectory between the end of the mission and the last eclipse arc would represent a small percentage of the total mission, so its optimization would not produce relevant improvements in results, unlike what occurs in a GTO-GEO transfer [20].

Nevertheless, also following the latest suggestion, it is significant to show how the Q-law algorithm identifies eclipses arcs without adding much computational expense, in order to discuss the eclipses effects in an orbital transfer using Q-law generated trajectories and to analyze their impact on the mission.

The studied transfer in this section is purposely not associated to the objective mission, especially regarding the inclination value, in order to enhance the impact of eclipses effects. Indeed, eclipses do not influence missions equally: in some transfers they may even be absent. By defining an initial RAAN in accordance with an initial date, the orbit can always be illuminated by solar light. That is one of the main reasons why SSO are exploited: by always maintaining the same relative position to the Sun and thanks to the inclination values (near-polar orbits), some orbits are defined in order to have the fewer passages possible in eclipses arcs during the year (dawn-dusk orbits) [44]. Taking as an example the first transfer of the objective mission of this thesis, this occurs if the mission starts on January 1st, 2020 at 00:00:00 with an initial RAAN value of  $\Omega = 18.05^\circ$  [37].

The analyzed transfer is summed up in Table 3.7, and the results in terms of orbital elements evolution and orbit visualization are reported in Fig. 3.13 and

Fig. 3.15. It is interesting as well analyzing the difference between this transfer and the same one where eclipses are not included, to highlight the impact of the integration of this constraint in the problem. This can be seen either in the orbits visualization in Fig. 3.15 and Fig. 3.16, or in Table 3.8.

	Parameter	Value	Unit
<b>Initial orbit</b>	$a$	6928	km
	$e$	0.01	-
	$i$	40	°
	$\Omega$	0	°
	$\omega$	0	°
	$\theta$	0	°
	<b>Target orbit</b>	$a_T$	7078
$e_T$		0.01	-
$i_T$		40	°
$\Omega_T$		Free	-
$\omega_T$		Free	-
$\theta_T$		Free	-
<b>Simulation</b>		Integration time step $dt$	600
	Integration method	RK45	-
	Starting date	2020/01/01 00:00:00	-
	Q-law tolerance	$10^5$	$s^2$
	$W_a$	1	-
	$W_e$	1	-
	$W_i$	1	-
	$r_p^{min}$	6578	km
	$k$	1000	-

**Table 3.7:** Parameters for eclipses example transfer

	Eclipses	No eclipses
<b>ToF [h]</b>	291.167	134.833
$m_{fuel}$ [kg]	0.14174055	0.10311880

**Table 3.8:** Eclipses impact on time of flight and fuel consumption

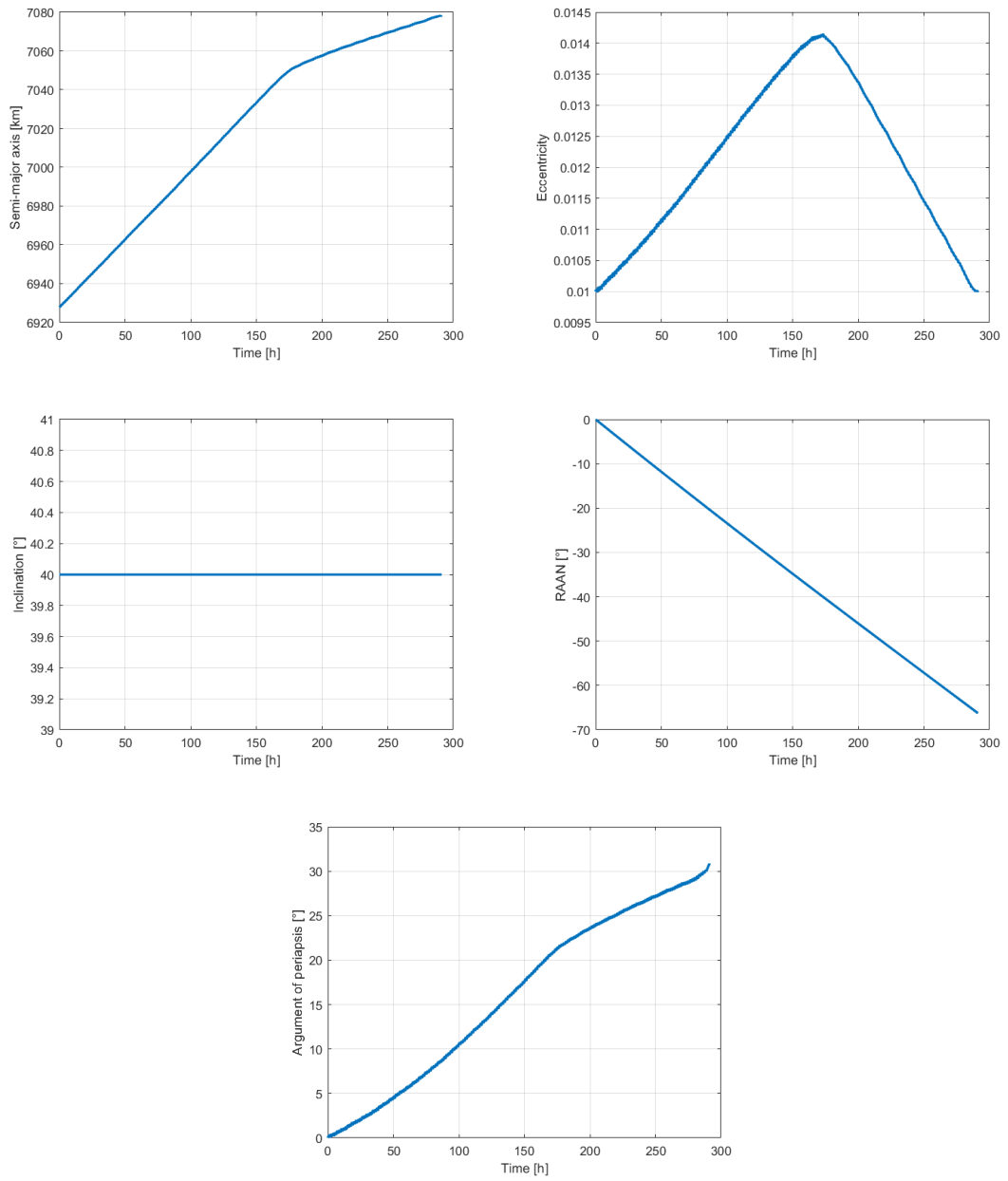


**Figure 3.13:** Orbital elements evolution for the transfer summarized in Table 3.7

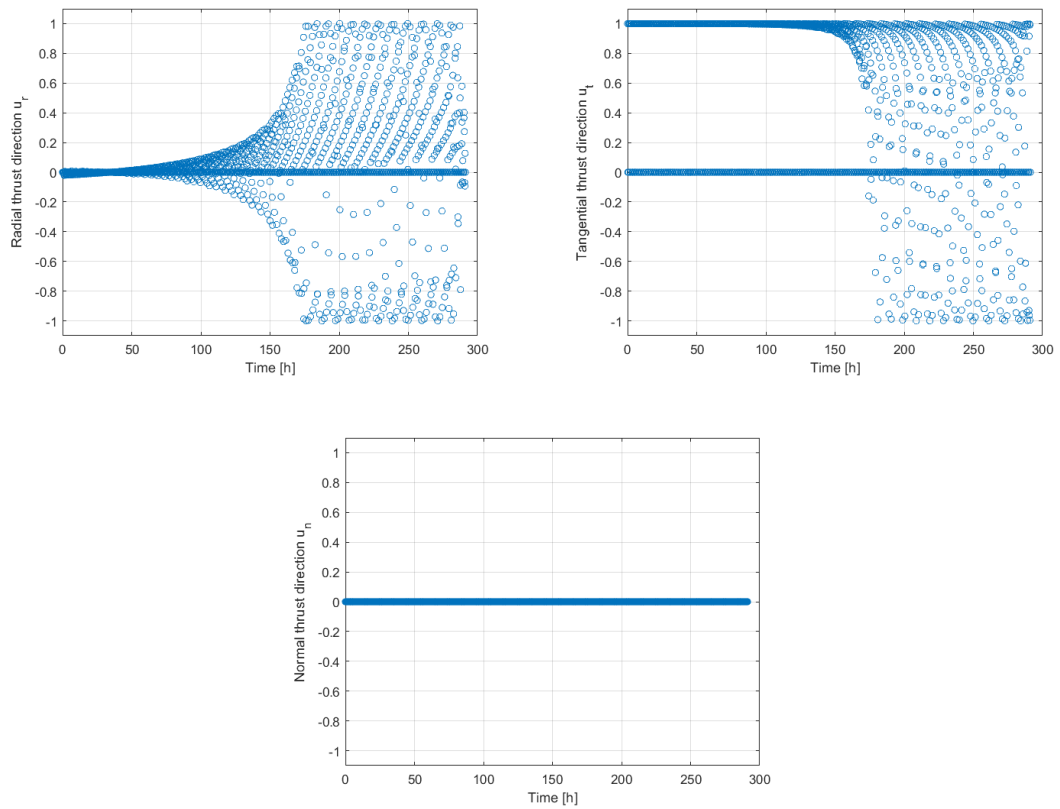
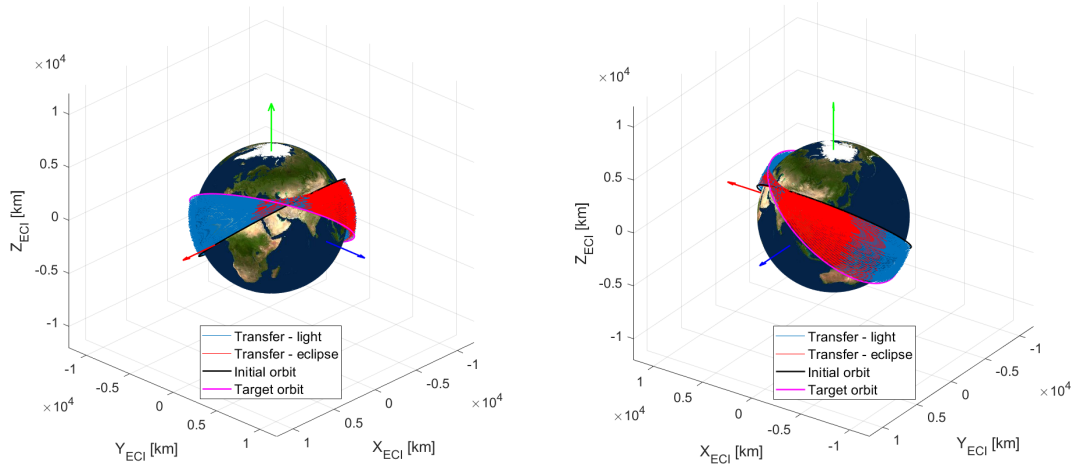
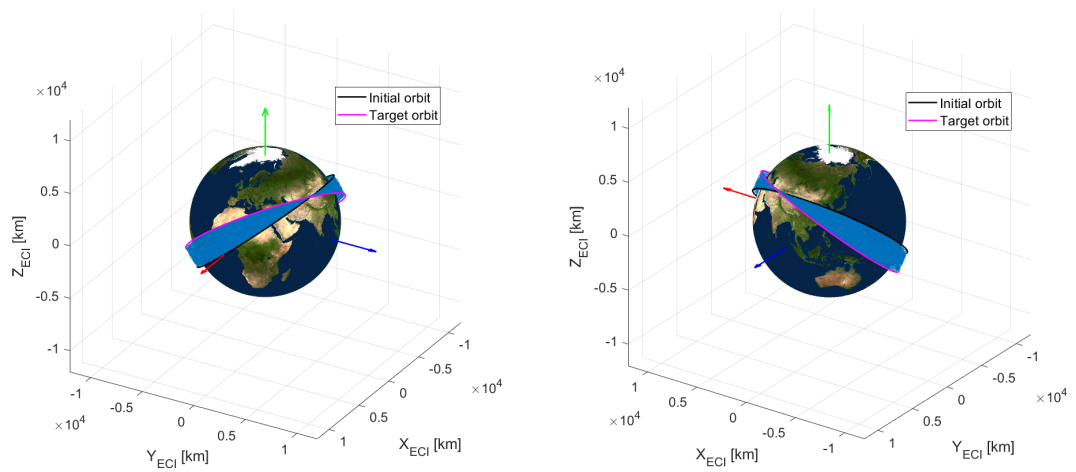


Figure 3.14: Thrust direction for the transfer summarized in Table 3.7



**Figure 3.15:** Orbital trajectory for the transfer summarized in Table 3.7 with eclipses



**Figure 3.16:** Orbital trajectory for for the transfer summarized in Table 3.7 without eclipses

### 3.5.1 Mesh refinement

The transition phases associated with entering and exiting eclipses arcs represent moments where the system dynamics are inherently stiff, so additional mesh points in the trajectory time grid are required to accurately model these transitions [20][31]. This is useful for a more accurate modeling of the orbital trajectory generated by the Q-law algorithm, leading to improved results, and for optimization processes in which these trajectories are used as initial guesses. Focusing on the latter, generally the optimization process, when eclipses are taken into consideration, is carried out optimizing the non-eclipsed arcs: if eclipse transitions are not accurately modeled, the non-eclipsed arcs may start or end in points that are not even close to the real points of transitions, leading to a solution that is not representative of the real situation.

The objective is therefore to have a finer time grid in correspondence of eclipse transitions.  $\Delta L$  is the mesh refinement interval and it is arbitrary, but since eclipse transitions for LEO spacecrafts occur in some seconds, it is worthless to consider it to be over a minute. To avoid useless mesh points that are too far from the transitions, a procedure to have a symmetrical refinement has been conducted. The mesh refinement has been carried out as follows:

- During the main Q-law algorithm with the predefined integration time step  $dt$ , the transition is detected by means of a value change of the logistic eclipse function (section 2.4).
- The state calculated after the transition is removed. The algorithm comes back to the point before the transition, and the Q-law procedure restarts with a finer time step  $dt_{search} \ll dt$ , without saving the state variables computed, until the transition point is found again.
- From the last computed state at the time  $t$ , the algorithm calculates the low extreme of the mesh refinement interval as  $t_{left} = t - \Delta L/2$ . Every state previously saved by the main Q-law algorithm at  $t > t_{left}$  is removed.
- The last point computed by the main Q-law algorithm before  $t_{left}$  is  $t_{last}$ . From this point, using a time step of  $dt' = t_{left} - t_{last}$ , the Q-law algorithm provides the states at  $t_{left}$ , point from where the real refinement occurs.
- $t_{left}$  is the starting point of the transition interval on which the refinement is desired. The Q-law procedure continues from  $t_{left}$  with a time step  $dt_{refinement} \ll dt$ , that is the actual step of the refined region, until  $t = t_{left} + \Delta L$ .
- The main Q-law algorithm with integration time step  $dt$  restarts, until a new transition is found.

To have a symmetrical refinement it is crucial to define the values of  $\Delta L$ ,  $dt_{search}$  and  $dt_{refinement}$  in accordance with each other, such that:

- The fraction  $\Delta L/dt_{refinement}$  is an integer odd number, leading to an even number of points ( $N_{points} = (\Delta L/dt_{refinement}) + 1$ ) in the refinement interval
- $dt_{search} \leq dt_{refinement}/2$ , if the procedure described above is followed, this relation governs the symmetrical distribution of the points around the transition

For  $dt_{refinement}$  it is recommended to choose a value in the order of a few seconds, to accurately identify the moment of transition. Consistently,  $\Delta L$  must be chosen in order to have not so many points around the transition, since this may lead to a useless memory overload.

The transfer chosen to present mesh refinements effects is the same as the one analyzed before, described in 3.7, and the additional parameters are chosen as follows:

$$\begin{aligned}\Delta L &= 25 \text{ s} \\ dt_{search} &= 2.5 \text{ s} \\ dt_{refinement} &= 5 \text{ s}\end{aligned}\tag{3.23}$$

A clear improvement in eclipse transitions detection can be seen in Fig. 3.17, with respect to the unrefined trajectory shown in Fig. 3.15.

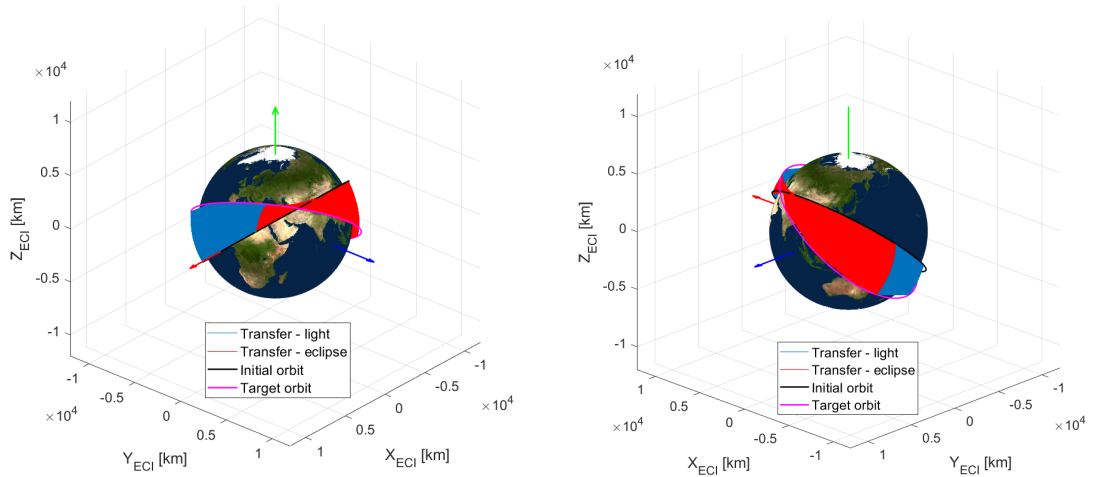


**Figure 3.17:** Orbital trajectory for the example transfer with mesh refinement

The details of the mesh refinement are further presented in Fig. 3.18 and in Fig. 3.19, where a piece of the thrust profiles of the unrefined and refined trajectory at the same moment are shown. It is clear to see how in the unrefined case, the transition is not accurately identified due to the large integration time step (600 s), while in the refined scenario, the small refinement integration time step (5 s) improves the accuracy of the transitions detection.

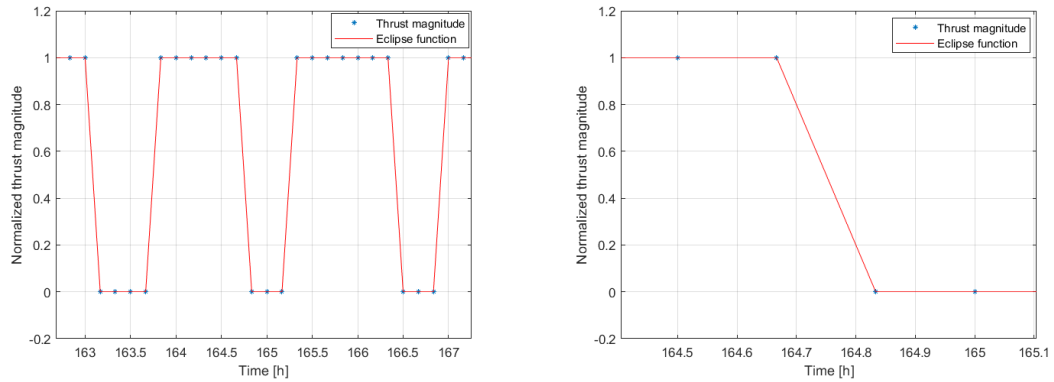


**Figure 3.18:** Thrust and eclipse function profiles without mesh refinement

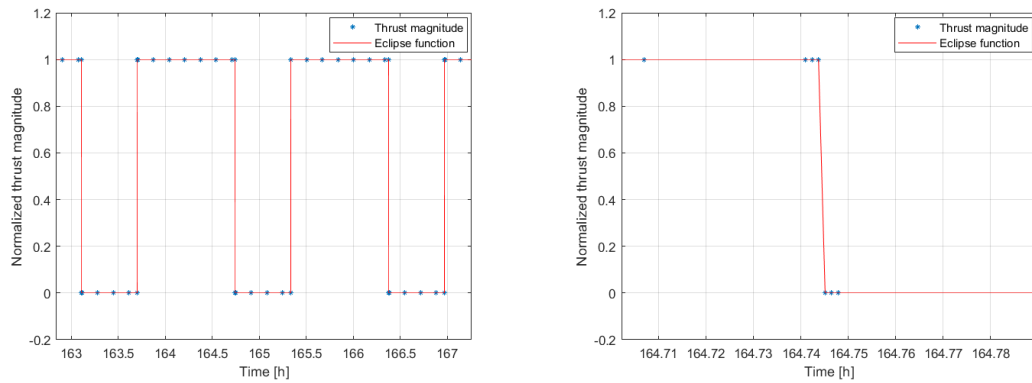


**Figure 3.19:** Thrust and eclipse function profiles with mesh refinement

Furthermore, at the cost of added computational time and memory footprint, the refinement also enhance the performances of the algorithm, as seen in Table 3.9: a coarse integration time step may cause the coasting arcs to go far beyond the real eclipses regions, so the refinement allows to exploit thrust for as long as possible, leading to a save in total time of flight.

	<b>With refinement</b>	<b>No refinement</b>
<b>ToF [h]</b>	262.326	291.167
<b><math>m_{fuel}</math> [kg]</b>	0.12757712	0.14174055
<b>Mesh nodes</b>	3398	1748
<b>CPU time [s]</b>	33.768744	5.691874

**Table 3.9:** Mesh refinement impact on Q-law algorithm performance

# Chapter 4

## Direct optimization

Low-thrust trajectory optimization belongs to the class of the optimal control problems for continuous time systems. No analytical solutions exist for this problem, even under two-body dynamics assumption. Therefore, numerical methods must be used.

One of these numerical methods consists in converting the continuous optimal control problem into a NLP problem, solving it for a set of discretized states and controls variables. This procedure is called direct transcription and the approach is known as direct method. In this chapter a discussion on these methods will be presented, focusing on the ones used for this work. Then the setup of *PSOPT* solver, employed in the optimization routines, will be discussed and some example results will be shown to highlight the effectiveness of this method.

### 4.1 Optimal trajectory design problem

In the more general form, given a set of  $n$  first-order differential equations, the classical optimal control problem (OCP) is expressed as follows [45]:

$$\dot{\mathbf{x}} = \mathbf{f}(\mathbf{x}, \mathbf{u}, t) \quad (4.1)$$

where  $\mathbf{x}(t) \in \mathbb{R}^n$  is the state variables vector of  $n$  dimension,  $\mathbf{u}(t) \in \mathbb{R}^m$  is the control variables vector of  $m$  dimension,  $t \in [t_i, t_f]$  represents the independent time variable. The objective of the optimization is to minimize the following performance index:

$$J = \varphi(\mathbf{x}(t_f), t_f) + \int_{t_i}^{t_f} L(\mathbf{x}, \mathbf{u}, t) dt \quad (4.2)$$

while satisfying  $q$ -dimensional final boundary conditions:

$$\psi(\mathbf{x}(t_f), \mathbf{u}(t_f), t_f) = 0 \quad (4.3)$$

An optimal trajectory design problem is a specialization of the classical OCP. The problem can be stated in a more convenient way for the use of direct approaches. Considering that the dynamics incorporate a set of constant parameters  $\mathbf{p}$ , the equation 4.1 can be rewritten as:

$$\dot{\mathbf{x}} = \mathbf{f}(\mathbf{x}(t), \mathbf{u}(t), \mathbf{p}, t) \quad (4.4)$$

while initial and final conditions can be defined within certain lower and upper bounds, as:

$$\begin{aligned} \boldsymbol{\psi}_{i,L} &\leq \boldsymbol{\psi}_i(\mathbf{x}(t_i), \mathbf{u}(t_i), \mathbf{p}, t_i) \leq \boldsymbol{\psi}_{i,U} \\ \boldsymbol{\psi}_{f,L} &\leq \boldsymbol{\psi}_f(\mathbf{x}(t_f), \mathbf{u}(t_f), \mathbf{p}, t_f) \leq \boldsymbol{\psi}_{f,U} \end{aligned} \quad (4.5)$$

Furthermore, the solution may include path constraints expressed as:

$$\mathbf{g}_L \leq \mathbf{g}(\mathbf{x}(t), \mathbf{u}(t), \mathbf{p}, t) \leq \mathbf{g}_U \quad (4.6)$$

and simple boundaries on the state and control variables:

$$\begin{aligned} \mathbf{x}_L &\leq \mathbf{x}(t) \leq \mathbf{x}_U \\ \mathbf{u}_L &\leq \mathbf{u}(t) \leq \mathbf{u}_U \end{aligned} \quad (4.7)$$

The trajectory optimization is based on the determination of the control variables vector  $\mathbf{u}(t)$  to minimize the performance index, rewritten here in the Mayer form [46] as:

$$J = \Phi(\mathbf{x}(t_f), t_f) \quad (4.8)$$

## 4.2 NLP

The direct optimization approaches rely on the conversion of the OCP into a NLP problem, in which dynamics are not involved. This is essentially a decisional problem concerning a scalar objective function and a constraints vector [47][48]. Suppose that the  $n$  variables of the states vector  $\mathbf{x}$  must be defined to solve:

$$\min_{\mathbf{x}} F(\mathbf{x}) \quad (4.9)$$

with  $m$  equality constraints:

$$\mathbf{c}(\mathbf{x}) = 0 \quad (4.10)$$

where  $m \leq n$ . The Lagrangian of this problem is a function of the  $n$  variables  $\mathbf{x}$  and the  $m$  Lagrange multipliers  $\boldsymbol{\lambda}$ :

$$L(\mathbf{x}, \boldsymbol{\lambda}) = F(\mathbf{x}) - \boldsymbol{\lambda}^T \mathbf{c}(\mathbf{x}) \quad (4.11)$$

A point  $(\mathbf{x}^*, \boldsymbol{\lambda}^*)$  is a constrained optimum of the problem only if the following system is solved:

$$\begin{cases} \nabla_x L(\mathbf{x}, \boldsymbol{\lambda}) = \nabla_x F - \mathbf{G}^T(\mathbf{x})\boldsymbol{\lambda} = 0 \\ \nabla_\lambda L(\mathbf{x}, \boldsymbol{\lambda}) = -\mathbf{c}(\mathbf{x}) = 0 \end{cases} \quad (4.12)$$

where  $\mathbf{G}$  is the Jacobian of the equality constraint vector  $\mathbf{c}(\mathbf{x})$ . Given an initial guess  $(\mathbf{x}, \boldsymbol{\lambda})$ , its corrections  $(\Delta\mathbf{x}, \Delta\boldsymbol{\lambda})$  to construct the new solution  $(\mathbf{x} + \Delta\mathbf{x}, \boldsymbol{\lambda} + \Delta\boldsymbol{\lambda})$  result from solving the following linear system, also called Karush-Kuhn-Tucker (KKT) system [49][50]:

$$\begin{bmatrix} \mathbf{H}_L & -\mathbf{G}^T \\ \mathbf{G} & 0 \end{bmatrix} \begin{bmatrix} \Delta\mathbf{x} \\ \Delta\boldsymbol{\lambda} \end{bmatrix} = \begin{bmatrix} -\nabla_x F \\ -\mathbf{c} \end{bmatrix} \quad (4.13)$$

where  $\mathbf{H}_L$  is the Hessian of equations 4.12 in  $x$ , that is:

$$\mathbf{H}_L = \nabla_x^2 F - \sum_{i=1}^m \lambda_i \nabla_x^2 c_i \quad (4.14)$$

The NLP problem can be generalized also for the case that occurs when inequality constraints are involved, in the form of:

$$\mathbf{c}(\mathbf{x}) \geq 0 \quad (4.15)$$

Therefore, in the most general case, the objective is to find  $n$  variables  $\mathbf{x}$  to solve equation 4.9, taking into account the  $m$  constraints defined as:

$$\mathbf{c}_L \leq \mathbf{c}(\mathbf{x}) \leq \mathbf{c}_U \quad (4.16)$$

where equality constraints  $c_j$  can be expressed imposing  $c_{j,L} = c_{j,U}$ , and state variables bounds:

$$\mathbf{x}_L \leq \mathbf{x} \leq \mathbf{x}_U \quad (4.17)$$

### 4.3 Direct transcription and collocation

Collocation methods are used to transcribe differential dynamic constraints into a set of algebraic constraints. The basic idea of these methods is to define a polynomial up to a certain degree with a number of points in the time domain

(collocation points), and to enforce these polynomials to satisfy the equations of motion and the constraints at the collocation points [51].

The differential equations can be transcribed into a finite set of equality constraints. If these constraints are respected, then the optimal trajectory design problem is solved within the degree of accuracy of the adopted numerical scheme [47][52]. The time domain can be discretized as:

$$t_i = t_1 < t_2 < \dots < t_N = t_f \quad (4.18)$$

where each time label is also called mesh point or node. The discretization is assumed to be uniform in this work, where the fixed step size is defined as:

$$h = \frac{t_N - t_1}{N - 1} \quad (4.19)$$

The states and control variables can be treated as a set of NLP variables, discretizing them over the time mesh as:

$$\begin{aligned} \mathbf{x}_k &= \mathbf{x}(t_k) \\ \mathbf{u}_k &= \mathbf{u}(t_k) \end{aligned} \quad (4.20)$$

Therefore, a whole variables vector for the problem may be defined as:

$$\mathbf{y} = \{\mathbf{x}_1, \mathbf{u}_1, \dots, \mathbf{x}_N, \mathbf{u}_N\}^T \quad (4.21)$$

In direct approaches the solution to the OCP is strictly connected to the numerical integration of the differential equations governing the motion of the spacecraft. These equations are replaced by a set of defects constraints, whose values depend on the adopted numerical integration scheme. The numerical integration influence the robustness of the method and the solution accuracy, so usually methods with high accuracy are likely to be used for practical applications. For now, just to proceed with a simple example, let's assume that a forward Euler scheme is used. In this case the defects are defined as:

$$\boldsymbol{\zeta}_k = \mathbf{x}_{k+1} - \mathbf{x}_k - h\mathbf{f}_k \quad (4.22)$$

where:

$$\mathbf{f}_k = \mathbf{f}(\mathbf{x}_k, \mathbf{u}_k, \mathbf{p}, t_k) \quad (4.23)$$

The transcription also involves the optimal control constraints described in Eq. 4.5 and Eq. 4.6, replaced by the following NLP constraints:

$$\mathbf{c}_L \leq \mathbf{c}(\mathbf{y}) \leq \mathbf{c}_U \quad (4.24)$$

with:

$$\begin{aligned} \mathbf{c}(\mathbf{y}) &= \{\zeta_1, \zeta_2, \dots, \zeta_{N-1}, \psi_i, \psi_f, \mathbf{g}_1, \mathbf{g}_2, \dots, \mathbf{g}_N\}^T \\ \mathbf{c}_L &= \{0, 0, \dots, 0, 0, 0, \mathbf{g}_{1,L}, \mathbf{g}_{2,L}, \dots, \mathbf{g}_{N,L}\}^T \\ \mathbf{c}_U &= \{0, 0, \dots, 0, 0, 0, \mathbf{g}_{1,U}, \mathbf{g}_{2,U}, \dots, \mathbf{g}_{N,U}\}^T \end{aligned} \quad (4.25)$$

This set of constraints shows that the first  $(n \cdot (N - 1))$  constraints are equality constraints on the defects  $\zeta_k$  for  $k = 1, 2, \dots, N - 1$ , which means that they satisfy the differential equations expressed in Eq. 4.4 within the accuracy of the adopted numerical integration scheme. The boundary conditions of Eq. 4.5 are imposed by the equality constraints on  $\psi_i$  and  $\psi_f$  and the inequality path constraints expressed in 4.6 are enforced at the mesh points. In a similar way, the objective function 4.8 is rewritten in terms of  $\mathbf{y}$  as:

$$F = F(\mathbf{y}) \quad (4.26)$$

and the optimal trajectory design problem can now be solved as a standard NLP problem using Eq. 4.9 - Eq. 4.14. The distinctive trait of each collocation method relies in the way the state and control variables are discretized and how the constraints are satisfied [53]. Some examples of collocation methods, accurately explained in [45][54], are trapezoidal, Hermite-Simpson, high order Gauss-Lobatto, pseudospectral and control parametrization methods.

### 4.3.1 Local discretization methods

When the problem requires a large number of nodes the NLP algorithm may have problems to converge if global collocation methods, such as pseudospectral methods [45], are used. This may be due to numerical difficulties within the NLP solver as the Jacobian and Hessian matrices may be too dense [54]. When faced with this problem, feasible solutions are either to split the problem into multiple segments to increase the sparsity of the derivatives, or to use local collocation methods.

Since the transfers studied in this work generally last many days, a step size defined in accordance with the maximum number of nodes (around 200 [54]) for an appropriate effectiveness of global optimization methods would be too large to achieve good results, especially for LEO missions. Therefore, global optimization methods are not suitable to perform a transfer optimization in this work. Because of that, local optimization methods are further analyzed and successively exploited to achieve a trajectory optimization in the studied transfers.

Direct collocation methods that use local information to approximate the functions associated with an optimal control problem are well established [46]. The main impact of a local discretization method as opposed to a global method is that, as the number of mesh points increases, the resulting Jacobian and Hessian matrices needed by the NLP solver are more sparse, which makes the NLP solution simpler. On the other hand, the disadvantage is that spectral accuracy in the discretization of the differential constraints by global methods is lost. Local mesh refinement methods are also possible: these methods concentrate more mesh points in areas of greater complexity in the function, which helps to improve the local accuracy of the solution.

The most used local discretization methods are trapezoidal method and Hermite-Simpson method. The former has an accuracy of  $O(h^2)$ , while the latter has an accuracy of  $O(h^4)$ , where  $h$  is the local interval between mesh points [54]. Both of these methods are widely used and have solved many challenging optimal control problems [46], and they differ on the way the defect constraints are computed.

In the trapezoidal method the defect constraints are defined as follows [46]:

$$\zeta_k = \mathbf{x}_{k+1} - \mathbf{x}_k - \frac{h_k}{2}(\mathbf{f}_k + \mathbf{f}_{k+1}) \quad (4.27)$$

where  $\zeta_k \in \mathbb{R}^n$  is the vector of differential defect constraints at the mesh node  $k$ ,  $h_k = t_{k+1} - t_k$  is the local step size, with  $k = 0, \dots, N - 1$ , and the other variables are introduced in section 4.3.

In the Hermite-Simpson method the defect constraints are computed as follows [46][54]:

$$\zeta_k = \mathbf{x}_{k+1} - \mathbf{x}_k - \frac{h_k}{6}(\mathbf{f}_k + 4\bar{\mathbf{f}}_{k+1} + \mathbf{f}_{k+1}) \quad (4.28)$$

where:

$$\begin{aligned} \bar{\mathbf{f}}_{k+1} &= \mathbf{f}[\bar{\mathbf{x}}_{k+1}, \bar{\mathbf{u}}_{k+1}, \mathbf{p}, t_k + \frac{h_k}{2}] \\ \bar{\mathbf{x}}_{k+1} &= \frac{1}{2}(\mathbf{x}_{k+1} + \mathbf{x}_k) + \frac{h_k}{8}(\mathbf{f}_k - \mathbf{f}_{k+1}) \end{aligned} \quad (4.29)$$

where  $\bar{\mathbf{u}}_{k+1} = \bar{\mathbf{u}}(t_{k+1})$  is a vector of midpoint controls, which are also decision variables. In this case a collocation point, over which state and control variables are calculated, appears also in the middle of the two adjacent mesh nodes  $(t_k, t_{k+1})$  [45].

In both cases, the number of differential defect constraints is  $n \cdot N$ , where  $n$  is the number of the  $\mathbf{x}$  state variables, and  $N$  the number of mesh points.

## 4.4 *PSOPT* setup

In order to implement a local optimization method in this work, the optimal control solver *PSOPT* has been used [54].

*PSOPT* is an open source optimal control package written in C++ that uses direct collocation methods. Through these methods, optimal control problems are solved by approximating the time-dependent variables using global (Legendre and Chebyshev pseudospectral methods) or local (trapezoidal and Hermite-Simpson methods) polynomials [54]. This allows to discretize the differential equations and continuous constraints over a grid of nodes, and to compute any integrals associated with the problem using quadrature formulas. A NLP solver is then used to find local optimal solutions. The used NLP solver is IPOPT, an open source C++ package for large-scale nonlinear optimization, which uses an interior point method [55]. *PSOPT* is able to deal with either single or multiphase problems, as well as problems with many other characteristics described in [54].

### 4.4.1 Problem formulation

The trajectory optimization problem to be implemented in *PSOPT* is formulated as a single phase problem, and it is defined as follows.

The objective of the optimization is to minimize a performance index  $J$  solving:

$$\min_{\mathbf{u}(t), \eta(t), t_f} J = \alpha t_f - (1 - \alpha)m_f \quad (4.30)$$

subject to:

$$\begin{aligned} \mathbf{x}(0) &= \mathbf{x}_i, m(0) = m_i, t(0) = t_i \\ \dot{\mathbf{x}}(t) &= \{\dot{a}(t), \dot{e}(t), \dot{i}(t), \dot{\Omega}(t), \dot{\omega}(t), \dot{\theta}(t), \dot{m}(t)\}^T \\ \mathbf{x}(t_f) &= \mathbf{x}_{target} \\ t_f^{min} &\leq t_f \leq t_f^{max} \\ \|\mathbf{u}(t)\| &= 1 \\ -1 &\leq u_r(t) \leq 1 \\ -1 &\leq u_t(t) \leq 1 \\ -1 &\leq u_n(t) \leq 1 \\ 0 &\leq \eta(t) \leq 1 \\ 0 &\leq \alpha \leq 1 \end{aligned} \quad (4.31)$$

where  $\mathbf{x}(t)$  is the state variables vector and  $\mathbf{u}(t)$  is the control variables vector in the RTN frame, respectively expressed as:

$$\begin{aligned}\mathbf{x}(t) &= \{a(t), e(t), i(t), \Omega(t), \omega(t), \theta(t), m(t)\}^T \\ \mathbf{u}(t) &= \{u_r(t), u_t(t), u_n(t)\}^T\end{aligned}\tag{4.32}$$

It is important to note that the mass is included in the state variables vector together with the classical orbital elements. The variables that appear in the problem formulation (4.31) are explained as follows:

- $\dot{\mathbf{x}}(t)$  represents the differential constraints of the problem, expressed through the rates of change of classical orbital elements and the fuel mass consumption. For the same reasons discussed in section 2.3.3 and in section 3.1.3, the model that is used to integrate the  $J_2$  zonal harmonic perturbation effects is the secular variations model. Therefore, the first six elements of the vector  $\dot{\mathbf{x}}(t)$  are the rates of change of classical orbital elements defined in Eq. 2.46. The mass consumption  $\dot{m}(t)$  is modeled as described in Eq. 2.36.
- $m_f = m(t_f)$  is the final mass value, from which fuel consumption can be derived.
- $t_i$  and  $t_f$  are respectively the initial and final time. The final time found by the optimization process is defined in an interval between a minimum and a maximum boundary values, respectively  $t_f^{min}$  and  $t_f^{max}$ .
- $\eta(t)$  is the thrust throttle that governs the thrust magnitude as well as the mass consumption: it is fixed to 1 in minimum time problems, while it is a control variable together with the thrust directions in optimal fuel problems.
- $\alpha$  is the parameter that defines the nature of the problem: with  $\alpha = 1$  the objective function becomes  $J = t_f$ , leading to a minimum time solution, whereas with  $\alpha = 0$  the objective function is  $J = -m_f$  and an optimal fuel solution is computed. Intermediate values in  $[0,1]$  could be used for a trade-off solution between time of flight and fuel mass consumption.

For the reasons presented in section 4.3.1 the optimization procedure is carried out by using local discretization methods, that are, in *PSOPT*, trapezoidal and Hermite-Simpson methods. Since, after different studied cases, no significant improvements were found by using the more accurate Hermite-Simpson method compared to results given by the less accurate but quicker trapezoidal method, the latter is employed to optimize the studied transfers shown in this thesis.

## 4.5 Example results

In order to show and analyze *PSOPT* example results in terms of orbital elements trends, a transfer of the same type as the first one of the objective scenario has been chosen, i.e. change of altitude and inclination with fixed eccentricity. It is however a shorter transfer, in order to reduce the computational expense and time while, at the same time, grasp sufficient information about the optimization of this type of transfer, essential to proceed with the more expensive analysis of the objective mission transfers. The transfer is described in Table 4.1, with initial orbit values discussed in section 1.3. The initial guess trajectory needed by the solver to start the optimization is generated by the Q-law algorithm, whose parameters vary depending on the desired optimization: for minimum time solution, a minimum time Q-law trajectory is given; for optimal fuel solution different Q-law trajectories are given in input to obtain and analyze a trade-off as seen in 4.5.2.

	Parameter	Value	Unit
<b>Initial orbit</b>	$a$	6928	km
	$e$	0.01	-
	$i$	97.5977	°
	$\Omega$	0	°
	$\omega$	0	°
	$\theta$	0	°
<b>Target orbit</b>	$a_T$	7078	km
	$e_T$	0.01	-
	$i_T$	97.9	°
	$\Omega_T$	Free	-
	$\omega_T$	Free	-
	$\theta_T$	Free	-

**Table 4.1:** Transfer for solver example results

The spacecraft model and the relative parameters are presented and discussed in section 2.5. The solver parameters are defined in accordance with the information found in *PSOPT* manual [54].

### 4.5.1 Minimum time

The first results are studied for the minimum time optimization problem. Thrust is always active, so the optimization parameters are the three thrust spacial directions in RTN frame  $\{u_r, u_t, u_n\}$ . The initial guess given in input is a Q-law minimum time trajectory, whose settings are summed up together with the chosen *PSOPT*

algorithm options in Table 4.2. The solver options that are not specified in the table are set to their default values. In the presented state variables evolution, the Q-law and solver results are plotted together to better catch the improvement given by the optimization method.

	Parameter	Value	Unit
<b>Initial guess parameters</b>	Integration time step	600	s
	Integration method	RK45	-
	Q-law tolerance	$10^5$	$s^2$
	$\eta_{cut}$	0	-
	$W_a$	1	-
	$W_e$	1	-
	$W_i$	1	-
	$r_p^{min}$	6578	km
	k	1000	-
<b>PSOPT parameters</b>	Nodes	1500	-
	Control variables	3	-
	$\alpha$	1	-
	NLP max iterations	1500	-
	NLP tolerance	$10^{-4}$	-
	Collocation method	Trapezoidal	-
	ODE tolerance	$10^{-5}$	-
	Mesh refinement	Automatic	-
	Defects scaling	Jacobian-based	-

**Table 4.2:** Algorithm options for solver minimum time example results

After an optimization carried out by using the trapezoidal collocation method, the mission is completed with a clear improvement in results for both total time of flight and fuel mass consumption, as also seen in Fig. 4.1. The improvements are proportional since a minimum time solution is considered, where thrust is active at each moment. The results and the comparison between solver and initial guess are summed up in Table 4.3.

	PSOPT	Q-law	Improvement
<b>ToF [h]</b>	175.276	182.333	3.87 %
<b><math>m_{fuel}</math> [kg]</b>	0.134049	0.139446	3.87 %

**Table 4.3:** Comparison between Q-law and *PSOPT* results

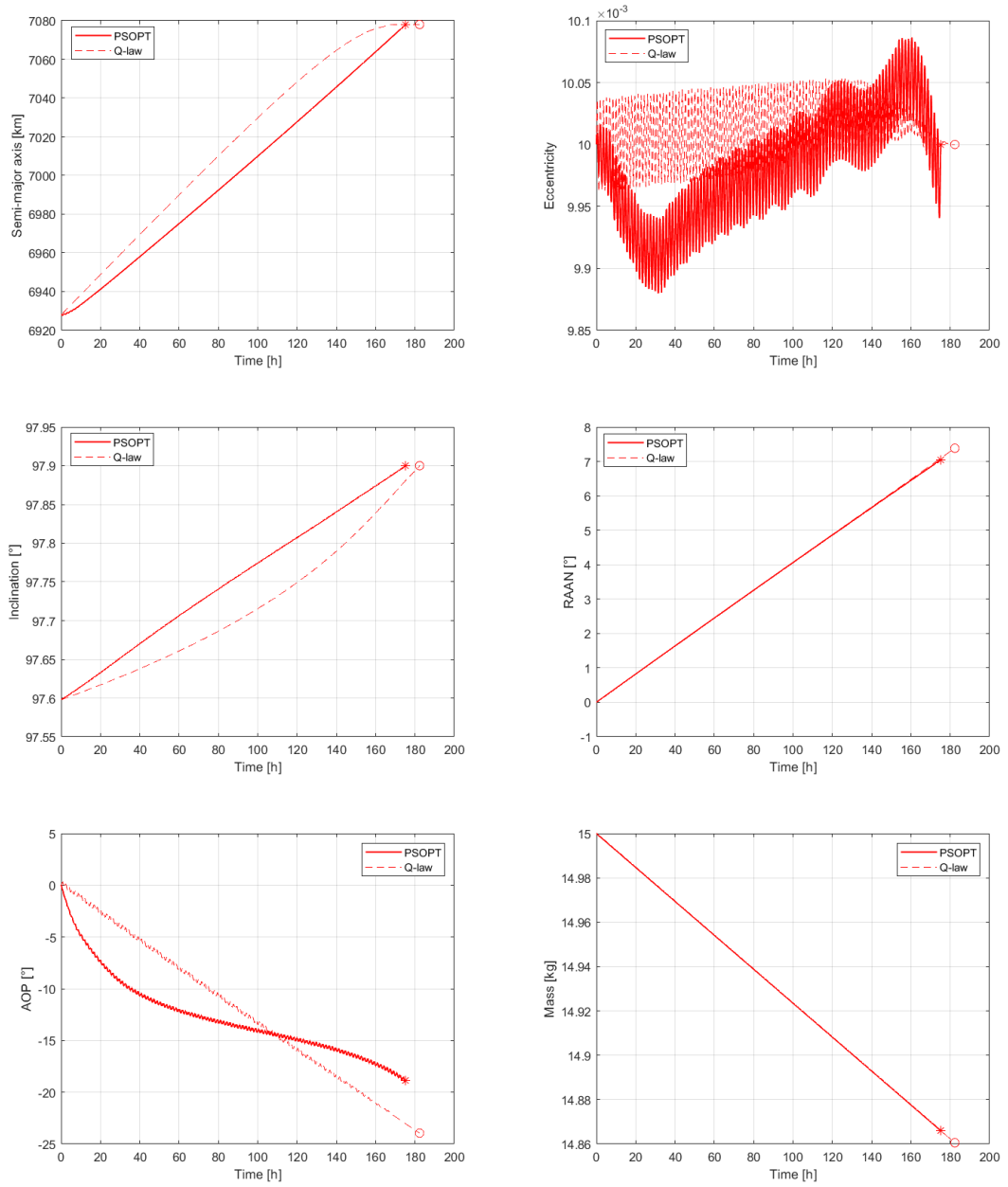


**Figure 4.1:** State variables evolution: minimum time optimization vs minimum time Q-law

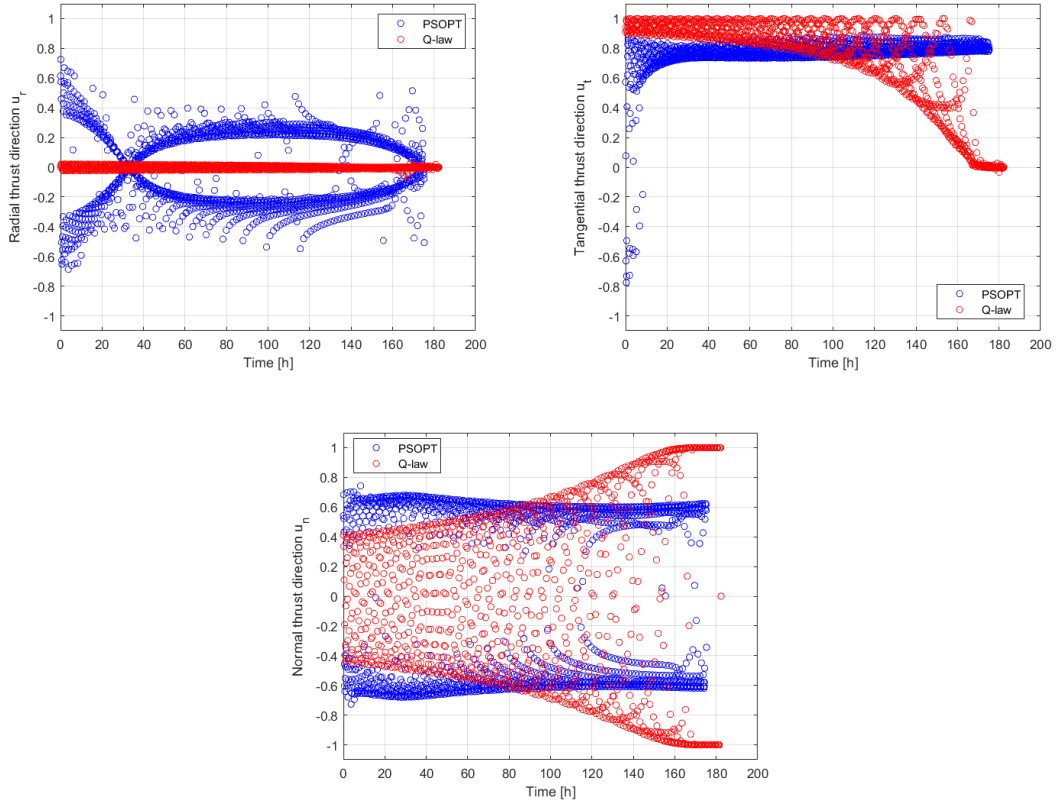


**Figure 4.2:** Thrust directions: minimum time optimization vs minimum time Q-law

### 4.5.2 Optimal fuel

As described in section 3.2.2, when considering an optimal fuel problem there is not an absolute best solution to the problem. In the same section, it has been presented how in the case of the Q-law the variation of the parameter  $\eta_{cutoff}$  leads to a trade-off solution between time of flight and fuel mass consumption. A similar situation arises when considering direct optimization. In section 1.2 direct optimization methods have been presented and discussed. One advantage of these methods is that, compared to indirect methods, they are associated to a large domain of convergence. This is an advantage because convergence does not depend on the accuracy of the initial guess, but on the other hand this also leads to the fact that the achieved solution is often not the global optimum, since it strongly depends on the initial guess. That is the reason why a trade-off must be conducted also for optimized results in case of optimal fuel solution.

To achieve a reasonable trade-off in this work, optimization processes with

several initial guesses are conducted. In particular, the case studied in this section are:

- **1.** Minimum time optimization with minimum time Q-law as initial guess
- **2.** Optimal fuel optimization with minimum time Q-law as initial guess
- **3.** Optimal fuel optimization, Q-law with  $\eta_{cutoff} = 0.9$  as initial guess
- **4.** Optimal fuel optimization, minimum time Q-law with halved maximum thrust as initial guess [45]

The Q-law generated initial guesses have been computed with the same parameters presented in Table 4.2, except for the trajectory 3 for which  $\eta_{cut} = 0.9$ . The control variables for optimal fuel problems are four, since the thrust throttle  $\eta$  is also a control parameter together with the three thrust direction in RTN frame  $\{u_r, u_t, u_n\}$ .

The solver options are described in Table 4.4. The ones that are not reported are already presented in Table 4.2, and they are the same also for these optimization processes.

Solutions with intermediate values of  $\alpha$ , parameter that define the objective function of the optimization (Eq. 4.31), have not been included since the consequent optimization has led to either not significantly improved results, or to an increased consumption associated with an increased time of flight.

	<b>1</b>	<b>2</b>	<b>3</b>	<b>4</b>
<b>Nodes</b>	1500	1500	1000	1200
<b>Control variables</b>	3	4	4	4
<b><math>\alpha</math></b>	1	0	0	0

**Table 4.4:** Optimization parameters for optimal fuel trade-off

	<b>1</b>	<b>2</b>	<b>3</b>	<b>4</b>
<b>ToF [h]</b>	175.276	183.662	217.751	363.387
<b><math>m_{fuel}</math> [kg]</b>	0.1341	0.1240	0.1220	0.1162

**Table 4.5:** Solutions for optimal fuel problem

The results confirm that convergence is found for each one of this initial guesses, even when the achieved optimal solution is not a global optimal. The state variables evolution is shown in Fig. 4.3 and the results are summed up in Table 4.5.

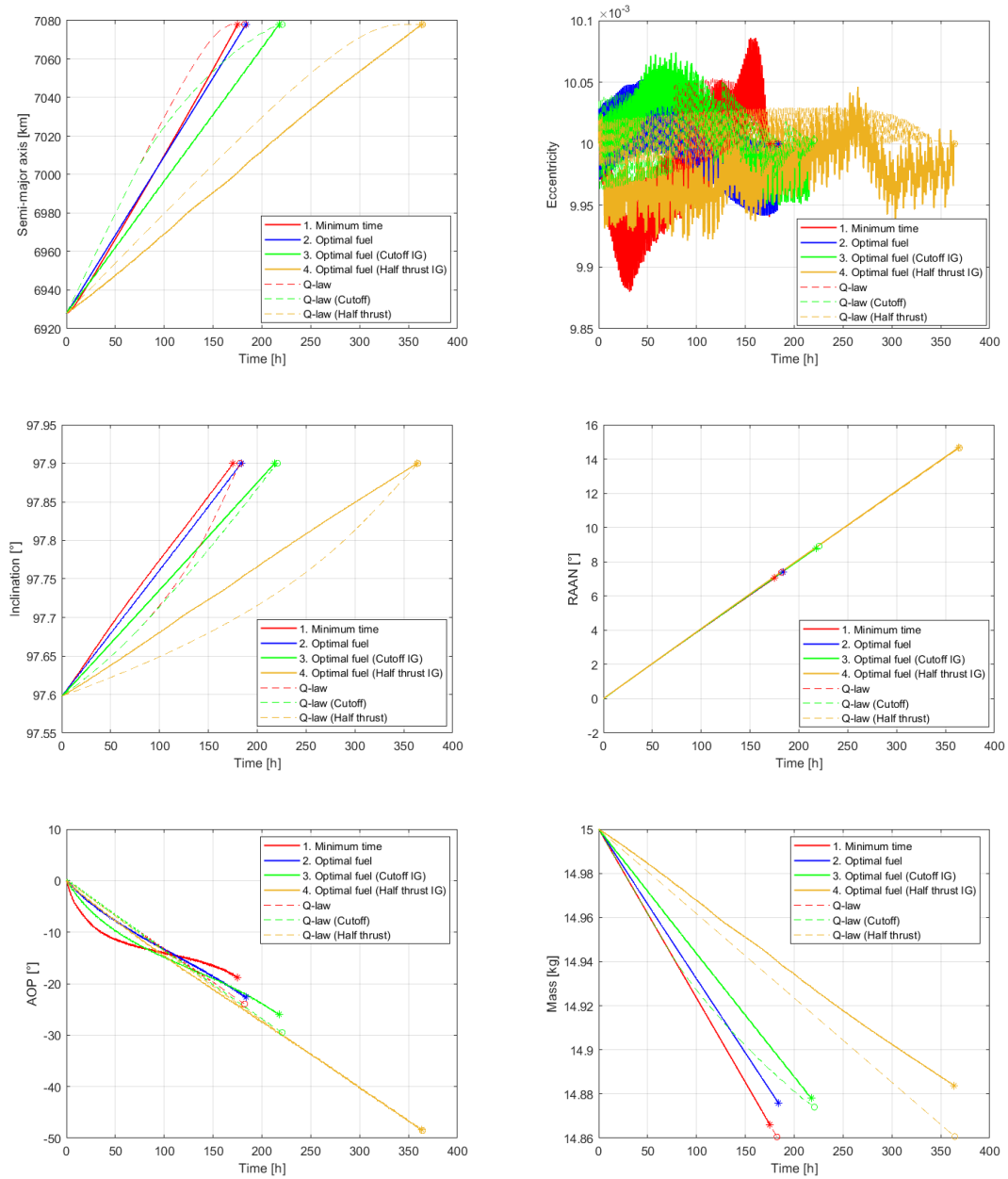


Figure 4.3: Optimal fuel solutions and initial guesses

These results also confirm that an absolute best solution does not exist. The mission designer must define which one of the possible solutions, that are many more than these presented, represents the best for the objective of the mission: through the mass plot in Fig. 4.3 it is clear that, also after the direct optimization

process, a reduction in fuel mass consumption is associated with an increase in time of flight. The bigger is the fuel saving and the less is the increase in time, the better is the found solution.

However, since in this work there are no constraints on maximum time of flight or maximum fuel consumption, the most suitable solution has been chosen by analyzing how much fuel is saved against how much time of flight is added to the mission. Taking the minimum time optimized solution as a reference (optimization 1), a comparison is carried out in Table 4.6 between the three optimal fuel results in terms of time of flight and fuel mass consumption.

	<b>2</b>	<b>3</b>	<b>4</b>
<b>ToF increase vs 1 [%]</b>	4.785	24.233	107.323
<b><math>m_{fuel}</math> reduction vs 1 [%]</b>	7.532	9.023	13.348

**Table 4.6:** Comparison between solutions for optimal fuel problem

Weighing up the pros and cons of each optimization, it has been chosen that the most suitable solution for this work is the optimization 2, i.e. the optimal fuel optimization ( $\alpha = 0 \rightarrow J = -m_f$ ) with minimum time Q-law as initial guess, because a significant improvement in fuel consumption is achieved at the cost of a very low increase in time of flight. This choice defines also the optimization that will be carried out for the objective mission of this thesis, since obtaining such a trade-off for the defined transfers (section 1.3) would be too computationally expensive.

# Chapter 5

## Simulation results

This chapter will be focused on the results of the objective scenario transfers optimization, presented in section 1.3. The chosen method will be based on the use of a direct trapezoidal collocation method that optimizes a sub-optimal initial guess provided by the Q-law algorithm. First there will be a discussion about minimum time results, and then the optimal fuel results will be presented. After that, the validation of Q-law controls will be carried out using the software General Mission Analysis Tool (GMAT).

### 5.1 Minimum time

	Parameter	Value	Unit
Q-law parameters	Integration time step	600	s
	Integration method	RK45	-
	Q-law tolerance	$10^5$	$s^2$
	$\eta_{cut}$	0	-
	$W_a$	1	-
	$W_e$	1	-
	$W_i$	1	-
	$r_p^{min}$	6578	km
	k	1000	-

**Table 5.1:** Q-law parameters for initial guess generation

The objective of this optimization is to obtain, for both the orbit change and the disposal, a set of control variables that leads to the quickest possible trajectory. As presented in Chapter 4, in this type of optimization the control variables are the

three thrust directions  $\{u_r, u_t, u_n\}$ , while the thrust magnitude is always fixed to the maximum value.

For both maneuvers, the Q-law minimum time trajectory will be generated using the parameters presented in Table 5.1.

### 5.1.1 Orbit change

An optimized solution through the direct trapezoidal collocation method has been achieved, using 1200 mesh nodes. The state variables initial and final values are presented in Table 5.2. The trajectories of the state and control variables as a function of time are shown in Fig. 5.1 and Fig. 5.2, and the performance results are summed up in Table 5.3.

Orbital element	Initial value	Final value	Unit
$a$	6928	7178	km
$e$	0.01	0.01	-
$i$	97.5977	98.6081	°
$\Omega$	0	17.8121	°
$\omega$	0	-58.2096	°
$\theta$	0	132.3259	°
$m$	15	14.6656	kg

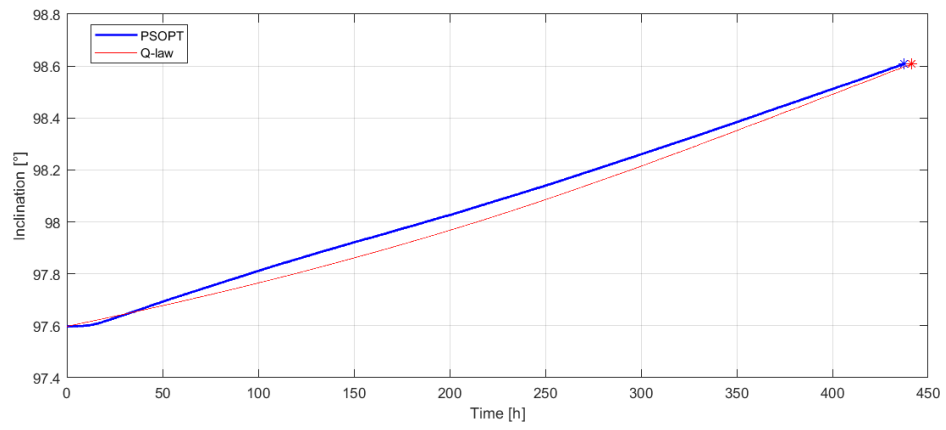
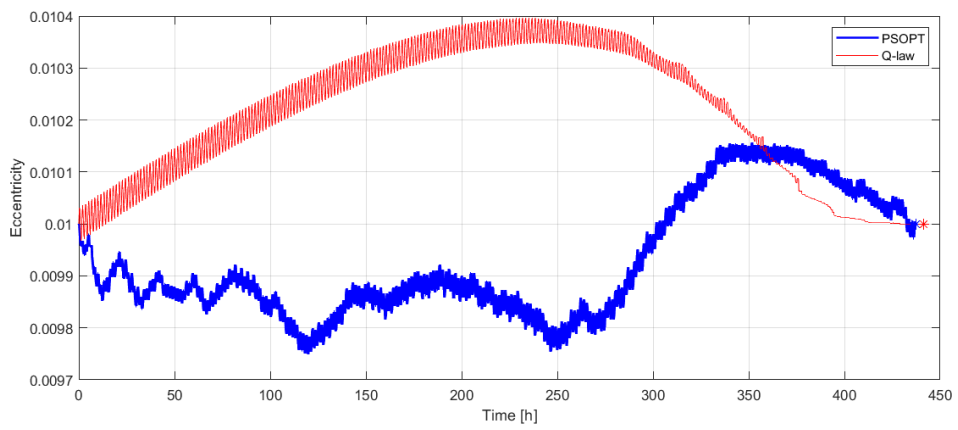
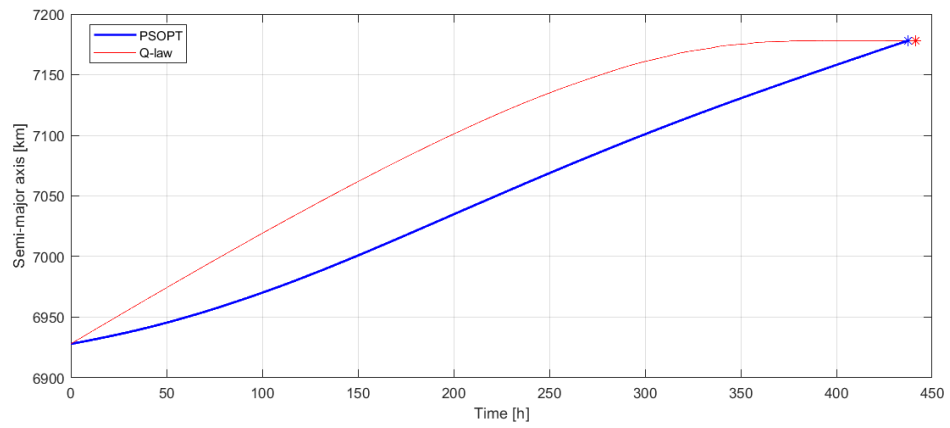
**Table 5.2:** Minimum time orbit change: initial and final state variables

Since a minimum time solution is considered, thrust is always active and it is equal to its maximum value. Therefore, the reduction in fuel consumption is proportional to the decrease in time of flight with respect to the Q-law initial guess, as seen in Table 5.3.

	PSOPT	Q-law	Improvement
<b>ToF [h]</b>	437.210	441.667	1.00 %
<b><math>m_{fuel}</math> [kg]</b>	0.3344	0.337781	1.00 %

**Table 5.3:** Minimum time orbit change: results

## Simulation results



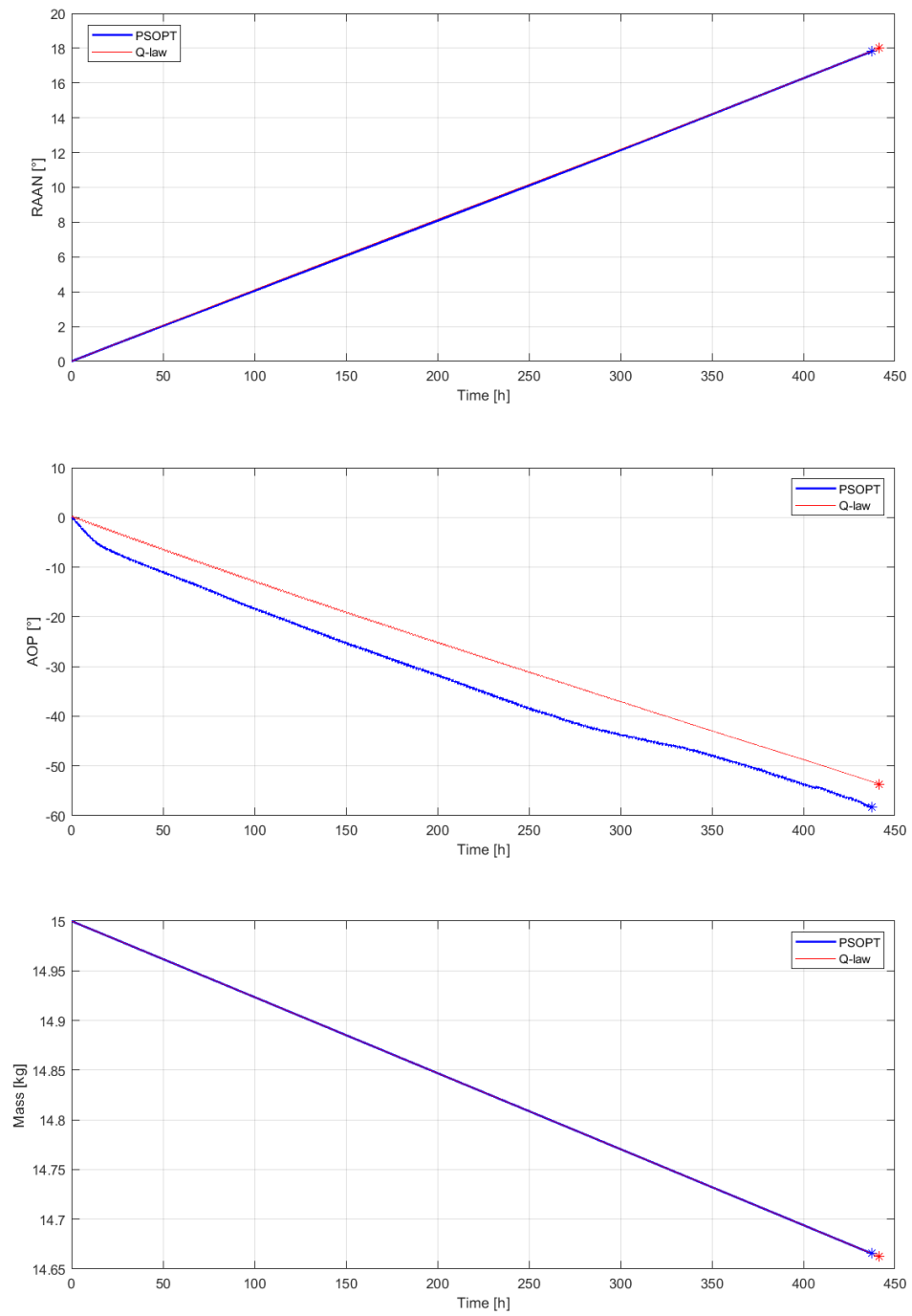


Figure 5.1: Minimum time orbit change: state variables

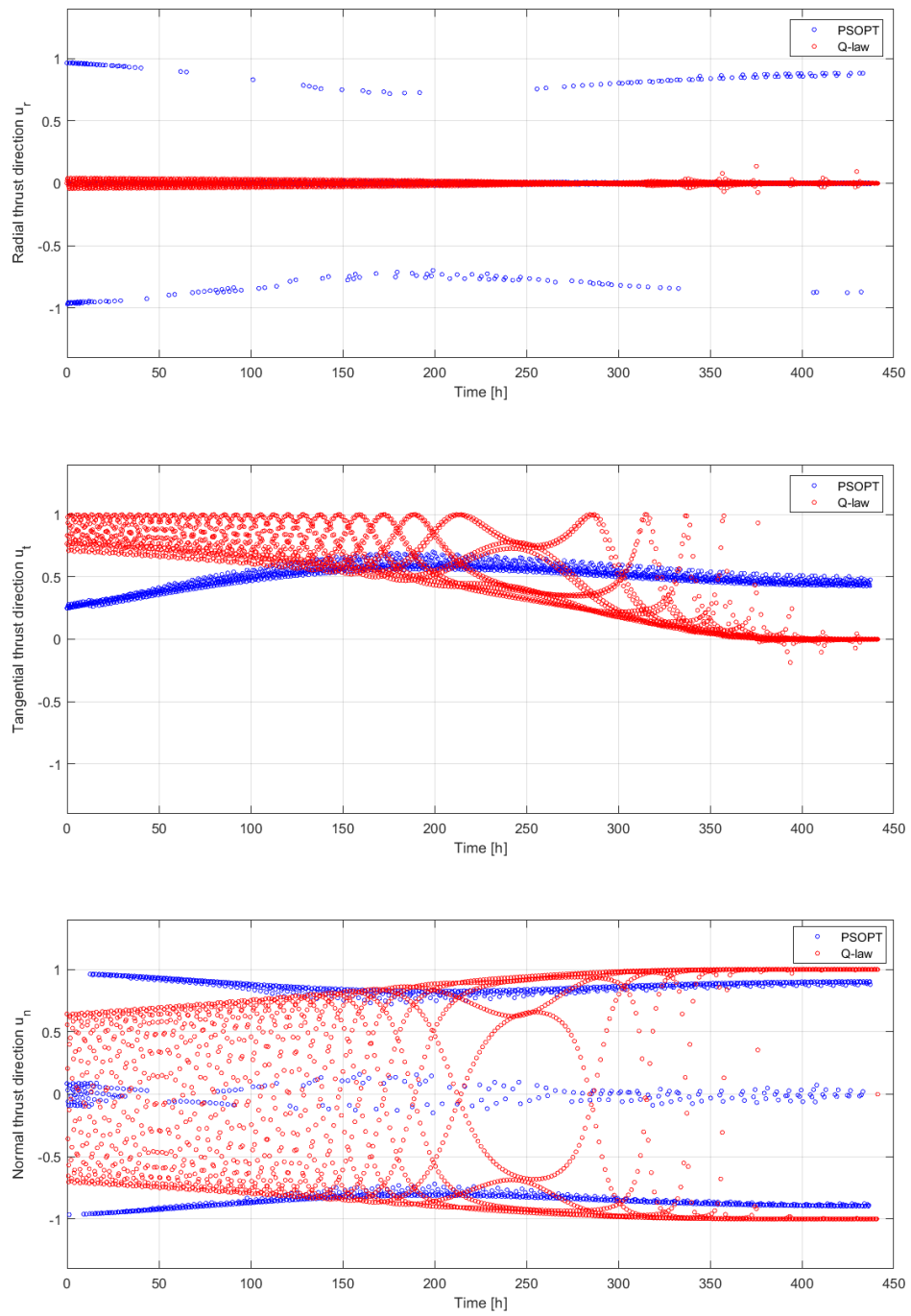


Figure 5.2: Minimum time orbit change: thrust directions

## 5.1.2 Disposal

As disclosed in Chapter 1, on-orbit operations for the assumed satellite are set to take place for 5 years. After this period, the goal is to reach an orbit where the satellite naturally decays, due to atmospheric drag, in less than 25 years. The initial values of this transfers depend on the evolution of the orbital elements during the operational period: apart from  $a$ ,  $e$  and  $i$  that, for how the problem is modeled in this work, do not vary in absence of thrust,  $\Omega$ ,  $\omega$  and  $\theta$  change under the other perturbations effects. The first two of these vary due to the  $J_2$  zonal harmonic, while the true anomaly  $\theta$  is modified because of the gravitational attraction of Earth. That is the reason why the initial values of  $\Omega$  and  $\omega$  have been defined in accordance with a 5-years propagation carried out in GMAT, in which  $J_2$  effects have been considered, and they are summed up in Table 5.4. It is important however to note that this is meant to just be an approximation, since many station-keeping maneuvers may occur in such a period, and they can affect the rate of change of orbital elements as well as modify the other elements. On the other hand, the definition of a precise  $\theta$  is not considered of relevance, since in LEO this element changes very quickly (orbital periods are around 90 minutes), so the initial value can be considered arbitrary and it is conventionally set to zero.

Orbital element	Initial value	Final value	Unit
$a$	7178	7178	km
$e$	0.01	0.01	-
$i$	98.6081	98.6081	°
$\Omega$	17.8121	12.5416	°
$\omega$	301.7904	23.1151	°
$m$	14.6656	14.6656	kg

**Table 5.4:** 5 years propagation: initial and final state variables

Since thrusting actions do not take place during on-orbit operations and station-keeping maneuvers are not considered, the mass initial value is the same as the final value of the first transfer of the mission, presented in Table 5.2.

In this case, the optimization carried out through the direct trapezoidal collocation method has converged to a solution using 900 mesh nodes. The state variables initial and final values are presented in Table 5.5. The trajectories of the state and control variables as a function of time are shown in Fig. 5.3 and Fig. 5.4, and the performance results are summed up in Table 5.6.

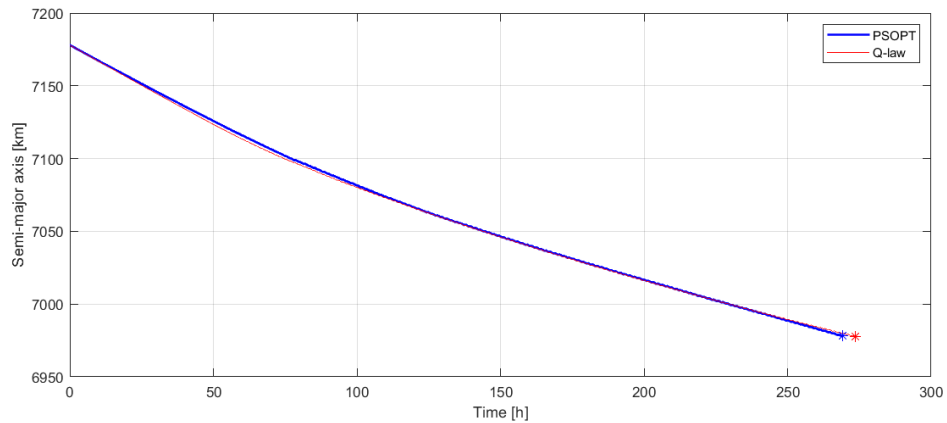
Orbital element	Initial value	Final value	Unit
$a$	7178	6978	km
$e$	0.01	0.02866151	-
$i$	98.6081	98.6081	$^\circ$
$\Omega$	12.5416	24.2574	$^\circ$
$\omega$	23.1151	5.3486	$^\circ$
$\theta$	0	354.1335	$^\circ$
$m$	14.6656	14.4597	kg

**Table 5.5:** Minimum time disposal: initial and final state variables

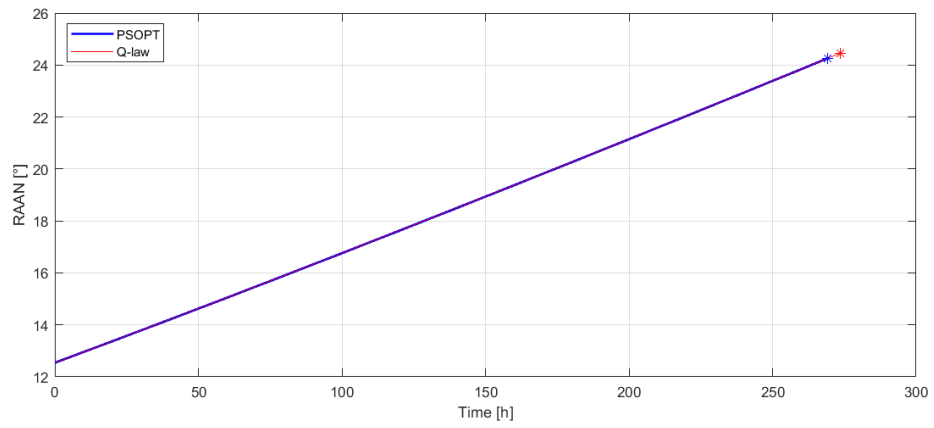
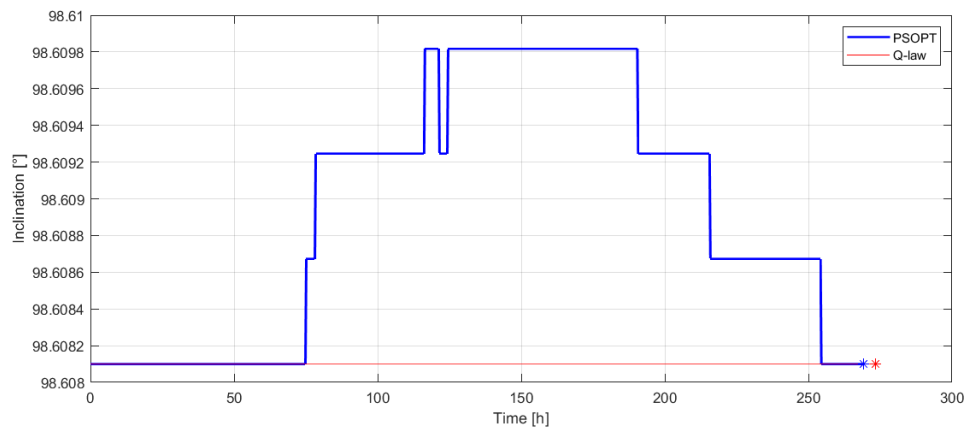
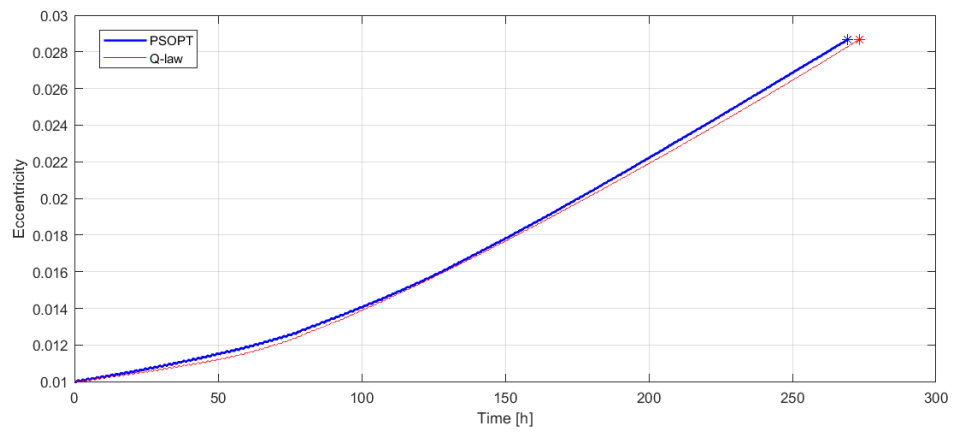
Also for this transfer, a minimum time solution is achieved, so the improvement in fuel consumption is strictly related to the improvement in time of flight, as seen in Table 5.6. The slight difference in the improvement percentages is only due to numerical approximation in *PSOPT* results.

	PSOPT	Q-law	Improvement
<b>ToF [h]</b>	269.175	273.5	1.58 %
$m_{fuel}$ [kg]	0.2059	0.209167	1.56 %

**Table 5.6:** Minimum time disposal: results



## Simulation results



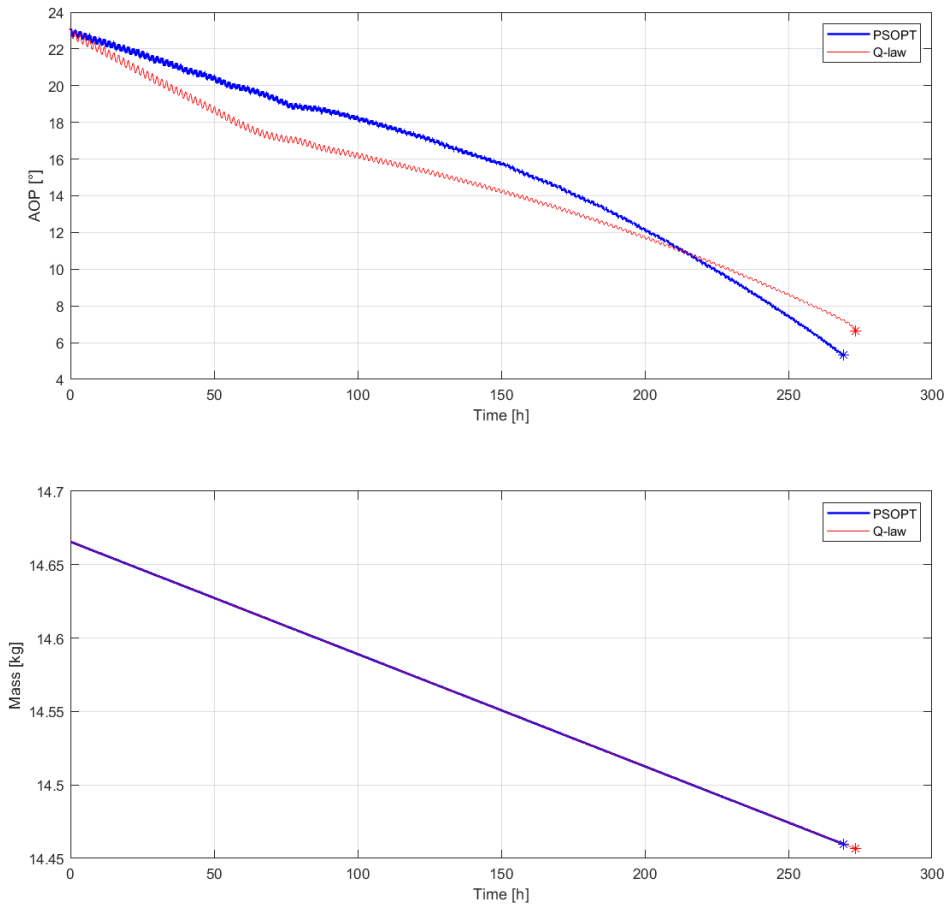
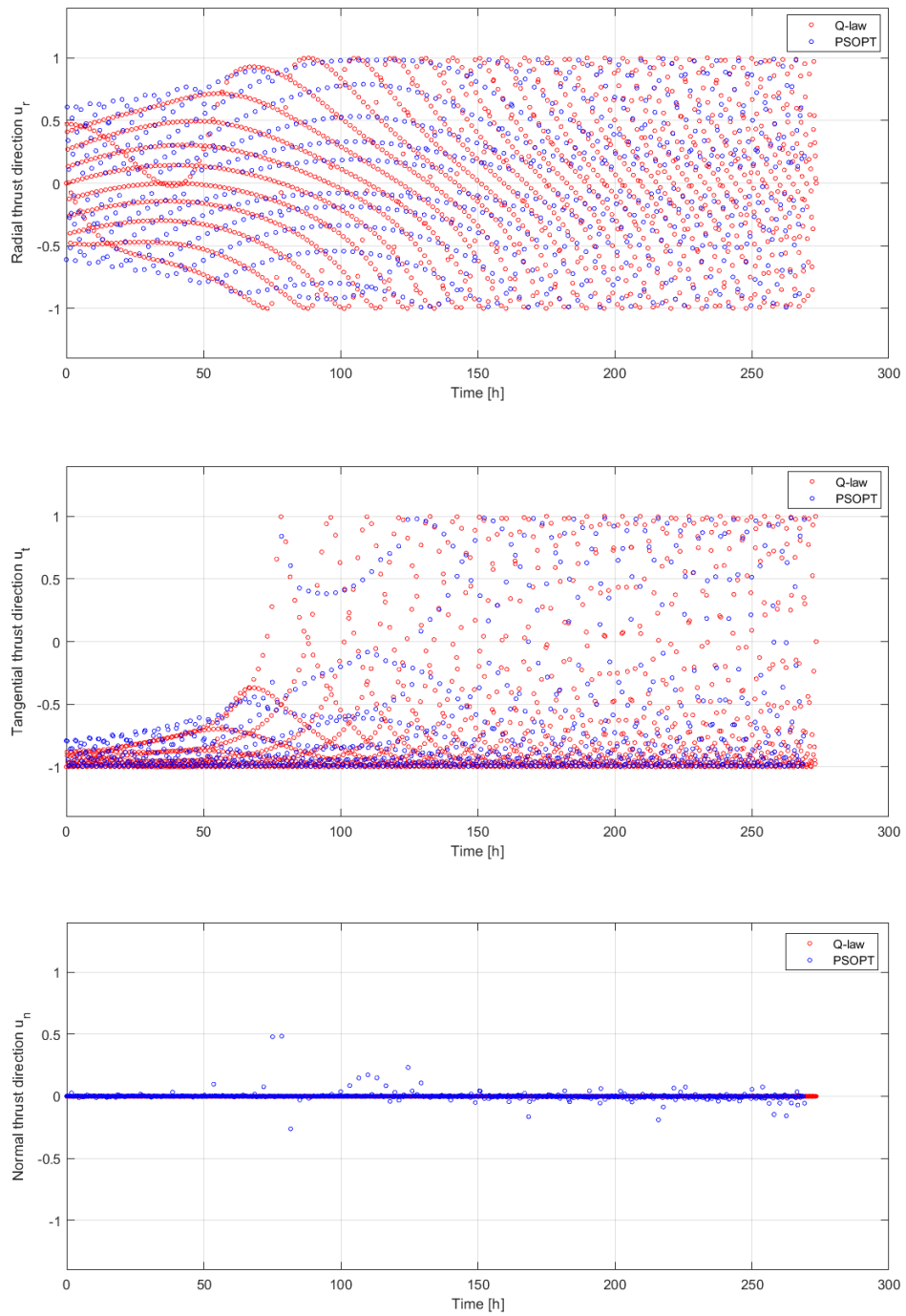


Figure 5.3: Minimum time disposal: state variables



**Figure 5.4:** Minimum time disposal: thrust directions

## 5.2 Optimal fuel

The objective of the optimization presented in this section is to obtain, for both the orbit change and the disposal, a set of control variables that leads to an optimized fuel consumption. In this case the thrust throttle may vary in the interval  $[0,1]$ , so it becomes an optimization control variable together with the three thrust directions  $\{u_r, u_t, u_n\}$ . As explained in section 4.5.2 there is not an absolute minimum for fuel consumption, since it strongly depends on how much additional time is accepted by the mission requirements. In the same section the solution adopted for this work has been defined: the direct method is a minimum fuel optimization ( $\alpha = 0 \rightarrow J = -m_f$ ) and takes a Q-law minimum time trajectory as initial guess. Therefore, for both maneuvers, the Q-law trajectory is the same as the one given in input for the minimum time optimization, defined in Table 5.1.

### 5.2.1 Orbit change

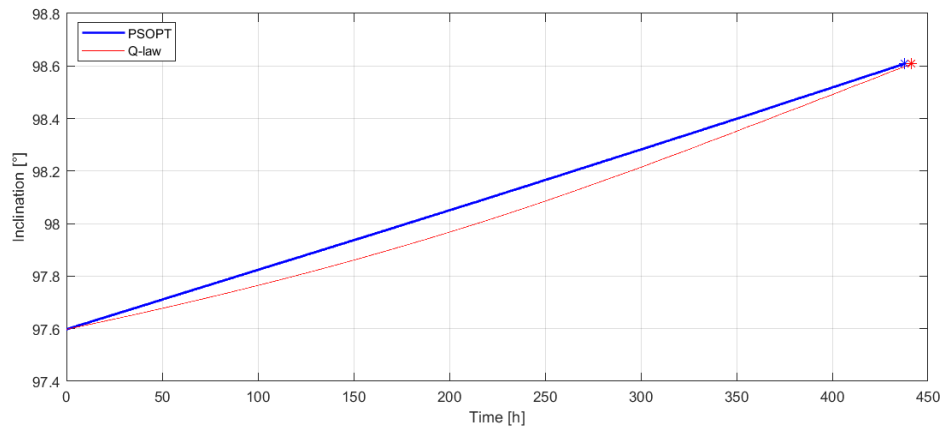
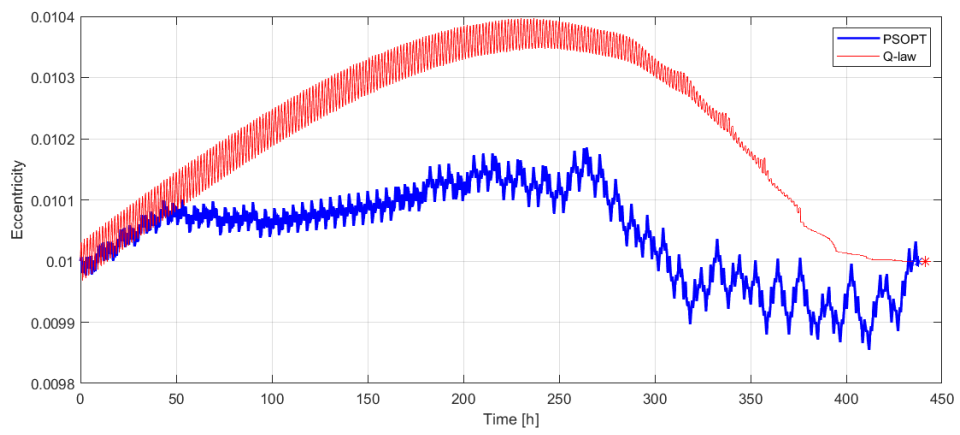
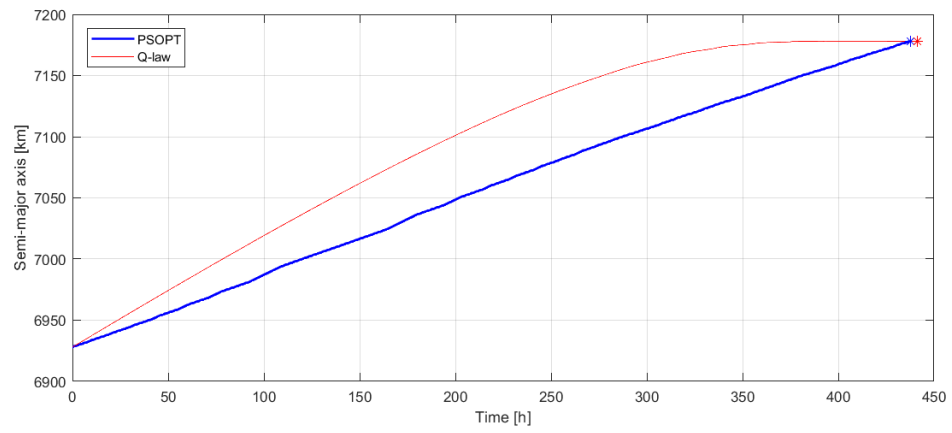
An optimized solution through the direct trapezoidal collocation method has been achieved for this scenario, using 900 mesh nodes. The state variables initial and final values are presented in Table 5.7. The trajectories of the state and control variables as a function of time are shown in Fig. 5.5 and Fig. 5.6, and the performance results are summed up in Table 5.8.

Orbital element	Initial value	Final value	Unit
$a$	6928	7178	km
$e$	0.01	0.01	-
$i$	97.5977	98.6081	°
$\Omega$	0	17.9592	°
$\omega$	0	-56.5823	°
$\theta$	0	67.0087	°
$m$	15	14.7213	kg

**Table 5.7:** Optimal fuel orbit change: initial and final state variables

As seen in Table 5.8, the solution of this case is particularly convenient since the formulation of an optimal fuel problem, and the consequent use of the thrust throttle as a control variable, not only lead to an expected reduction in fuel consumption but also to a reduction in time of flight, whereas most of the time a saving of fuel is related to an increase in time of flight.

## Simulation results



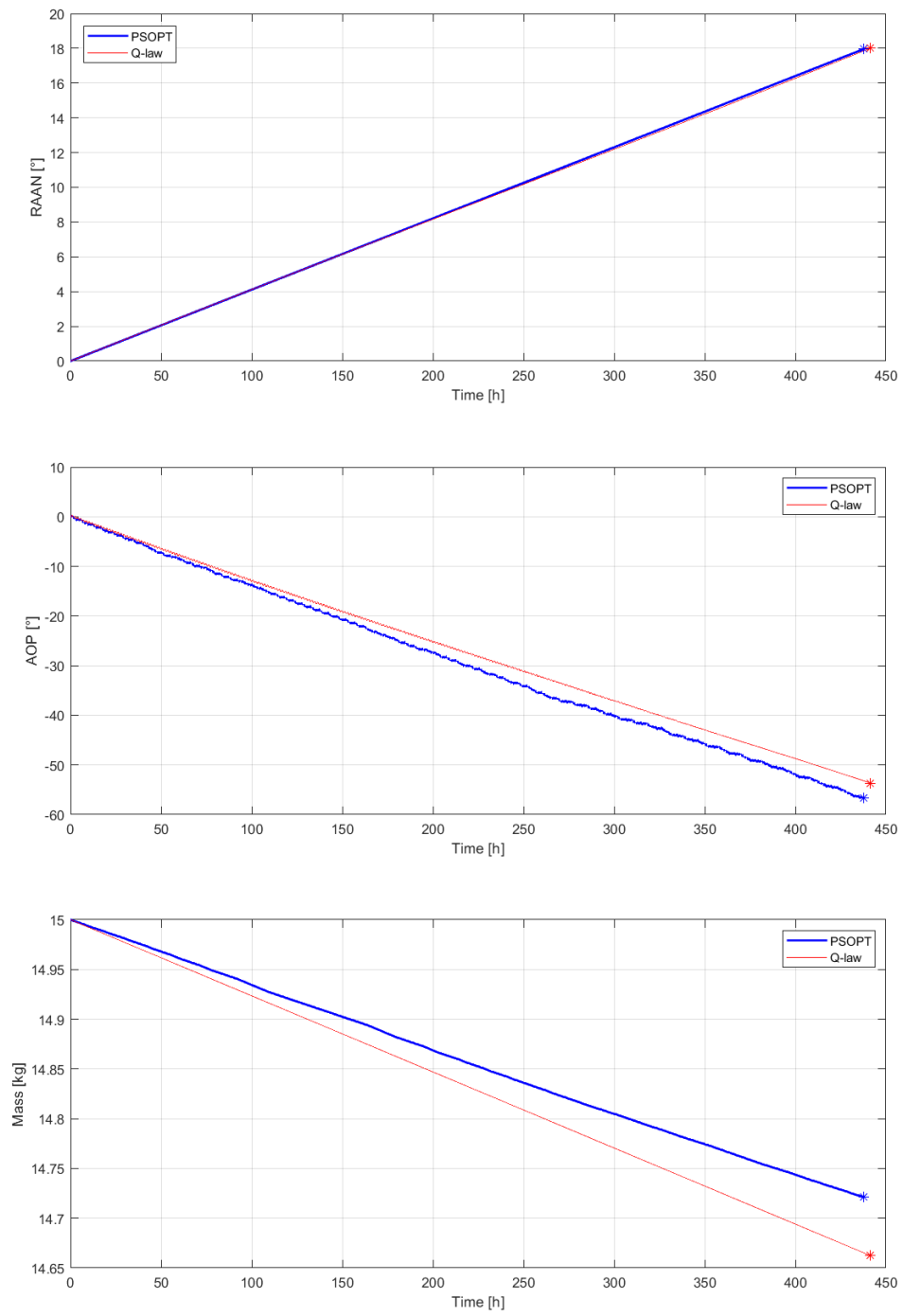
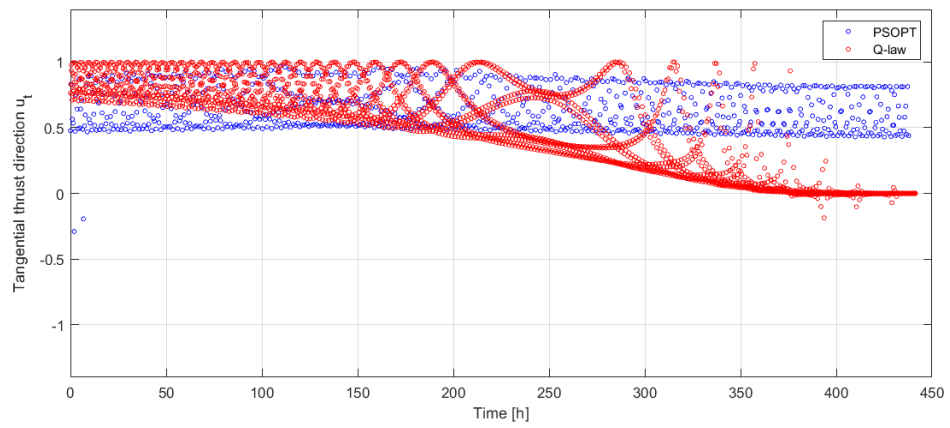
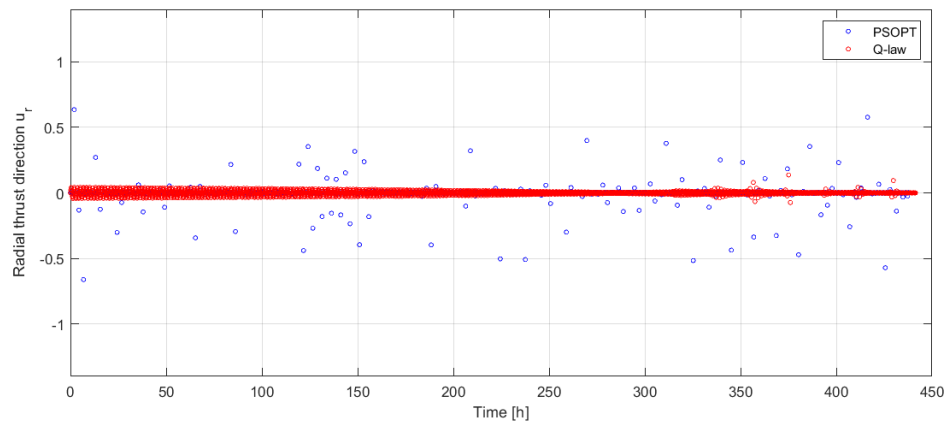
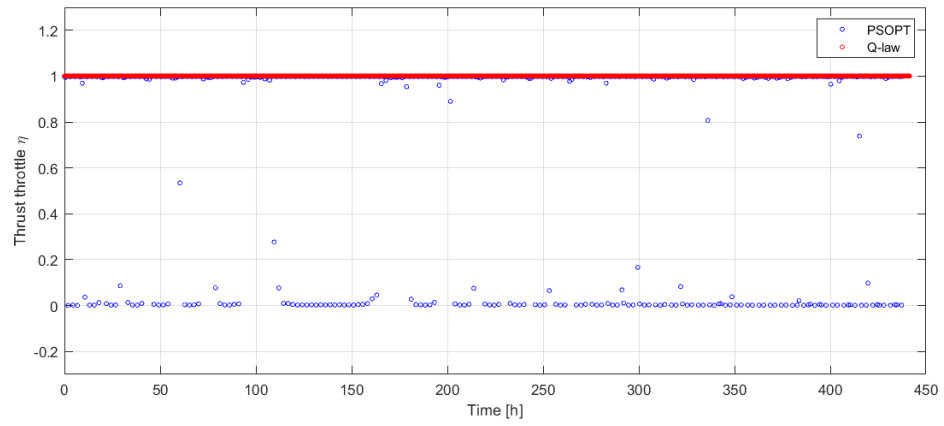
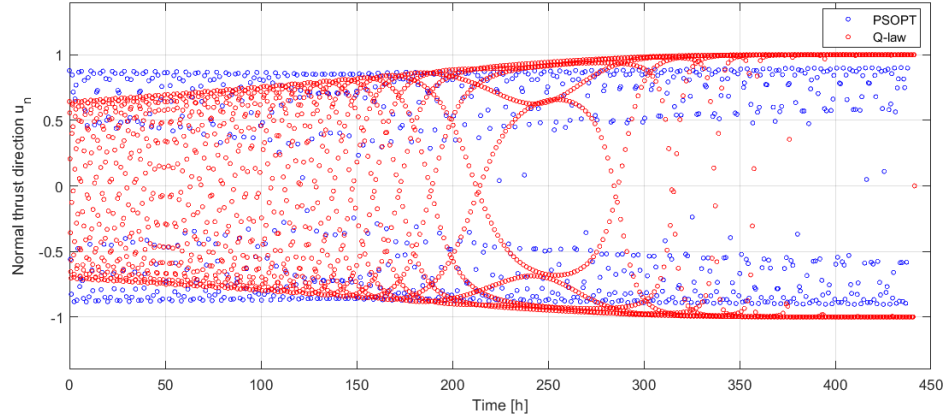


Figure 5.5: Optimal fuel orbit change: state variables

## Simulation results





**Figure 5.6:** Optimal fuel orbit change: thrust throttle and directions

	PSOPT	Q-law	Improvement
<b>ToF [h]</b>	437.751	441.667	0.89 %
$m_{fuel}$ [kg]	0.2787	0.337781	17.49 %

**Table 5.8:** Optimal fuel orbit change: results

## 5.2.2 Disposal

Noticing the very slight differences between the final values of  $\Omega$  and  $\omega$  at the end of the optimal fuel orbit change transfer and the respective values obtained for the minimum time transfer, it is reasonable to assume the same initial values for the disposal maneuver that starts after the 5-years period of on-orbit operations. An option for the definition of the mass initial value is to choose it in accordance with the final value of the first transfer, as done in the minimum time scenario. However, the mass initial value is here considered the same as the initial mass of the minimum time disposal maneuver, to more clearly visualize the comparison in the performance results.

In this scenario, the optimization conducted through the direct trapezoidal collocation method has converged to a solution using 1100 mesh nodes. The state variables initial and final values are presented in Table 5.9. The trajectories of the state and control variables as a function of time are shown in Fig. 5.7 and Fig. 5.8, and the performance results are summed up in Table 5.10.

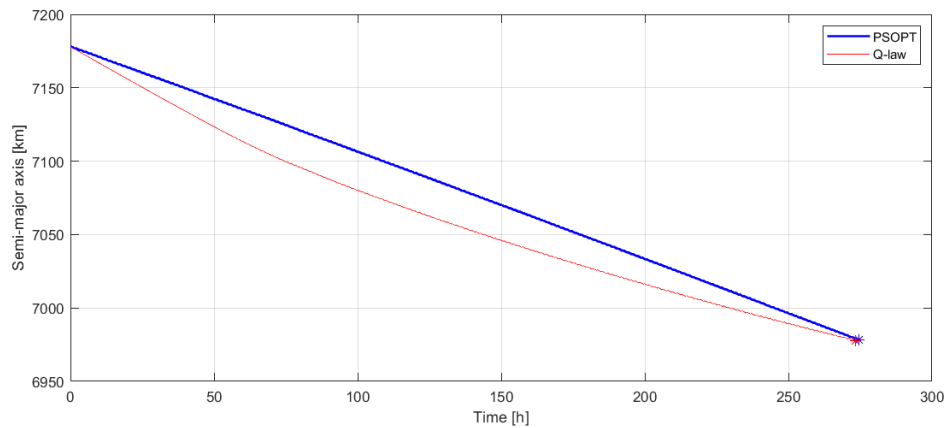
Orbital element	Initial value	Final value	Unit
$a$	7178	6978	km
$e$	0.01	0.02866151	-
$i$	98.6081	98.6081	°
$\Omega$	12.5416	24.4071	°
$\omega$	23.1151	5.3514	°
$\theta$	0	285.9769	°
$m$	14.6656	14.4919	kg

**Table 5.9:** Optimal fuel disposal: initial and final state variables

The results summed up in Table 5.10 show that the significant saving of fuel is associated to a very slight increase in time of flight, so such a solution may be really convenient if a trade-off between the two parameters is considered.

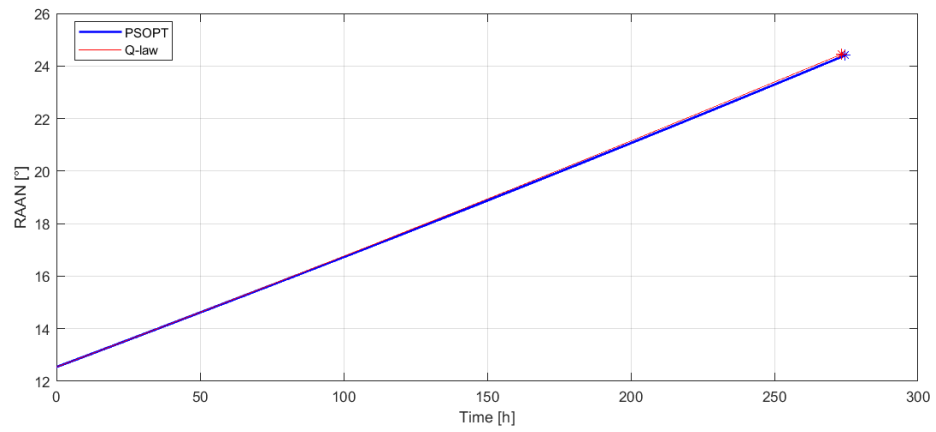
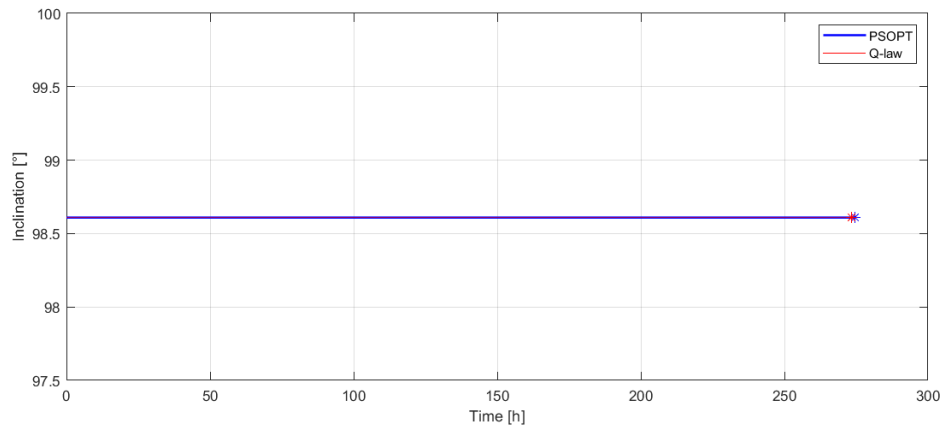
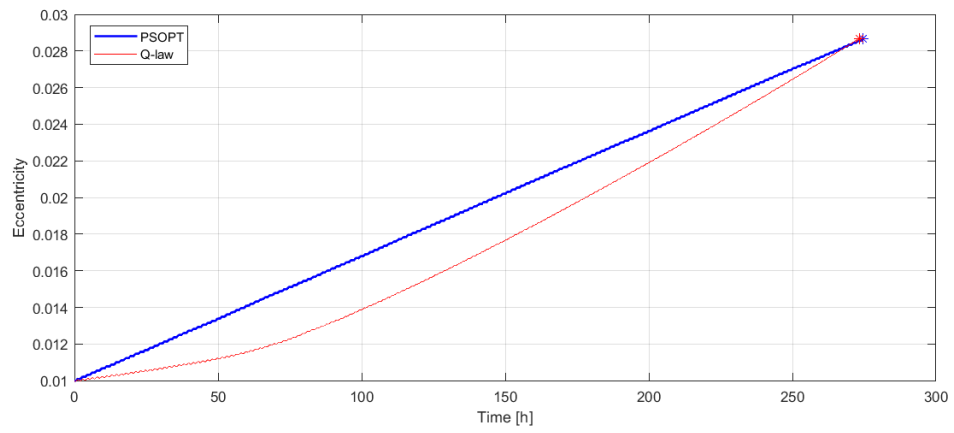
	PSOPT	Q-law	Improvement
<b>ToF [h]</b>	274.671	273.5	-0.43 %
<b><math>m_{fuel}</math> [kg]</b>	0.1737	0.209167	16.96 %

**Table 5.10:** Optimal fuel disposal: results



## Simulation results

---



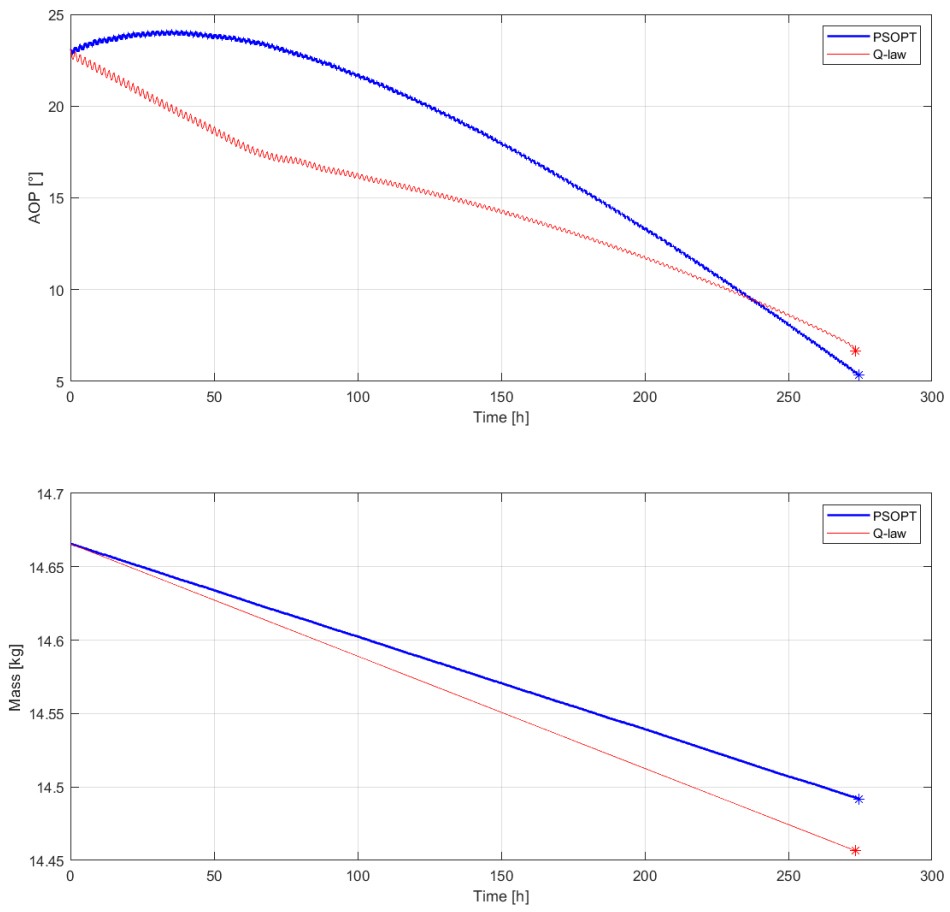
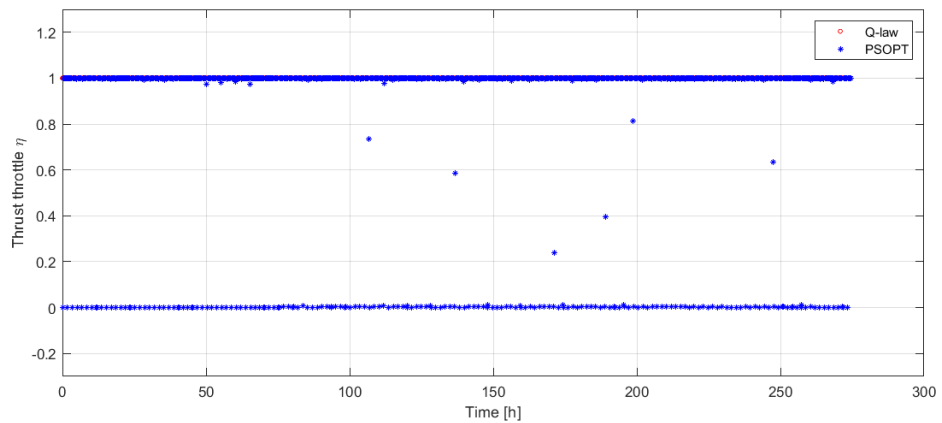


Figure 5.7: Optimal fuel disposal: state variables



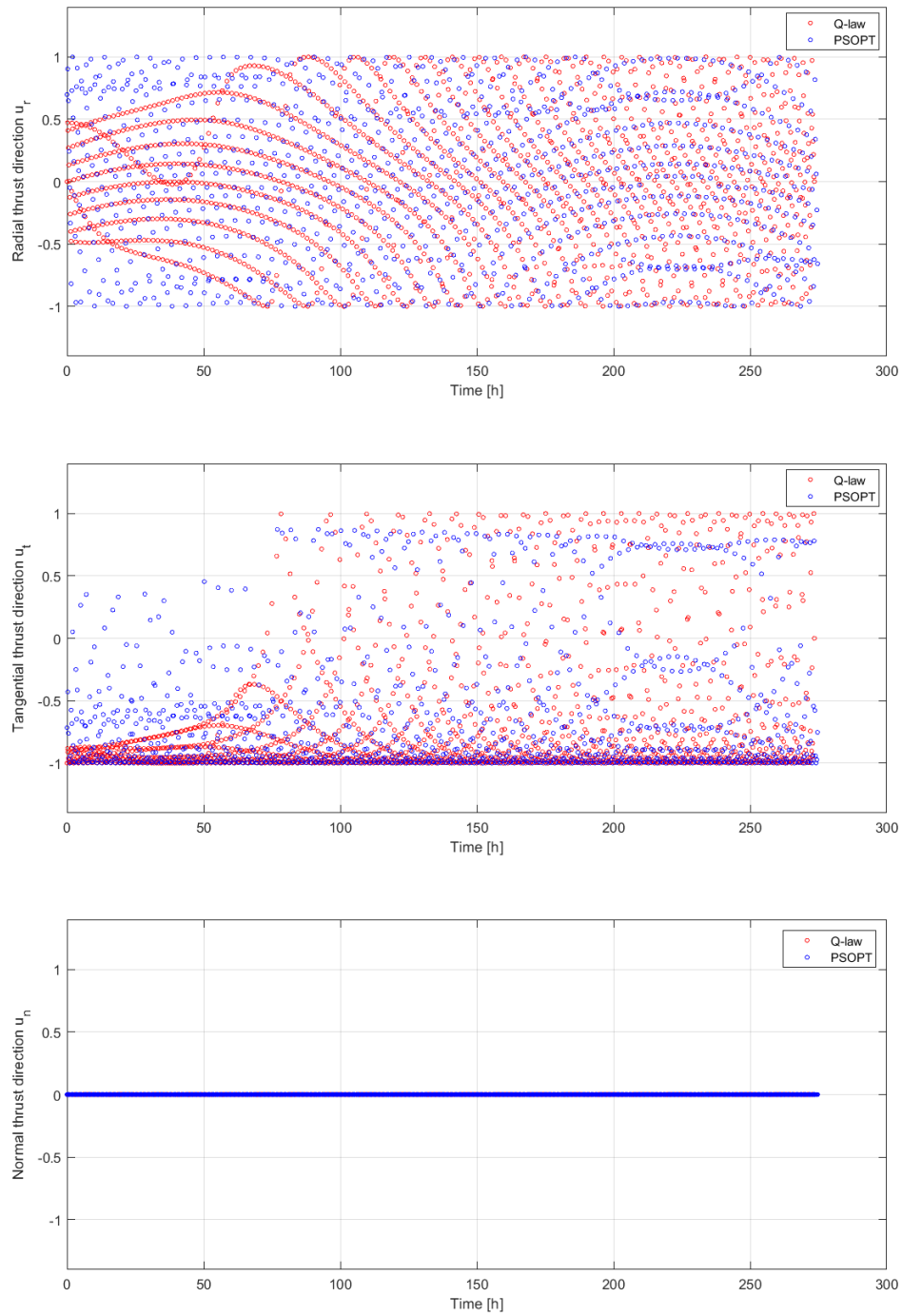


Figure 5.8: Optimal fuel disposal: thrust throttle and directions

## 5.3 GMAT validation

In this section the focus will be on the validation of the set of control variables given in output by the analyzed method. A method to validate the controls generated by the Q-law algorithm is discussed and presented; however, the same procedure has been tried on the *PSOPT* controls, but since no good results have been achieved and further investigation on the solver functioning are needed, the validation of the controls given by the optimization process is still underway.

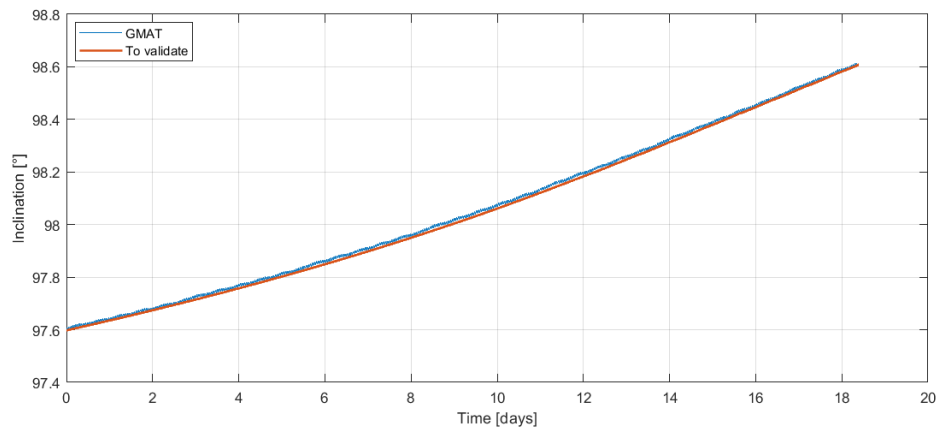
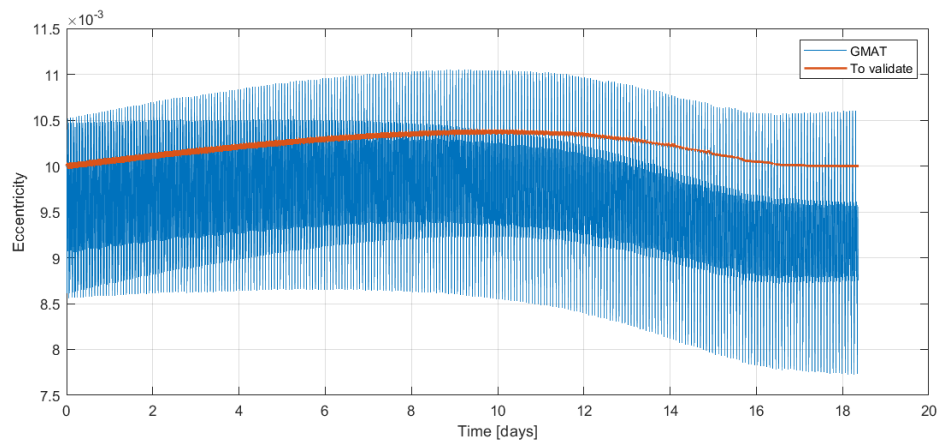
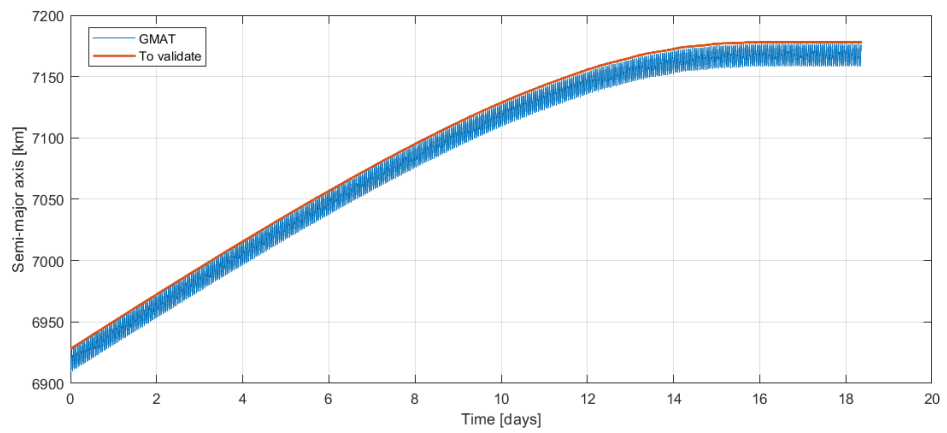
In order to perform the validation of the Q-law generated set of controls, the software General Mission Analysis Tool (GMAT), an open source space mission analysis software developed by NASA [56], has been used. The two Q-law trajectories that provide the orbit change and the disposal maneuver, and that are used as initial guesses for both minimum time and optimal fuel optimizations in the previous sections, have been chosen as the transfers to validate. The two transfers are presented in Table 1.2 and the Q-law parameters are shown in Table 5.1). Significant results on the validation of these trajectories would allow to consider validated the implementation of the Q-law algorithm and the definition of the system and orbital dynamics model.

The goal is to prove that the control variables defined by using the chosen perturbation model ( $J_2$  secular effects) produce the desired trajectory also in a real scenario with long-period, short-period and secular effects of the considered perturbations: in this case only  $J_2$  zonal harmonic effects are included. In order to do so, the spacecraft model parameters as well as the initial values of orbital elements have been imported in GMAT. Then, the control variables, that are the three thrust directions in the RTN frame  $\{u_r, u_t, u_n\}$  and the thrust magnitude, are enforced. However, it is crucial to note that each set of control variables given in output by the Q-law is associated to a time instant and a true anomaly value: in order to properly perform the validation in such a perturbed environment, it is necessary to enforce these actions at the respective true anomaly values, and not at the time instants. As a result, since the two compared dynamic models are not the same, there will be a slight difference in final time between the trajectory to validate and the validated GMAT solution, just like a subtle difference in true anomaly would be generated if actions were enforced at the respective time instant.

### 5.3.1 Orbit change

The orbital elements evolution presented in Fig. 5.9 show that, imposing the thrust controls as described above, the trajectories of the elements in the model to validate follow the trajectories of the elements in a real perturbed scenario, modeled by GMAT. Therefore, it is reasonable to consider validated the Q-law solution for this case and the assumed dynamics model.

## Simulation results



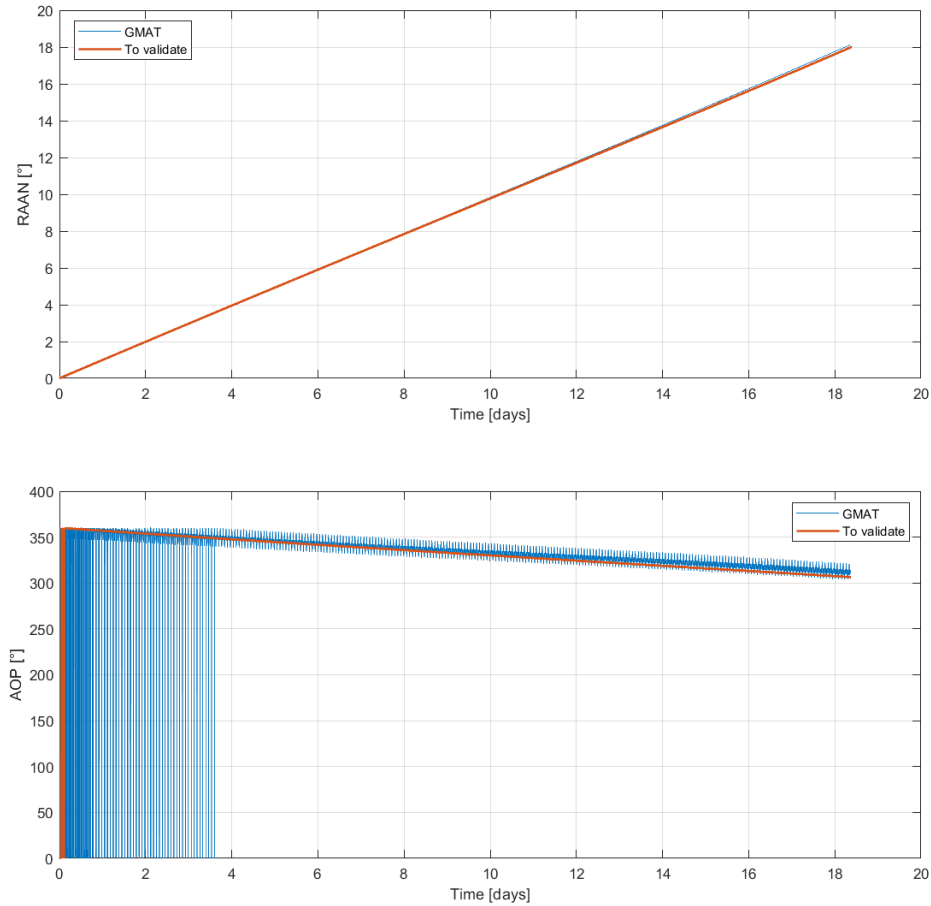
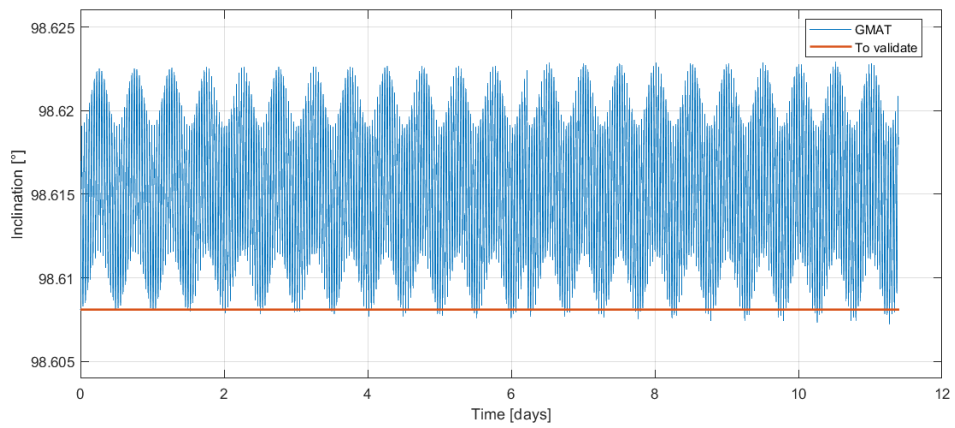
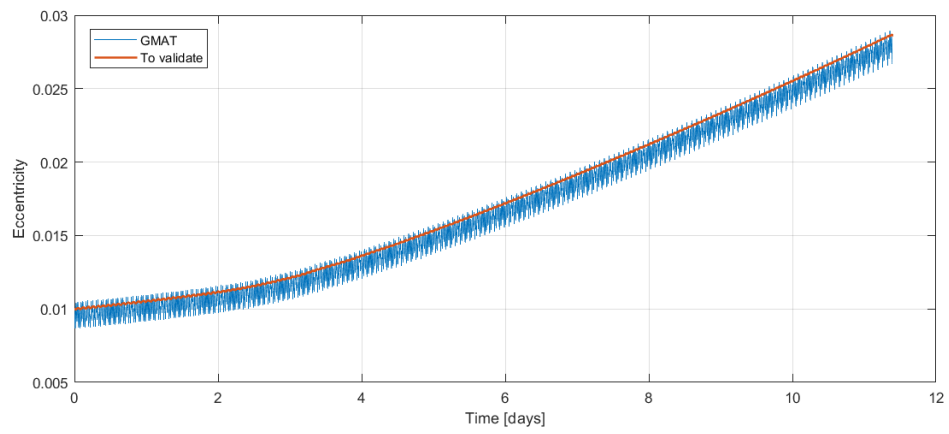
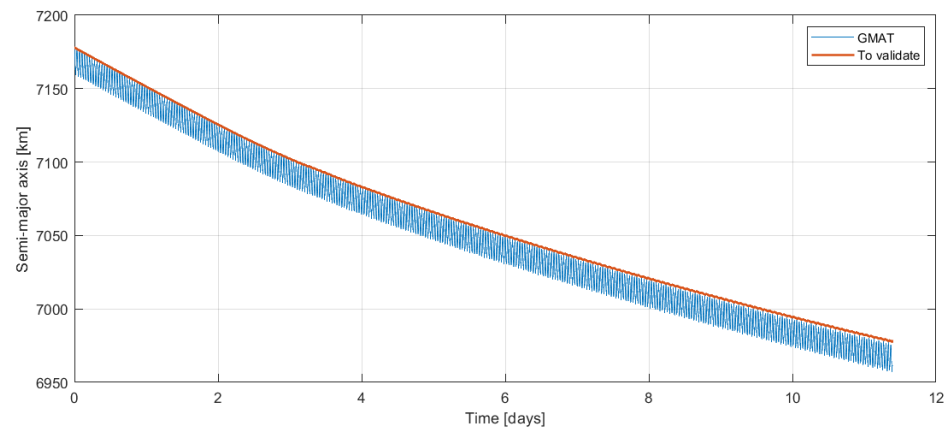


**Figure 5.9:** Orbit change: GMAT validation on orbital elements evolution

### 5.3.2 Disposal

In Fig. 5.10 it is shown that, also for the disposal transfer, the evolution described by the model to validate accurately follow the secular variation due to the thrusting actions in a real perturbed scenario. Thus, the Q-law solution and the model dynamics are validated for this case as well.

## Simulation results



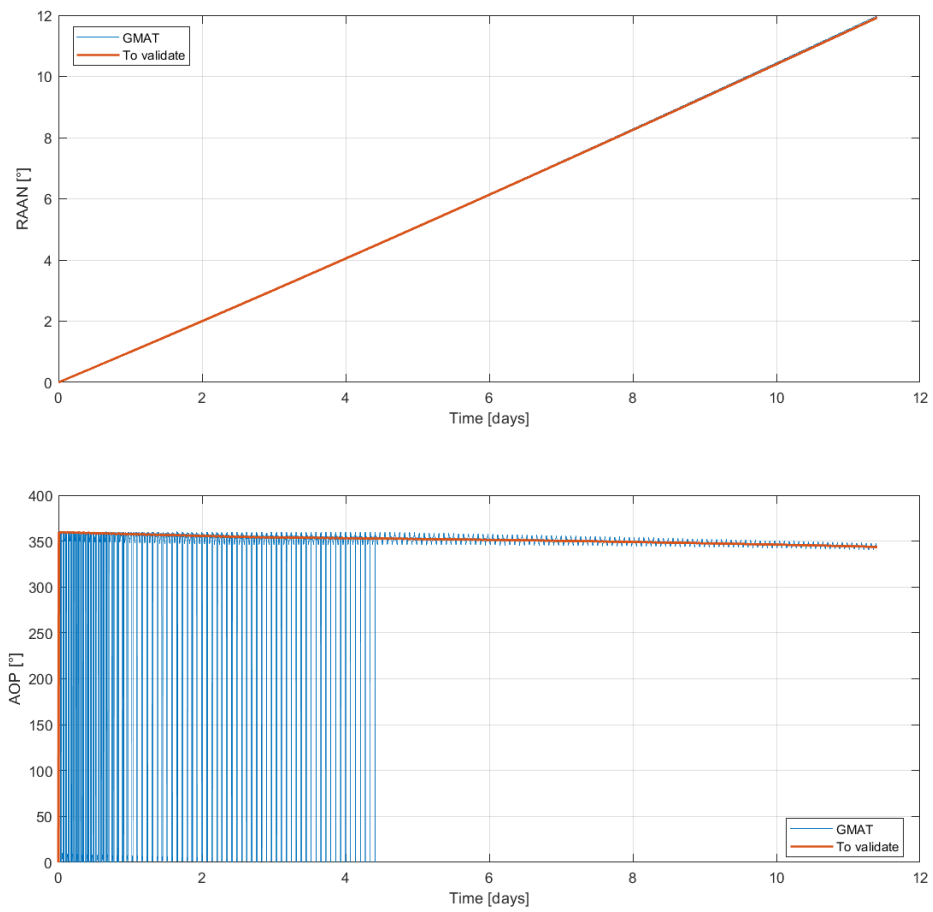


**Figure 5.10:** Disposal: GMAT validation on orbital elements evolution

# Chapter 6

## Conclusions

Analyzing the results obtained in Chapter 4 and in Chapter 5, it is clear that an improvement on results can be obtained through the proposed approach, which achieves an optimization employing a direct collocation method with the use of a Q-law generated initial guess trajectory.

It is interesting however to finally sum up the performances of the two types of optimization for the two transfer of the objective mission (section 1.3): the orbit change optimized transfer is performed with a 1% reduction in time of flight and fuel consumption employing a minimum time optimization (Table 5.3), whereas, using the same initial guess, the optimal fuel problem exploit the thrust throttle control to achieve a 17.49 % reduction of fuel consumption, even with a very slight reduction in time of flight (Table 5.8). This represents a very convenient solution, since generally a fuel consumption reduction requires an increase in time of flight, as also seen in the effectivity cutoff mechanism described for the Q-law algorithm (Fig. 3.5). The disposal maneuver optimization presents a similar behaviour: a slight improvement in both time of flight and fuel consumption is achieved with a minimum time optimization method (Table 5.6), while an optimal fuel problem leads to a much wider improvement of 16.96% in fuel consumption at the cost of a very subtle increase in time of flight with respect to the Q-law initial guess (Table 5.10).

Proceeding with the same reasoning discussed in section 4.5.2 and weighing up the pros and cons of each optimization, it is sensible to say that an optimization on fuel consumption, for these type of transfers with a Q-law generated initial guess, seems to be more convenient in terms of a global result. It is however reasonable to consider minimum time optimization, especially if a constraint on maximum time of flight is specified, since it also leads to an improvement with respect to the initial guess. Of course these results strongly depend on how the initial guess is generated: as a matter of fact, they confirm that the Q-law mechanism is well established for the generation of a rapid close to optimal minimum time trajectory.

## 6.1 Future work

In this section some suggestions for future works are given to further improve the accuracy of the proposed methods.

First of all, the implementation of RAAN and true anomaly phasing maneuvers, introduced in section 3.1.3, would be relevant for this work [40][41][3]. The first one is important especially when dealing with Sun-Synchronous orbits, since RAAN value is essential to define how much the orbit is exposed to eclipses and sunlight throughout the year: for example, dawn-dusk orbits are commonly designed to maximize the exposure to sunlight, crucial for electric propulsion systems. The second one is crucial when an optimized design of rendezvous maneuvers is desired.

Another significant addition to this work would be represented by the implementation of eclipses in the optimization procedure: as presented in Chapter 4, this process may require a multi-phase problem implementation [20] and can lead to more realistic results in terms of orbital elements evolution, time of flight and fuel consumption. The possibility to implement an eclipse model in the optimization process would consequently allow to exploit the eclipse model, discussed in section 2.4, in the Q-law algorithm, together with the effective symmetrical mesh refinement (section 3.5.1).

The proposed method may also be generalized in order to perform an optimization of longer trajectories, such as GTO to GEO transfers. In this case, an optimization on Q-law weights becomes relevant, as seen in [20]: the Q-law trajectory given as initial guess can be even closer to the optimal solution, so it improves the performance of the proposed optimization, which strongly depends on the accuracy of the initial guess. For this reason, Genetic Algorithms may be implemented in order to perform the Q-law weights optimization [27][20].

Lastly, another important addition to this work would be the possibility to consider a target on the argument of periapsis: an optimization may be achieved for other type of trajectories, such as transfers to Molniya orbits [29], that are commonly exploited for communications services and remote sensing coverage over high latitudes thanks to their property of not having an apsidal precession (section 2.3.3).

# Bibliography

- [1] SLO Cal Poly. *The CubeSat Program, CubeSat Design Specification Rev. 13*. 2014 (cit. on p. 1).
- [2] Paul Lascombes. «Electric propulsion for small satellites orbit control and deorbiting: The example of a Hall Effect thruster». In: *2018 SpaceOps Conference*. 2018, p. 2729 (cit. on p. 2).
- [3] A Fiorentino Lascombes and P Dewost. «Electric Propulsion for Small Satellites. A case study». In: *36th International Electric Propulsion Conference*. 15-20. 2019 (cit. on pp. 2, 5, 9, 45, 110).
- [4] Lamberto Dell’Elce. «Satellite orbits in the atmosphere: Uncertainty quantification, propagation and optimal control». In: (2015) (cit. on pp. 3, 25).
- [5] David Morante, Manuel Sanjurjo Rivo, and Manuel Soler. «A survey on low-thrust trajectory optimization approaches». In: *Aerospace* 8.3 (2021), p. 88 (cit. on p. 3).
- [6] Lev Semenovich Pontryagin. *Mathematical theory of optimal processes*. CRC press, 1987 (cit. on p. 3).
- [7] Charles R Hargraves and Stephen W Paris. «Direct trajectory optimization using nonlinear programming and collocation». In: *Journal of guidance, control, and dynamics* 10.4 (1987), pp. 338–342 (cit. on p. 3).
- [8] Richard Bellman and Robert E Kalaba. *Dynamic programming and modern control theory*. Vol. 81. Citeseer, 1965 (cit. on p. 4).
- [9] Michael R Caputo. «Dynamic Programming and the Hamilton-Jacobi-Bellman Equation». In: *Foundations of Dynamic Economic Analysis: Optimal Control Theory and Applications; Cambridge University Press: Cambridge, UK* (2005), pp. 511–536 (cit. on p. 4).
- [10] H Lomax, Thomas H Pulliam, and David W Zingg. «Time-Marching Methods for ODE’S». In: *Fundamentals of Computational Fluid Dynamics*. Springer, 2001, pp. 81–114 (cit. on p. 4).
- [11] Anastassios E Petropoulos. «Simple control laws for low-thrust orbit transfers». In: (2003) (cit. on pp. 5, 39).

- [12] M Yakovlev. «The “IADC Space Debris Mitigation Guidelines” and supporting documents». In: *4th European Conference on Space Debris*. Vol. 587. ESA Publications Division Noordwijk, The Netherlands. 2005, pp. 591–597 (cit. on p. 9).
- [13] Roger R Bate, Donald D Mueller, Jerry E White, and William W Saylor. *Fundamentals of astrodynamics*. Courier Dover Publications, 2020 (cit. on pp. 12, 13, 15–17, 23, 24, 26).
- [14] MJH Walker, B Ireland, and Joyce Owens. «A set modified equinoctial orbit elements». In: *Celestial mechanics* 36.4 (1985), pp. 409–419 (cit. on pp. 24, 27).
- [15] MJH Walker. «A set of modified equinoctial orbit elements». In: *Celestial mechanics* 38.4 (1986), pp. 391–392 (cit. on pp. 24, 27).
- [16] Jung-Hyun Jo, In-Kwan Park, Nam-Mi Choe, and Man-Soo Choi. «The Comparison of the Classical Keplerian Orbit Elements, Non-Singular Orbital Elements (Equinoctial Elements), and the Cartesian State Variables in Lagrange Planetary Equations with J 2 Perturbation: Part I». In: *Journal of Astronomy and Space Sciences* 28.1 (2011), pp. 37–54 (cit. on p. 24).
- [17] David A Vallado. *Fundamentals of astrodynamics and applications*. Vol. 12. Springer Science & Business Media, 2001 (cit. on p. 26).
- [18] Anastassios E Petropoulos. «Refinements to the Q-law for the low-thrust orbit transfers». In: (2005) (cit. on pp. 26, 39, 44, 50).
- [19] Davide Guzzetti et al. «Multi-revolution low-thrust trajectory optimization using symplectic methods». In: *Science China Technological Sciences* 63.3 (2020), pp. 506–519 (cit. on p. 27).
- [20] Jackson L Shannon, Martin T Ozimek, Justin A Atchison, and Christine M Hartzell. «Q-law aided direct trajectory optimization of many-revolution low-thrust transfers». In: *Journal of Spacecraft and Rockets* 57.4 (2020), pp. 672–682 (cit. on pp. 27, 44, 58, 59, 61, 66, 110).
- [21] Jerome R Vetter. «The evolution of Earth gravitational models used in astrodynamics.» In: *Johns Hopkins APL Technical Digest* 15.4 (1994), pp. 319–335 (cit. on p. 28).
- [22] Nikolaos K Pavlis, Simon A Holmes, Steve C Kenyon, and John K Factor. «The development and evaluation of the Earth Gravitational Model 2008 (EGM2008)». In: *Journal of geophysical research: solid earth* 117.B4 (2012) (cit. on p. 28).
- [23] *Orbit perturbations*. URL: [http://www.ingaero.uniroma1.it/attachments/2298\\_Part8\\_OrbitPerturbations1920.pdf](http://www.ingaero.uniroma1.it/attachments/2298_Part8_OrbitPerturbations1920.pdf) (cit. on pp. 28, 29).

- 
- [24] Andrea Forestieri. «Optimal low Earth orbit transfers with drag sails». PhD thesis. Politecnico di Torino, 2021 (cit. on p. 28).
- [25] Wikipedia contributors. *Earth Gravitational Model — Wikipedia, The Free Encyclopedia*. 2022. URL: [https://en.wikipedia.org/w/index.php?title=Earth\\_Gravitational\\_Model&oldid=1089953758](https://en.wikipedia.org/w/index.php?title=Earth_Gravitational_Model&oldid=1089953758) (cit. on p. 29).
- [26] Haoyi Shen, Shibe Xue, and Dewei Li. «MPC-based Low-thrust Orbit Transfer Under J 2 Perturbation». In: *2020 39th Chinese Control Conference (CCC)*. IEEE, 2020, pp. 2467–2472 (cit. on p. 29).
- [27] Gábor I Varga and JM Sánchez Pérez. «Many-revolution low-thrust orbit transfer computation using equinoctial q-law including j2 and eclipse effects». In: *6th International Conference on Astrodynamics Tools and Techniques*. 1. Darmstadt Germany, 2016 (cit. on pp. 29, 42, 45, 59, 110).
- [28] Marco Gomez Jenkins, David Krejci, and Paulo Lozano. «CubeSat constellation management using ionic liquid electrospray propulsion». In: *Acta Astronautica* 151 (2018), pp. 243–252 (cit. on p. 30).
- [29] Yu F Kolyuka, NM Ivanov, TI Afanasieva, and TA Gridchina. «Examination of the lifetime, evolution and re-entry features for the “Molniya” type orbits». In: *Proceedings of the 21st International Symposium on Space Flight Dynamics—21st ISSFD, Toulouse, France*. Vol. 650. 2009 (cit. on pp. 30, 110).
- [30] Jonathan Aziz, Daniel Scheeres, Jeffrey Parker, and Jacob Englander. «A smoothed eclipse model for solar electric propulsion trajectory optimization». In: *Transactions of the Japan Society for Aeronautical and Space Sciences, Aerospace Technology Japan* (2019), pp. 17–181 (cit. on pp. 34, 36).
- [31] Mirko Leomanni, Gianni Bianchini, Andrea Garulli, Renato Quartullo, and Fabrizio Scortecci. «Optimal low-thrust orbit transfers made easy: A direct approach». In: *Journal of Spacecraft and Rockets* 58.6 (2021), pp. 1904–1914 (cit. on pp. 34, 36, 66).
- [32] Mauro Pontani. «Optimal Space Trajectories with Multiple Coast Arcs Using Modified Equinoctial Elements». In: *Journal of Optimization Theory and Applications* 191.2 (2021), pp. 545–574 (cit. on p. 34).
- [33] P Kenneth Seidelmann. *Explanatory supplement to the astronomical almanac*. University Science Books, 2006 (cit. on p. 34).
- [34] Bruce Yost, Sasha Weston, Gabriel Benavides, Frederic Krage, John Hines, Stephanie Mauro, Selasi Etchey, Kiara O’Neill, and Barbra Braun. «State-of-the-art small spacecraft technology». In: (2021) (cit. on p. 37).

- [35] Akshay Reddy Tummala and Atri Dutta. «An overview of cube-satellite propulsion technologies and trends». In: *Aerospace* 4.4 (2017), p. 58 (cit. on p. 37).
- [36] Dillon O'Reilly, Georg Herdrich, and Darren F Kavanagh. «Electric propulsion methods for small satellites: A review». In: *Aerospace* 8.1 (2021), p. 22 (cit. on p. 37).
- [37] Giada Staniscia. *Development of a Low Earth Orbit Mission Preliminary Analysis Tool*. 2019 (cit. on pp. 37, 61).
- [38] Andrea Verri and Lorenzo Casalino. «Low-Thrust Many-Revolutions maneuver optimization for future active debris removal applications». In: () (cit. on p. 37).
- [39] Yuqing He and Jianda Han. «Control Lyapunov functions: new framework for nonlinear controller design». In: *IFAC Proceedings Volumes* 41.2 (2008), pp. 14138–14143 (cit. on p. 39).
- [40] James E Pollard. *Simplified analysis of low-thrust orbital maneuvers*. Tech. rep. AEROSPACE CORP EL SEGUNDO CA TECHNOLOGY OPERATIONS, 2000 (cit. on pp. 45, 110).
- [41] Scott King, Mitchell Walker, and Craig Kluever. «Small satellite LEO maneuvers with low-power electric propulsion». In: *44th AIAA/ASME/SAE/ASEE Joint Propulsion Conference & Exhibit*. 2008, p. 4516 (cit. on pp. 45, 110).
- [42] Armando Ruggiero, Pierpaolo Pergola, Salvo Marcuccio, and Mariano Andrenucci. «Low-thrust maneuvers for the efficient correction of orbital elements». In: *32nd International Electric Propulsion Conference*. 2011, pp. 11–15 (cit. on pp. 54, 55).
- [43] Marilena Di Carlo and Massimiliano Vasile. «Analytical solutions for low-thrust orbit transfers». In: *Celestial Mechanics and Dynamical Astronomy* 133.7 (2021), pp. 1–38 (cit. on p. 55).
- [44] *ESA - Types of Orbits*. URL: [https://www.esa.int/Enabling\\_Support/Space\\_Transportation/Types\\_of\\_orbits](https://www.esa.int/Enabling_Support/Space_Transportation/Types_of_orbits) (cit. on p. 61).
- [45] Francesco Topputo and Chen Zhang. «Survey of direct transcription for low-thrust space trajectory optimization with applications». In: *Abstract and Applied Analysis*. Vol. 2014. Hindawi. 2014 (cit. on pp. 70, 74, 75, 82).
- [46] John T Betts. *Practical methods for optimal control and estimation using nonlinear programming*. SIAM, 2010 (cit. on pp. 71, 75).
- [47] John T Betts. «Survey of numerical methods for trajectory optimization». In: *Journal of guidance, control, and dynamics* 21.2 (1998), pp. 193–207 (cit. on pp. 71, 73).

- [48] Bruce A Conway. *Spacecraft trajectory optimization*. Vol. 29. Cambridge University Press, 2010 (cit. on p. 71).
- [49] William Karush. «Minima of functions of several variables with inequalities as side constraints». In: *M. Sc. Dissertation. Dept. of Mathematics, Univ. of Chicago* (1939) (cit. on p. 72).
- [50] Harold W Kuhn and Albert W Tucker. «Nonlinear programming». In: *Traces and emergence of nonlinear programming*. Springer, 2014, pp. 247–258 (cit. on p. 72).
- [51] Paul J Enright and Bruce A Conway. «Discrete approximations to optimal trajectories using direct transcription and nonlinear programming». In: *Journal of Guidance, Control, and Dynamics* 15.4 (1992), pp. 994–1002 (cit. on p. 73).
- [52] Albert L Herman and Bruce A Conway. «Direct optimization using collocation based on high-order Gauss-Lobatto quadrature rules». In: *Journal of Guidance, Control, and Dynamics* 19.3 (1996), pp. 592–599 (cit. on p. 73).
- [53] Stephen Paris, John Riehl, and Waldy Sjawu. «Enhanced procedures for direct trajectory optimization using nonlinear programming and implicit integration». In: *AIAA/AAS astrodynamics specialist conference and exhibit*. 2006, p. 6309 (cit. on p. 74).
- [54] Victor M. Becerra. *PSOPT Optimal Control Solver User Manual Release 5.0*. URL: [https://github.com/PSOPT/psopt/blob/master/doc/PSOPT\\_Manual\\_R5.pdf](https://github.com/PSOPT/psopt/blob/master/doc/PSOPT_Manual_R5.pdf) (cit. on pp. 74–76, 78).
- [55] Andreas Wächter and Lorenz T Biegler. «On the implementation of an interior-point filter line-search algorithm for large-scale nonlinear programming». In: *Mathematical programming* 106.1 (2006), pp. 25–57 (cit. on p. 76).
- [56] Steven P Hughes, Darrel J Conway, and Joel Parker. «Using the general mission analysis tool (GMAT)». In: *AAS Guidance and Control Conference*. GSFC-E-DAA-TN39043. 2017 (cit. on p. 104).